UNIVERSITY OF AGDER

Signal Analysis, Modeling and Simulation of Vehicle Crash Dynamics

Students:
Debela Yadeta Midjena
Sanin Muraspahic

Supervisors:
Prof. Hamid Reza Karimi
Prof. Kjell Gunnar Robbersmyr

A thesis submitted in partial fulfillment of the requirements for the degree of Master of Science in Mechatronics

in the

Department of Engineering
Faculty of Technology and Science
University of Agder

June 2013

Abstract

Vehicle crash safety has been a strong point of interest for long time in many countries due to the reason that safety statistics show high fatality rate of vehicle occupants involved in road accidents. All vehicles which are going to appear on the road must go through several serious crash investigations to approve whether they conform to the relevant safety standards. There are large crash test facilities built by big companies for these operations. However, a wide and full-scale crash testing is complex, difficult and expensive that demands many things to be fulfilled. Because of these and other reasons, mathematical models could be developed to represent real world vehicle crash scenarios. This work is devoted to developing a vehicle crash modeling and a reconstruction of physical models composed of springs, dampers and mass arrangements to simulate a real car collision with a rigid pole. First, an extensive signal analysis is carried out to understand the vehicle full-scale frontal crash in time domain and frequency domain. Next, 2D and 3D mass-spring-damper model are presented and equations of motion for the dynamic model are being established and subsequently solutions to obtain differential equations are formulated. The models' parameters are obtained by fitting their response equations to the real data measurement from vehicle crash experiment. The identified parameters with the proposed 2D and 3D mathematical models are used for the simulation, and the response from the models are verified by comparing them with the real data from experiment. The comparison and validation show that the model represented are well suited to the real vehicle crash scenario.

Acknowledgements

We would like to express our gratitude to our advisors Prof. Hamid Reza Karimi and Prof. Kjell Gunnar Robbersmyr for the continuous support, encouragement and good advice through the learning process of this master thesis. Besides our advisors, we would like thank the rest of vehicle crash research group for their insightful comments and questions.

Contents

List of Figures

List of Tables

Chapter 1

Introduction

1.1 Problem Statement

Vehicle crash tests are important part of the comprehensive investigation on the crash-worthiness of the vehicle engineering practices. However, a vehicle crash test is very expensive experiment which incorporate many complex components and practices. Therefore, much effort is going by many researchers to use modeling tools such as Finite Element Method(FEM) or Lumped Parametric Model(LPM) to represent crash tests. It is desirable to involve in this research-field to make further advancement by introducing a new 3D mathematical model for vehicle crash test that was carried out by Agder Research Foundation.

1.2 Scope of Work

Road traffic accidents constitute a major health and economic problems everywhere around the world. During recent years traffic accidents have gain big focus, and attempts to minimize these problems has increased in many countries. The effort to bring the changes have forced many sectors including automotive industry to look into vehicle crash safety seriously. Because of this fact, all vehicles which are going to appear on the road must go through a serious crash investigation to approve whether they conform to the relevant safety standards or protocols applicable to different countries. At the same time every equipments that are placed along side of the roads for example lighting columns, sign masts, road and bridge railings, central reservations, etc, must be tested and approved if they satisfy the safety requirements. This require well established and organized information from different research sources. Due to this reason and other described information in this project there is a great interest to develop mathematical models that could represent real world vehicle crash scenarios.

The University of Agder has been involving for over two decades in several theoretical and practical crash test researches to participate in this interesting field of work. This project is the continuation

of this research trend. Despite much research which was going on in this field of interest, good 3D models have yet to be implemented for use. The key aim of this project can be stated in few words as to establish a 3D mathematical model that would represent the dynamics of real-time crash. That is of course a very general specification and in this case the aim is to cover large level of details for the scope of this work to achieve the specified target.

- Review the signal analysis of vehicle crash data obtained from experimental measurements conducted by Agder Research Foundation.
- Present mathematical model in 2D and 3D mode that can represent a vehicle to barrier collision from the experiment carried out.
- Perform Simulation for vehicle crash models derived and check their effectiveness by comparing them with the real data obtained from the conducted experiment.
- Evaluate the performance of the models derived by experimenting or applying them on different set of data obtained from another vehicle crash and suggest possible solutions for further investigations.

1.3 Aims and Motivations

As stated in the proceeding description, the first task in this project is to analyze signals obtained from vehicle crash experiment. Depending on this analysis, a mathematical model have to be formulated to represent the kinematics and dynamics of vehicle crash from the experiment. Simulation of the model have to be performed using MATLAB software to compare the simulation results from the mathematical models and the experimental data. Lastly, the presented mathematical model performance have to be evaluated by testing if they have the same performance on similar crash experiment so that they can be used for future work. The sensitive experimental data used for references in this work is obtained from a full scale physical impact test carried out by team of researchers from Agder Research Foundation.

Important comprehensive information for vehicle crash is needed by many organizations as well as vehicle users. Manufacturers need to carry out the rigorous crash experiments to meet the standard requirements and improve their car design to make reliable products. At the same time government bodies or other responsible organizations should make extensive and complex research on vehicle crash to place regulatory standards, to asses the models of existing or new manufactured cars, to update the information for consumers or manufactures regularly [10],[11],[3],[12]. In general cases the experimental tests should be carried out at many stages throughout the design phases of the vehicles or the development of road side equipments to make sure that the preliminary design safety requirements are satisfied. However, wide and full-scale crash experiments are complex and difficult because it demands many things to be fulfilled. For example, it requires properly equipped research center to conduct the test measurement precisely, it needs qualified staff members for the

work or correct measuring devices. Another issue is high cost expenses for setting up a full scale vehicle crash, and carrying out the experiments is time consuming [13].

Vehicle crash is also of great interest for researchers and car producers who want to improve the safety standards and performances. In the recent years, many researches have been going on vehicle crash tests and several mathematical models have been developed and published to represents the actual crash tests. For example, Matthew Huang in his book named Vehicle Crash Mechanics described different contents for a car crash that includes crash pulse and kinematics, crash pulse prediction by convolution method, crash pulse characterization, basics of impact and excitation modeling and so on [5]. Reconstruction of crash pulse of a vehicle involved in crash event is made by using a wavelet-based approach in [14]. A novel 3D building and query algebra for reconstructing is defined for a car crash scene in [15]. A new intelligent adaptive method for occupant restraint system has been used in [16]. Even though, there were many researches going on for long time in this field of interest, there are still many problems that need more work because of the complexity and magnitude of the challenges.

Due to the factors mentioned above or other details there is a huge amount of motivational force behind this work to establish mathematical models that can represent a full-scale impact and provide results that could be used instead of the experimental tests. The derived model should be accurate enough to predict a behavior of vehicle during collision or vehicle crash, so that derived models will be utilized for developing equipment and preliminary tests without performing complicated crash tests. A mathematical model can be considered genuine and accurate if it proves to be valuable by representing different impact testings of similar or identical cases. Then a single mathematical model can be used to reconstruct and simulate full-scale vehicle crash test, which would be used to improve the safety of occupants during real time crash.

1.4 Problem Solution

To achieve a good solution for the problem stated in chapter 1.1, a better understanding of the procedures for crash analysis is needed, in both practical and mathematical aspects. Since the main focus is developing a new mathematical model, a good survey needs to be conducted through published papers and literature studies for a better understanding of car crash analysis and modeling procedures [[13],[5],[14],[15]]. In parallel to this, a research is needed to familiarize how the crash test experiments work and how the relevant data is gathered from it[[10],[11],[3],[12]]. Based on the gathered information and having a good understanding of the concepts, an analysis of the crash data needs to be done in order to study and verify the crash behavior. The better the verification is, the better the crash data can be used as a reference to ongoing creation of mathematical models. Before creating the final 3D model, a comprehensive study of the modeling process needs to be conducted. Primarily, a 1D model is to be created for a better understanding of the concept and the use of various equations. Secondly, a 2D model is to be created and at the end the final 3D

model. The final model would be verified with the reference data to check if the model corresponds good to the gathered data from the real crash scenario.

1.5 Project Plan

There are two members involved in this project namely Debela Yadeta Midjena and Sanin Muraspahic. At the beginning of the project realization it was decided to proceed in with weekly meetings of the project with advisors and other members of research groups working on similar project on vehicle crash. The meetings have been taking place every Wednesday for one hour. The project tasks from the preceding week is briefly discussed with the advisors and at same time look on to the following weekly plans.

The tasks in the project were divided between the members of the project team from the beginning and everything was being in progress with good cooperation to stick to the time table. The project work was expected to be executed according to a time table presented below in the Appendix A. It is noted that the shown version is the final one, since throughout the project realization some changes were needed in the project planning. The time table was presented using Gantt chart and modification and updates were being made accordingly throughout the project phases.

The different tasks of the project were indicated in the left part of the chart and the allocated time interval of the tasks were indicated by the color at the right columns. Each task was expected to be started at the beginning of the colored zone and be completed at the end of the colored zone. The major tasks were also identified as major parts in the project documentation, and the details break down of the project tasks were taken as section and subsection in the documentation of the project. Even though the project had been delayed about a month due to some inconvenient reasons, it can be observed the task plans were strictly followed according to the time table by successive hard work of the project members.

As the title of the project indicates the project includes tasks that require knowledge from different fields and availability to a number of different reference sources. In addition, the project was conducted as a team work and a lot of various materials, calculations, drawings, concepts, designs, etc. were produced. In order to improve effectiveness of work and knowledge sharing, it was decided to use a well known Internet tool: DropboxTM (https://www.dropbox.com/). Thanks to this powerful information sharing tool, both of the group members had a direct access to everything done or shared by other member of the team in convenient and straight-forward form. The report writing was being conducted starting from the beginning of project duration in parallel to the project realization. This helped the project team to facilitate the summarization and the documentation of the results available in timely manner as well as intelligible way.

1.6 Project Outline

The report is organized into the chapters briefly described as follows:

Chapter 1

The first chapter is the Introduction part. It starts with a definition of the problem and scope of the work. The scope description part mentions some important and interesting scientific problems that is tried to be solved in this project. There are four major parts to be carried out which are itemized in the scope of the project. The introduction part addresses the aims of the project and the motivation behind the whole work. The plan followed to realize the work is another part described here, and the time needed for different levels of the plan is placed in the index part for further reference.

Chapter 2

The second chapter includes background information which is necessary to start a project. It starts with a section defining or answering questions such as: what is a vehicle crash or traffic accident?, what causes the vehicle crashes everywhere?, and what is the extent of the problem ?. Three different standard procedures followed to make a test experiment on a vehicle crash, and what data these experiments provide are also described in detail here. Further, it is explained how these data are used in the interest of enhancing crash safety. Some few examples of crash test experiments are also listed. Two main approaches for the vehicle crash modeling which are the Finite Element Analysis Method(FEM) and Lumped Parameter Modeling(LPM) are described briefly. Finally, a custom methodology is created to describe the steps followed to solve the problem stated at the beginning of the introduction.

Chapter 3

In the third chapter the experimental setup was described in detail. The explanation starts with how the test site was organized and what the test facility incorporated. The information about the car used for the full-scale collision, the dimensions of the vehicle and the barrier used for the collision purpose are also described. Lastly, the instruments used for collecting the data and the method of data acquisition are described in detail here.

Chapter 4

The Signal Analysis is one main focus area of the project that is described in the fourth chapter. The content of experimentally obtained data set is explained at the beginning of this section. In the next step the raw data set is put into analysis to investigate the data in time domain and

frequency domain. Then the data is filtered using Butterworth low-pass filter to reject unwanted frequencies and to have as flat a frequency response as possible in the passband. Finally, the filtered data is put into signal analysis to find important information such as crash time, deformation and maximum dynamic crush.

Chapter 5

Finding new mathematical model is the major part of the project which is carried out in the fifth chapter. First, a description of planar kinematics of rigid vehicle is presented and the planar dynamic aspect of a rigid vehicle is carefully studied. Using mass-spring-dampers in combination with the concept presented in the planar dynamics section, a new 2D mathematical model is proposed for a representation of a vehicle to barrier collision. The next step was a careful study of 3D kinematics and dynamics of a rigid vehicle. Then, three pairs of spring-dampers are each parallely connected to a mass for a representation of a vehicle to barrier collision. Finally, using the kinematics and dynamic knowledge gained, an equation of motion is presented for the system representing a vehicle to barrier collision in 3D.

Chapter 6

The MATLAB simulation has helped a lot to elaborate the essence of the proposed mathematical model and it is presented well in the sixth chapter. MATLAB is used to estimate or find the values of the parameters for the simulation process and the comparison of the real data and the model response is carried out in this section using the powerful simulation tools. Lastly, the validation of the model is made here using data from another vehicle crash with different angle of impact and different intial speed.

Chapter 7

The discussion and evaluation provides an overview of the project outcome. In the discussion and evaluation section the result obtained from the signal analysis are discussed. Then the expected performance of proposed 3D mathematical model response is compared to the real data signal analysis result. At last the validity of the results is discussed along with pros and cons of the proposed models.

Chapter 8

This section outlines the conclusion drawn based on the execution of the project. The points of conclusion are made to clarify that the objectives of the problem statement are met. Finally some suggestions for further work relevant to this project is proposed.

Chapter 2

Theoretical Background

2.1 Vehicle crash

2.1.1 Definition

The term Car crash also known as a traffic accident (motor vehicle collision, motor vehicle accident, car accident, automobile accident, road traffic collision, or car smash) refers to the general term used for a traffic accident involving collisions or impact between an automobile and another automobile, collision between vehicle and roadside hazards, pedestrians, or animals[17].

Roadside hazard is a stationary obstruction by the side of a road that could increase the probability of vehicle crash or occupant injury or fatality if a motor vehicle leaves the roadway. The fixed obstructions may include trees, utility poles, luminaries supports, sign posts, bridge rails and end treatments, fences, embankments and cuttings, ditches, guard rails (and guard rail end treatments), mail boxes and drainage structures [18].

2.1.2 Causes of Vehicle Crashes

Different factors contribute to the risk of vehicle collision that may include equipment failure, roadway design or poor roadway maintenance. A behavior of a driver, driver skill and/or impairment and speed of operation are another factor that could lead to vehicle accidents. The vehicle design and road environment are also factors in vehicle collisions [17].

2.1.3 Problems of road traffic injury

Road traffic accident is a big challenge in all societies today. It is a complex and dangerous system which people deal with every day. Vehicle crashes are one of the traffic accidents that lead to the death or fatality of occupants, pedestrians, animals or cause a great damage to roadside safety equipments or properties.

The traffic injury cause dozens of survivors live with short-term or permanent disabilities that may lead to a continuous restriction on their physical functioning, psychosocial consequences or a reduced quality of life. People counted in millions spend long weeks in hospital each year after severe crashes and may never have the same potential as before the crashes happened. About 50 million people are injured worldwide every year and an estimated 1.2 million people are killed in road accidents. Projections indicate that these figures will increase by about 65 % over the next couple of decades. This indicates there should be new commitment to prevention [19].

The traffic accidents have also bad economic consequences. In low-income countries the cost of road crash injuries is estimated at roughly 1% of gross national product (GNP) in economic terms. It is estimated 1.5% in middle-income countries and 2% in high-income countries [20]. The direct economic costs of global road crashes have been estimated at 387.67 euro($ 518) billion. In European Union (EU) countries alone road crash injury contributes 5% to the global death toll which exceed 180 euro billion in economic terms [19].

2.2 Vehicle Crash Testing Procedures

Crash safety of vehicles is very important because of the direct or indirect involvement of human in automobile accidents [21]. Even though fatality rates of cars are declining and the cars are getting safer each year, car crashes are still one of the leading cause of death and injury in many communities [22]. Cars have been getting safer because of well-established testing programs. Instrumented and controlled collisions are used recently by manufacturers to build improved crash safety into their vehicles [21]. Vehicle crash testing is quite extensive and it composes many kinds of objects in the struck and different type configurations. Full scale vehicle is the crucial for impact testing in addition to other instrumentation and components [23].

In this topic for testing procedures we intended to focus on full scale barrier impact testing for ,three of the most widely consulted consumers safety programs [12] which are European New Car Assessment Program(Euro NCAP), National Highway Traffic Safety Administration(NHTSA) and Insurance Institute for Highway and Safety (IIHS). The content is description about the basic testing procedure and some points their rating criteria.

2.2.1 European New Car Assessment Program(Euro NCAP)

Euro NCAP is European organization that was set up by the Transport Research Laboratory for the UK Department for Transport, and was backed by several European governments and the European Union. Euro NCAP encourage safety improvements to new car design [1]. Cars for the evaluation and testing are purchased from dealers randomly [12].

Euro-NCAP organizes crash test using frontal and side collisions and publish test results that provide accurate information to motoring consumers based-on a realistic and independent assessment

of safety performance for most popular cars sold in Europe [24][1]. EEVC WG17 safety assessment protocol is used by Euro-NCAP for occupant safety as well as pedestrian safety [12]. According to [1], for the Frontal Impact test a speed of 64km/h is used to strike the car to deformable barrier that is offset see Figure 2.1. 50th percentile male HYBRID III dummies are fitted into the driver and front passenger seat belted to carry out the test [12] and the assessment given to adult front occupants is carried out depending the readings taken from these dummies [1].

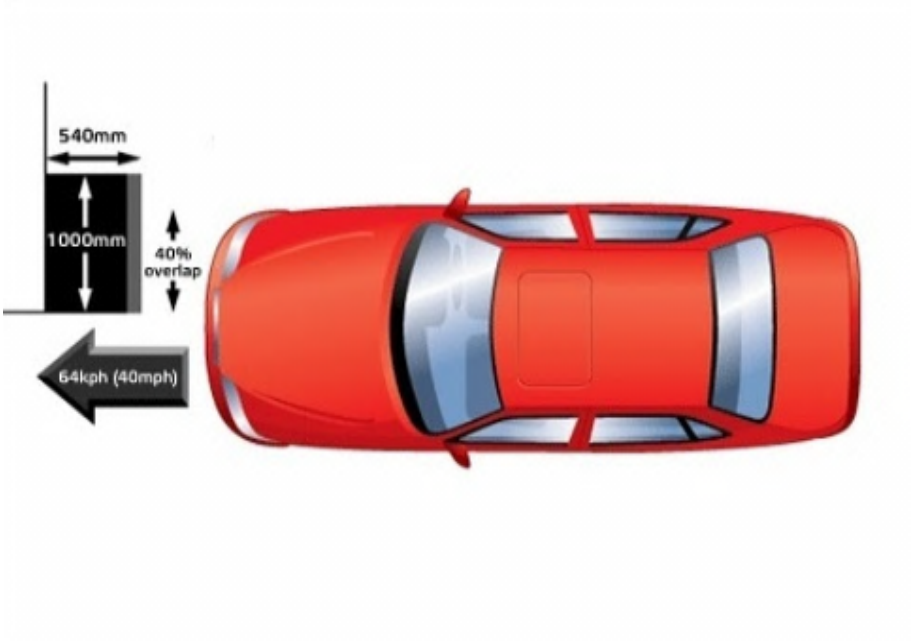

FIGURE 2.1: *Euro-NCAP Frontal Impact Test Set-Up (RH drive)* [1].

The offset frontal impact is made into an immovable block fitted with a deformable aluminum honeycomb face [24] [1]. The offset test with the impact across 40 percent of test car's front is made to replicate one car having a half width frontal impact with another car of equivalent size and weight. This test is made in order to identify the car's ability to survive the impact without suffering passenger compartment intrusion. The speed of collision of 64km/h between a car and an immovable block represents a car to car collision with each car traveling at around 55 km/h. The energy absorbed by the deformable face makes the difference in speed [1].

A quarter of all serious-to-fatal injuries happen in side impact collisions in Europe. The side impact test which includes car-to-car side impact and pole-to-side impact is the second most important crash configuration. A mobile deformable barrier (MDB) is used to impact the driver's door at the speed of 50km/h for the replicate of car-to-car side impact see Figure 2.2.

The second side impact test is carried out by making the car tested propel sideways at 29km/h into a rigid pole for the simulation of pole-to-side impact see Figure 2.3 [1]. A 50th percentile male Euro-SID I dummy is fitted belted into the driver seat [12] to assess the injury protection.

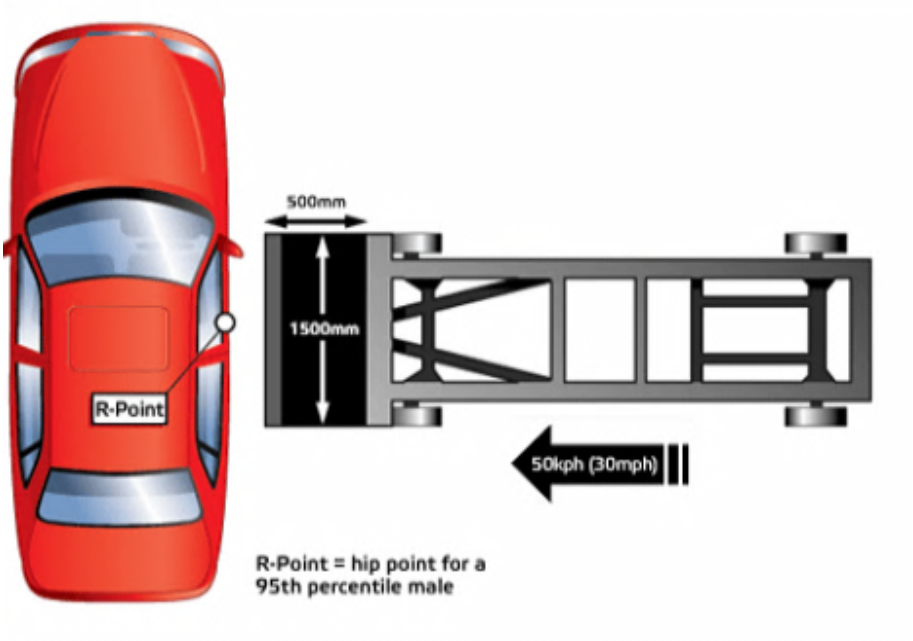

FIGURE 2.2: *Euro-NCAP Side Impact Test Set-Up (RH drive)* [1].

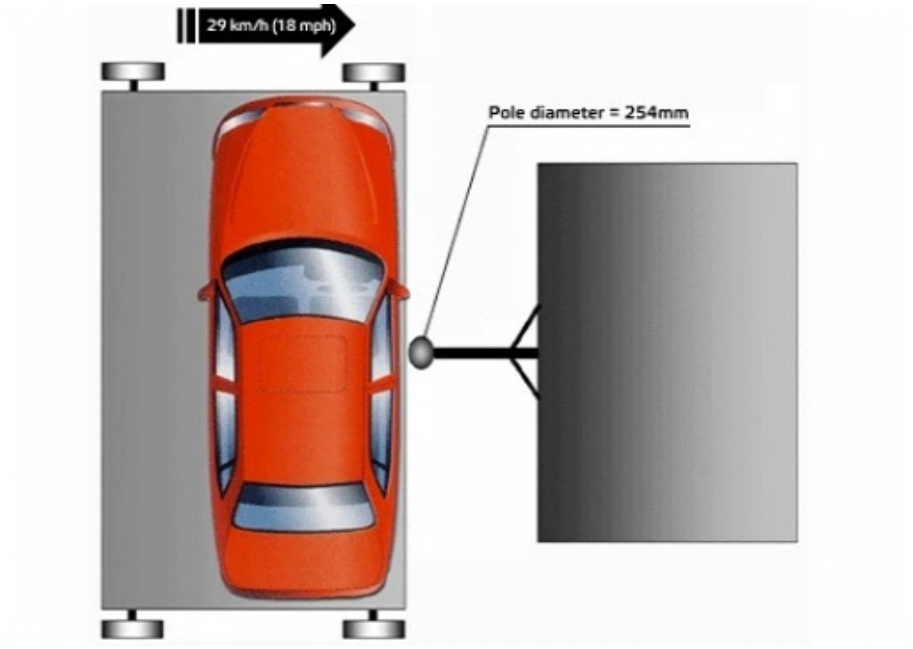

FIGURE 2.3: *Euro-NCAP Pole Impact Test Set-Up (RH drive)* [1].

2.2.2 National Highway Traffic Safety Administration(NHTSA)

NHTSA is an agency of the Executive Branch of the U.S. government, part of the Department of Transportation. It has been providing important comprehensive information for long years which composes frontal and side crash test results to consumers to assist in car purchasing decision [12]. It has also the responsibility for setting and monitoring the standard for traffic and safety for all motor vehicles in U.S. [25]. Results are published for the information of consumers, as the US arm of the international New Car Assessment Program (NCAP)[24].

They use a protocol FMVSS208 [2] for checking how well occupants would be protected in a passenger vehicle during an event of a serious real world crash. This protocol has elevated occupant crash protection by encouraging the improvement of vehicle structure and restraint system. The structural design of a car should lessen the gravity of two adverse effects of a crash which are the degradation of the occupant compartment survival space, and the occupant compartment deceleration severity. These two effects have the potential to cause death or fatality. NHTSA use several frontal crash procedures and try to find out if the frontal collision procedure meets the required objectives. The procedures prescribed by the protocol FMVSS208 includes: the full frontal fixed rigid barrier test, the oblique frontal fixed rigid barrier test, the generic sled test, the offset frontal fixed deformable barrier test, the perpendicular moving deformable barrier (MDB) test, the oblique moving deformable barrier test and the full frontal fixed deformable barrier (FFFDB) test [2].

As mentioned above US-NCAP conducts a frontal impact test and a side impact test to investigate occupant safety [12]. A rigid barrier crash test is applied and the test involves belted and unbelted 50th percentile male anthropomorphic dummies for impact conditions. The vehicle speed is often from 0 to 48 km/h, and impact angle is from 0 to 30 degrees [2]. For the full width frontal impact which is illustrated in Figure 2.4. 50th percentile male HYBRID III dummy are fitted in the driver and front passenger seats and the vehicle crashes head-on into rigid concrete barrier at 56km/h(35mph). The occupant restraint system such as belts and air bags are evaluated from this particular test [24].

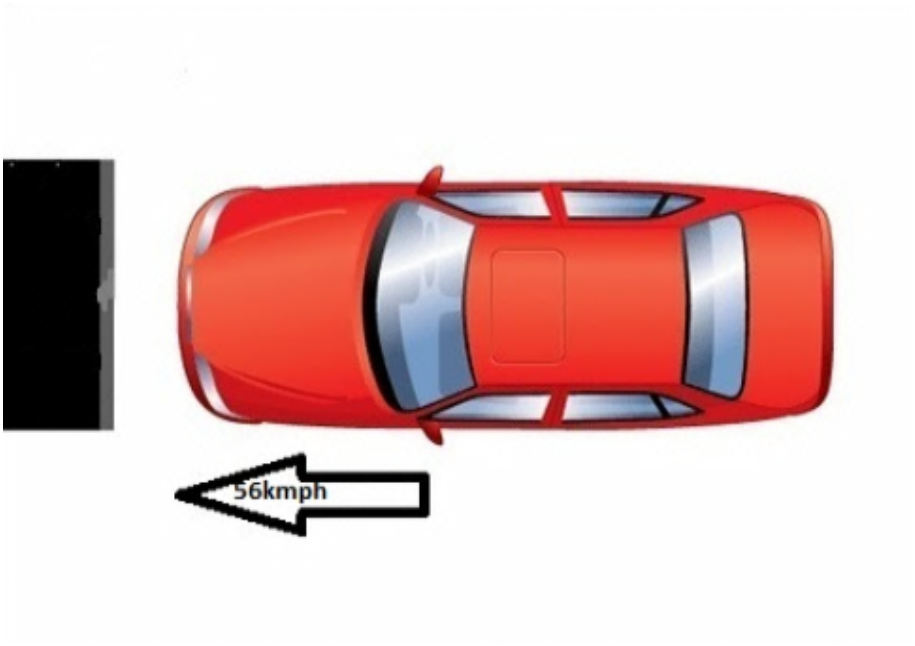

FIGURE 2.4: *US-NCAP Frontal Impact Test Set-Up* [2].

The FMVSS 214 is side barrier impact protocol with increased impact speed, i.e., 61.9km/h (38.5mph) vs. 53.9km/h (33.5mph). The 50th percentile male US-SID dummies are belted and positioned in the driver and driver side rear passenger seats while the trolley impacts the targeted

in crabbed configuration [12]. The frontal impact and side barrier impact performance are presented separately with an individual star rating for each dummy positioned in the vehicle under assessment by US-NCAP [12].

2.2.3 Insurance Institute for Highway and Safety (IIHS)

The IIHS is an independent, nonprofit scientific and educational organization that has been working to reduce the number of motor vehicle crashes , the rate of injuries ,amount of property damage in the crashes that still occur, and it has been finding out what works and does not work to prevent vehicle crashes from happening [3]. It focuses on countermeasures aimed at human, vehicular, environmental factors ,and on interventions that can occur before, during, and after crashes to reduce losses. IIHS rates vehicles and publish the result by performing the low-speed bumper crash tests, head restraints tests and frontal impact crash tests [12].

The frontal impact test is carried out in two different modes which are a moderate overlap test and a small overlap test. A vehicle traveling at speed of $64.4 \pm 1 km/h$ impacts a deformable face made of aluminum honeycomb barrier with $40 \pm 1\%$ overlap on the driver side see the Figure 2.5 [3]. A HYBRID III dummy representing an average-sized man is fitted and belted into the driver seat [3, 12]. This test represent a frontal offset crash between two vehicles of the same weight both traveling at speed 65km/h [3].

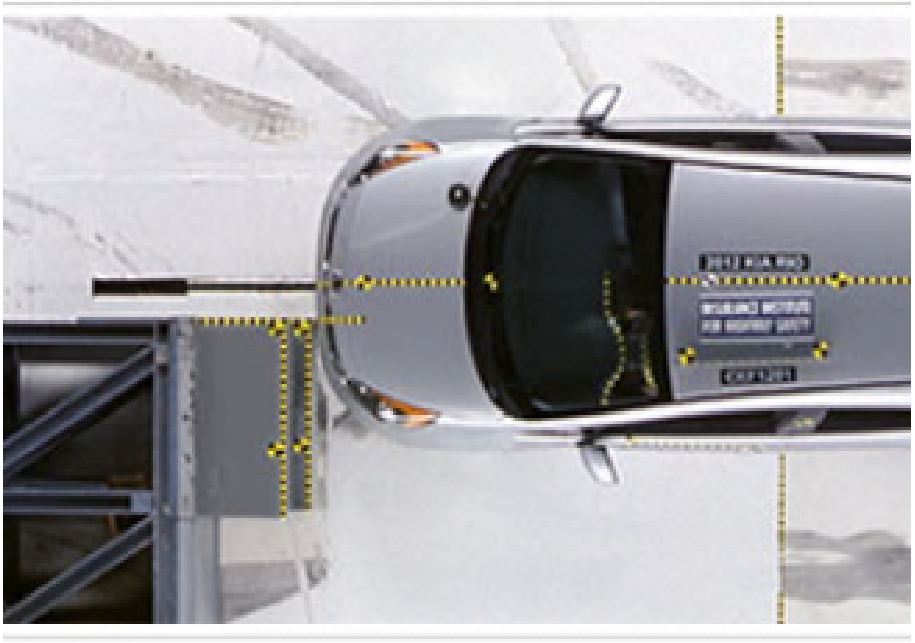

FIGURE 2.5: *IIHS Moderate Overlap Frontal Impact Test Set-Up* [3].

The second FI test is Small overlap frontal test which is introduced in 2012. A vehicle traveling at speed of $64.4 km/h$ is made to impact $1.524 m$ tall rigid barrier to replicate what happens when front corner of a vehicle collides with other vehicle or object like a tree or utility pole. The vehicle hits the barrier with 25% of the total width overlap on the driver side that is shown in Figure 2.6.

A HYBRID III dummy representing an average-sized man is fitted and belted into the driver seat [3].

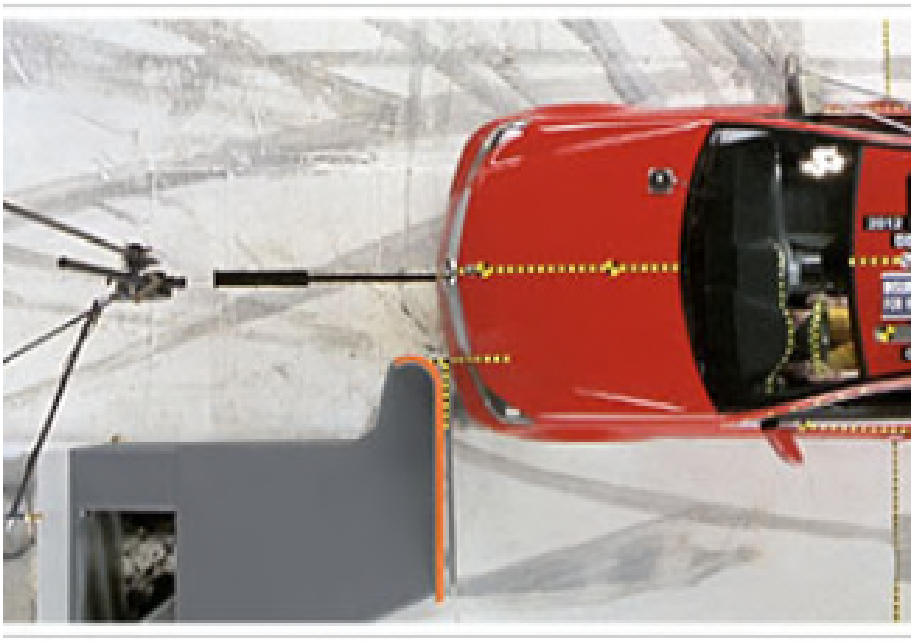

FIGURE 2.6: *IIHS Small Overlap Frontal Impact Test Set-Up* [3].

Three factors are assessed in the moderate overlap and small overlap frontal tests. The three factors engineers use include structural performance, injury measures and dummy kinematics to determine each vehicle overall crash-worthiness evaluation [3, 12].

IIHS performs also a side impact test. The side impact test is performed by 1496.85kg SUV-like barrier. The barrier strikes the driver side of the vehicle at speed of 50km/h as shown in the Figure 2.7. The test is carried out using two SID-II dummies representing small (5th percentile) women or 12-year-old children. These dummies are placed in the driver seat and the rear seat behind the driver. The side impact test rating is determined by looking at driver and passenger injury measures, head protection and structural performance [3].

2.2.4 Some other Crash Testing Techniques

There are several other vehicle crash testing procedures. For example, National Road Motorists Association(NRMA) is an organization in Australia that involves assessment program of new cars. The Australasian New Car Assessment Program (ANCAP) carry out crash testing new model vehicles under strictly controlled conditions. It compares injury levels of occupants involved in frontal and side impacts and publish results [10, 24].

Another Vehicle Crash testing procedure is carried out by Japan NCAP. Japan NCAP is the Japanese organization that works under the guidance of Ministry of transport. The safety performance of automobile currently available in Japan is evaluated using its own procedure [11, 24]. There is also several automotive industry Vehicle crash testing facilities in different countries.

FIGURE 2.7: *IIHS Side Impact Test Set-Up* [3].

Some examples are Ford Company Test Facility, General Motors Corporation Automotive Crash test Facility ,Crash Test Techniques at FIAT and so on.

2.3 Vehicle Crash Modeling

2.3.1 Finite Element Analysis Method

Vehicle crash modeling is one of the challenges in the area to determine the crash-worthiness. There are two main approaches to the modeling of the vehicle crash. The first method is carried out by a use of a virtual environment software which is called a Finite Element Analysis Method (FEM) [26] and the second method is by a use of Lumped Parameter Modeling(LPM) [27],[28].

The two different approaches have their own advantages and disadvantages that need to be considered when one wants to use either of them. The major advantage in using FEM is the ability to represent the geometrical and material details of structure in virtual environment software. However, FEM consumes more time and is more expensive than the LPM that could be considered as its major disadvantages. On the other hand, the LPM has a major advantage of low use of computer resource and simplicity of modeling. Finding the values for the lumped parameters is a problem in the LPM [26].

FEM is considered a most powerful in the vehicle crash analysis that is suitable for creation and simulation of a 3-dimensional car model. There are several types of modeling and simulation software that could be used in the simulation and analysis of vehicle crash dynamics and kinematics. Two FEM software are briefly described below as an example for a use in vehicle crash as well as occupant safety modeling and simulation.

LS-DYNA

LS-DYNA is a general-purpose, explicit finite element program capable of simulating and analyzing the complex real world problems which are nonlinear dynamic response of three-dimensional structures. It was developed by Livermore Software Technology Corporation [29]. LS-DYNA is used by several industries that include automobile, aerospace, construction, military, manufacturing, and bioengineering sectors. LS DYNA minimizes a design time for a system by predicting how a prototype will respond to real-world events. Fully developed collision analysis is incorporated in LS-DYNA and it has also a built in features for errors in defining the surface contacts between mating surfaces. It is user friendly software and it is easy to run all types of vehicle crash analysis [30].

IMPETUS AFEA SOLVER

This is another FEM software package that can be used for non-linear computational mechanics such as vehicle crash analysis. According to the developers website information it is primarily developed to predict large deformations of structures and components exposed to extreme loading conditions. Impetus is a volume element based programming. The package comprises different solver modules such as Finite Element(FE) module, Discrete Particle (DP) module, WELDSIM module and Smoothed Particle Hydrodynamics (SPH) module.

It has also a post processor feature which is a professional engineering tool for analysis and post processing of the Solver's database. The tool can be used to high quality graphics, animations and plots which can be used directly for reports and company presentations [31].

2.3.2 Lumped Parameter Modeling

The theory of lumped parameters has been developed from the background of spring stiffness. It is an analytical way of solving a vehicle crash. It uses dynamic and kinematics equations. For example, a mass-spring and damper model to describe a car colliding with a hazardous obstacle [32]. Finding solutions to differential equations allow us to obtain the acceleration for the entire vehicle and by integrating it one can obtain the speed and displacement of the vehicle during and after impact. This method is good for representing a real crash and because of its simplicity compared to FEM makes it a good candidate for assessment of car crash data.

The models can be made by a simple Kelvin model or a more complex dynamic model which represents for example the front panel with equations of mass, suspensions, engine and other mechanical units for better approximation. The disadvantage of this modeling approach is to estimate the parameters of the spring and damper which are mostly found on the basis of the real crash for a certain case. It can be used for good approximation for the case where the real data is collected [26].

In recent years there were a lot of theories and publications of different car crash models. In any damage analysis, where a crash or impact occurs, whether it is a plane crash, train or in this case a car crash, the total energy of the impact will be absorbed and used in balancing equations. As mentioned earlier in the text, first the data from the accelerometers and other sensors needs to be gathered. Then the acquired measurements from the real case should be processed for further creating models and simulations to best fit the real data analysis.

In the LPM different software can be used to generate a model which represents the actual case. Using curve fitting toolbox from MATLAB one can estimate a function for the acceleration graph which is generated from the real data. It could be a Gaussian or an exponential function with several terms. Acceleration pulse approximation can also be made to describe the real data by using basic functions of sine, haversine or smoothing spline. Another approach is using wavelets functions to reconstruct the acceleration signal from the wavelets coefficient matrix for the major frequency components as described in [33] and gave satisfactory results comparing with real crash data.

Other method use neural networks and fuzzy logic which is a newer type of intelligent technologies and it has good result when comparing with the actual acceleration pulse signal. Fuzzy logic is explained by fuzzy sets that are representation of probability. Fuzzy rules can be used to describe a system of uncertainty where it is difficult to use a mathematical model [26].

2.4 Project Methodology

.

The goal set previously put forward in the introduction part of the project will be reached by following custom methodology designed for this specific task Figure 2.8. The first step handled in the starting part of this project was to clearly define what is the problem at hand. Based on the clarification, information gathering has taken place for further investigation and determining method to solve the problem. To work for a reliable car accident reconstruction the first thing required is an estimation of the change in the velocity (acceleration) that a vehicle experiences during a collision. In this case the data is obtained from previously carried out full-scale crash experiment.

The next step was to make a detailed signal analysis that helped in the decision making of how to approach the problem. The raw data was put into MATLAB software and necessary information was obtained to select Lumped mathematical modeling approach for modeling and simulation process. The methodology used to reach at the final step of Establishing Mathematical Model for the crash test can easily be seen in the Figure 2.8.

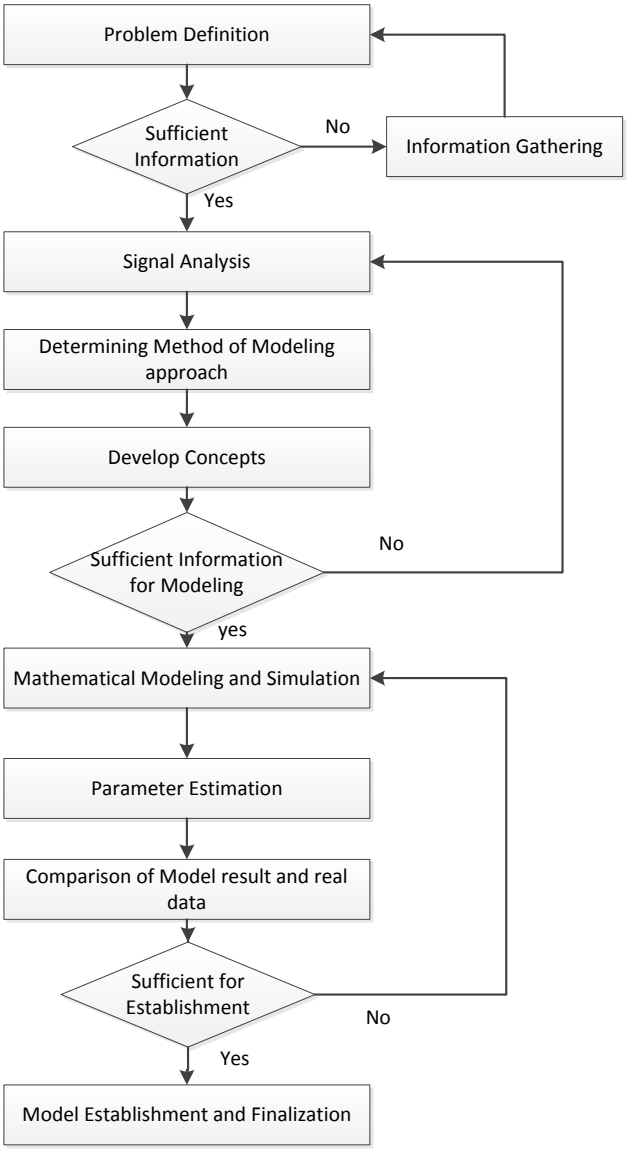

FIGURE 2.8: *Flowchart for the problem solution*

Chapter 3

The Experimental Setup for the Collected Data

3.1 Test Facility

The test was carried out at a test field Lista Airport in Farsund, Norway on 20, September 2004. The test facility was built considering safety issue for this experimental purposes of the vehicle crash scenario. The test was conducted by teamwork of researchers from Agder Research Foundation. The test site was arranged to have an acceleration field of 100 meter long that consists of two anchored parallel pipelines. The pipelines were arranged to give a distance of 5 meter clearance to the front wheel tires. The release mechanism was placed 2 meters in front of the end of the pipelines and a truck and tackle was used to accelerate the test vehicle. The distance between the end of the pipelines and the test item was made about 6.5 meters. The experimental setup can be seen in Figure 3.1.

Because of high cost expenses of a full scale crash testing a standard vehicle was used. The test vehicle was Ford Fiesta 1.1L,1987 model. The vehicle identification number was "WFOBXXGAFBHM40099". The front and left side of the test vehicle looks like Figure 3.2 before the impact.

A belted dummy without fully loaded instrumentation was seated at driver seat. The inertial test mass measured was 789kg.The total test mass was 873kg including the test dummy and measuring equipments. The center of gravity of the test vehicle was calculated and the result was recorded before the test. The lowest point of the vehicle was 0.12 meters above the ground level. The width of the vehicle was 1.58 meters, the length was 3.64 meters and the height was $1.39m$. The vehicle dimensions and the center of gravity position are shown in the Figure 3.3 and the Table 3.1. The vehicle was executed with a target impact speed of $35 \pm 3km/h$ and the measured vehicle's impact velocity was $35.4km/h$.

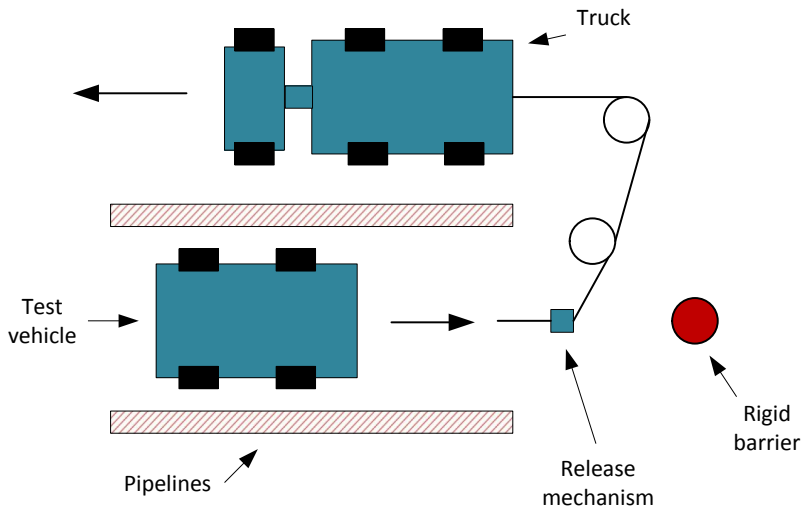

FIGURE 3.1: *Experimental Setup of the car crash [4].*

FIGURE 3.2: *Test vehicle before impact [4].*

Reference no.	Width [m]	Length [m]	Height [m]	Wheel track -front axel -rear axel	Wheel bas[m]	Frontal overhang[m]	Rear Over hang[m]
04-02	1.58	3.64	1.39	1.38 1.34	2.28	0.66	0.70

TABLE 3.1: *Vehicle dimensions [4].*

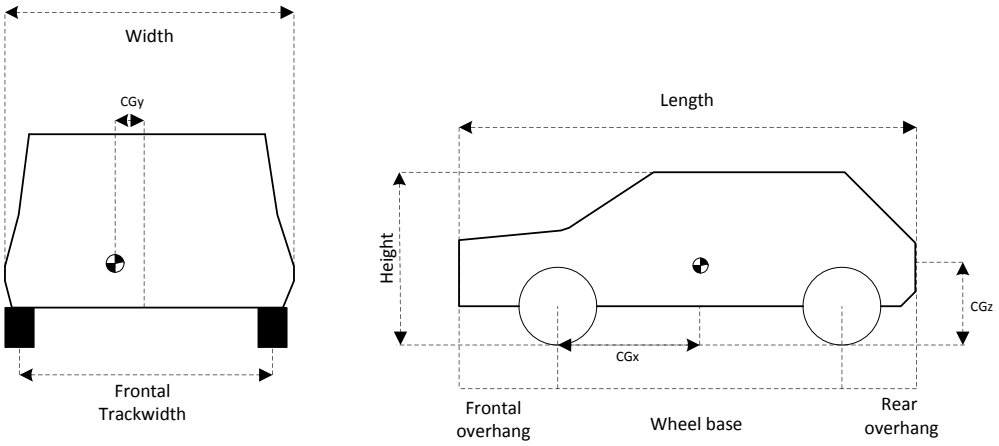

FIGURE 3.3: *Vehicle Dimensions. [4].*

Four load cells were used for weighing the test vehicle to determine the position of center of gravity in the horizontal position . Then the vehicle was tilted by lifting the front of the vehicle. The following parameters were recorded in both position[4].

- m_1:front left wheel load,
- m_2:front right wheel load,
- m_3:rear left wheel load,
- m_4:rear right wheel load,
- m_v:frontal left wheel load,
- θ: tilted angle,
- l: wheel base,
- d: distance across the median plane between the vertical slings from the lift brackets at the wheel and the load cells.

Longitudinal location: The horizontal distance between the center of gravity and the front axle centerline [4]:
$CG_x = \left[\frac{m_3+m_4}{m_v}\right] l$
Lateral location: The horizontal distance between the longitudinal median plane of the vehicle and

the center of gravity(positive to the left) [4]:

$$CG_y = \left[\frac{m_1+m_3-(m_2+m_4)}{m_v}\right]\frac{d}{2}$$

Location of the center of gravity above a plane through the wheel centers [4]:

$$CG_z = \left[\frac{(m_1+m_2)-m_f}{m_v tan\theta}\right] l$$

where:

m_f: front mass in tilted position

m_b: rear mass in tilted position

The measured values for the parameters in the above equations are shown in the Table 3.2.

Ref no.	m_1 [Kg]	m_2 [Kg]	m_3 [Kg]	m_4 [Kg]	m_v [Kg]	m_f [Kg]	m_b [Kg]	d[m]	l[m]	theta [degr]
04-02	257	237	154	150	798	444	354	1.73	2.28	28.4

TABLE 3.2: *Vehicle dimensions [4].*

The vehicle was targeted to stop after it hits the rigid steel obstruction. The Figure 3.4 shows the test vehicle during the impact. The dummy placed at driver's seat is also easy to identify in this picture. The test vehicle after the impact is shown in the Figure 3.5. The barrier was fixed from the back to an industrial shovel of a heavy loader machine.

It can be seen from the Figure 3.6 the obstruction was a rigid steel with 275mm outer diameter and it was welded to a heavy steel plate. The rigid cylinder was fixed in such away that it must not be displaced statically more than 10mm during the test when measured at contact surface. To fulfill this rigidity the cylindrical steel barrier is filled with concrete and welded to a heavy steel plate which is bolted by four bolts to the pavement. It was arranged to be hit by the test vehicle in the vehicles symmetry axis. The base plate was made to measure 740mmx410mmx25mm and the length of the pipe was 1290mm. The obstruction was arranged to give an impact angle of 0 degree.

FIGURE 3.4: *Test Vehicle during the impact [4].*

FIGURE 3.5: *Test Vehicle After impact [4].*

3.2 Instrumentation

A 3 dimesnional accelerometer was used to gather the accelerations for the test vehicles in three axes of directions at the center of gravity of the vehicle during the collision. There are different choices of accelerometers. The most common in use is the strain gauge measurements which provide an output voltage which is equivalent to the change of strain. Others use change in the capacitors or within crystals (piezoelectric) for an output voltage. The basics of piezoresistive accelerometer is shown in the Figure 3.7 [5].

FIGURE 3.6: *The test Barrier(Obstruction) [4].*

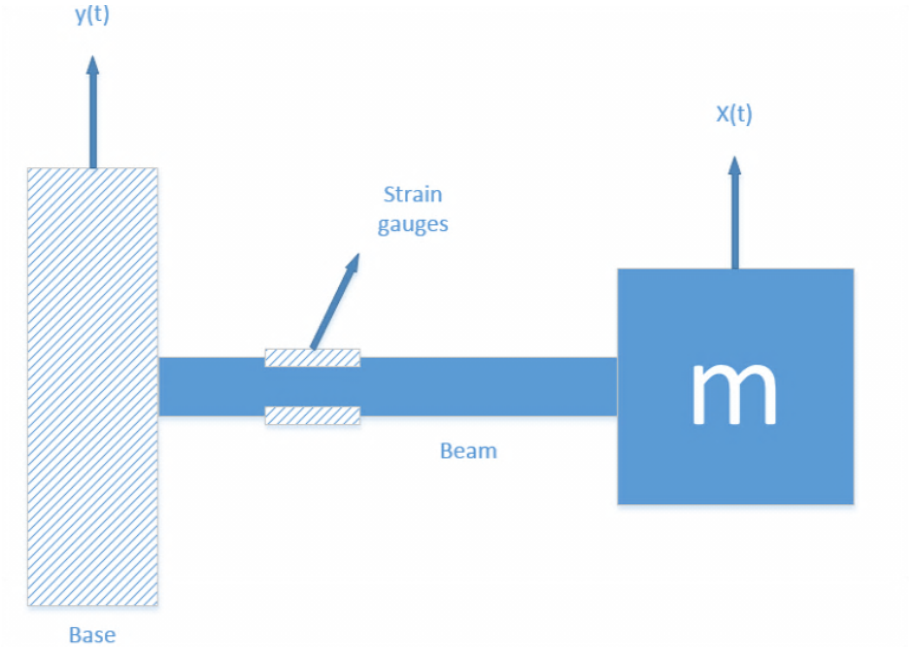

FIGURE 3.7: *Piezoresistive accelerometer [5].*

The other type of accelerometer used is piezoelectric crystal accelerometer which is shown in the Figure 3.8 [5]. There were two-triaxial piezoresistive accelerometers used in this experiment which were mounted on a steel bracket close to the vehicles center of gravity. The bracket was fastened by screws to the vehicle chaises. The accelerometer used in the damage and the bodies were visualized

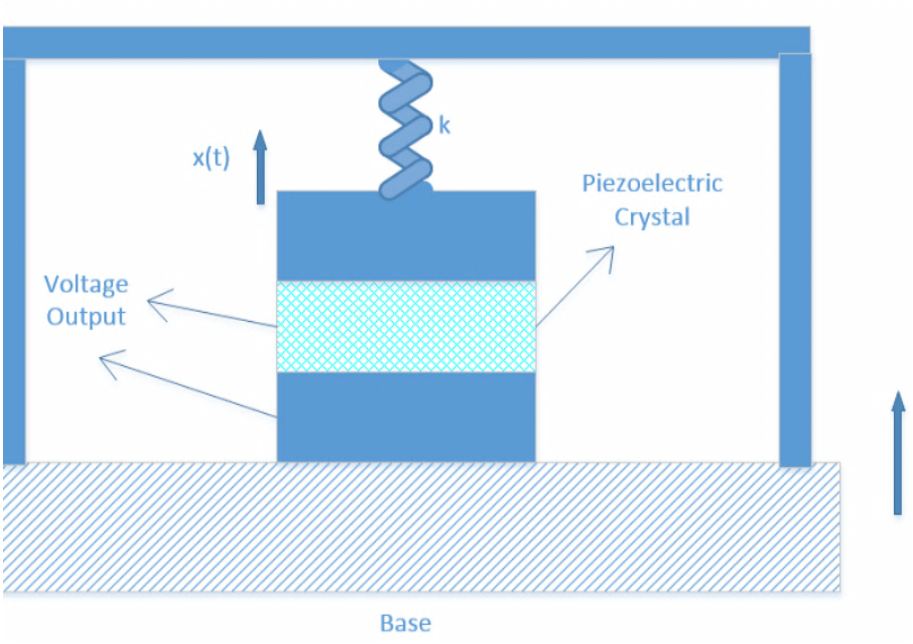

FIGURE 3.8: *Piezoelectric accelerometer [5].*

by using still pictures and high speed video films. These normal speed and high speed cameras were used to record the behavior of the obstruction and the test vehicle during the collision. To get a full overview of the impact, seven cameras were mounted around the scene to provide good visual images and documentations. This is also done for proving that the physical test was closely accurate to the assumptions and statements made by the project group. The layout Figure 3.9 shows the camera alignment with respect to the speed direction line. Kodak and Sony brand cameras were used. An inductor monitor was used to monitor the speed of the vehicle. The inductive sensor used was a type N4-S12-AP6X and it was directed towards a perforated disc mounted on a wheel. The wheel for this purpose was mounted on the right side of the test vehicle. The accelerometer was calibrated according to the procedures pointed out by the supplier [4].

3.3 Data Collection Technique

Data from the vehicle full scale frontal crash was collected from several mounted sensors attached within the car. The measuring instruments used were two 3-D accelerometers, a gyroscope and an inductive vehilce speed monitor. They were attached to important points within the car for the best possible readings. The speed of the vehicle before the impact and through the collision was measured using the inductive vehilce speed monitor. The vehicle accelerations in three axis directions was measured by accelerometers which were mounted on a steel bracket close to the vehicles center of gravity. The vehicles yaw rate was measured using the gyroscope that recorded 1

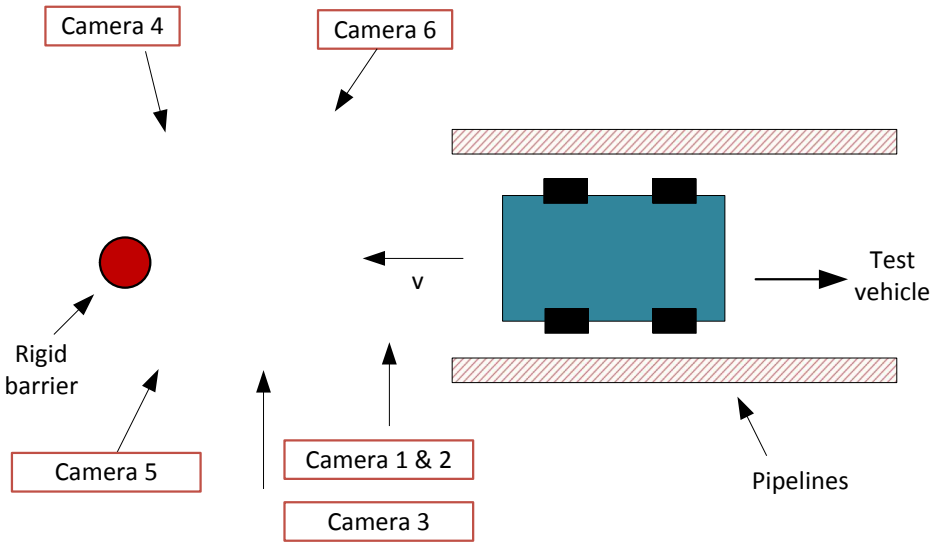

FIGURE 3.9: *The Alignment of Cameras [4]* .

deg/msec. High speed and normal speed cameras were used to record the behavior of the vehicle during the collision.

The front characteristic of the vehicle used for the full scale testing of road masts was made in accordance with the requirements set forth in the European standard NS-EN 12767:2000:"Passive safety of support structure for road equipment-Performance requirements and test methods" [4]. Other issues were the crash configuration. There can be many different configurations for the test to be performed according to different protocols and standards. This research was conducted for direct front impact or hitting hazardous obstacle with impact angle of 0 degree. The initial speed of the car at the impact was 35km/h.

A pipe which was bolted to the concrete runway has guided the steering test vehicle to hit the obstruction. The vehicle was made to steer freely 7m before it hits the obstruction. The measurements were taken for accelerations in three axes(X,Y and Z-axis) and yaw rate about Z-axis that could be used to calculate a velocity-time and displacement-time graphs for the test vehicle. The vehicle was supposed to stop when it hits the rigid steel obstruction. Safety issues were also considered if the car would start to change the initial angle and begin to shift. The car was accelerated by a truck at the other side connected through a release mechanism and wire connections [4].

Chapter 4

Signal Analysis

4.1 Data Set

The received data from the different sensors are described here. As discussed in the experimental setup section, the data collected includes important sensors' data set. The set as shown in Table 4.1 and Table 4.2 contains data from two accelerometers in three dimensions separately mounted close to the center of gravity of the vehicle. Another important data from the measurements was the rotational angle measurement taken for the car about the vertical direction to the ground. There was also an inductive speed monitor used to measure the speed of the vehicle.

The data gathered from the data acquisition system was unfiltered type. In the unfiltered or wide-band data there are unwanted frequencies and noise that can cause disturbances or discrepancies in the signal for analysis. As mentioned earlier, the sampling rate of the data acquisition was of 10kHz which means that one sample was gathered every $1/10000Hz = 0.00001s$. There were 33008 samples collected from each sensor. Each channel of the sensors could gather up to 6.5 s of data and it has sufficient memory for each channel. The yaw rate was measured with respect to the y-axis as the x-axis is the reference point of the frontal impact. The Table 4.1 shows brief description of the parameters gathered from the data acquisition system.

In analysis part of this project the acceleration data is used to be integrated and provide many important information such as, the velocity, the dynamic crush, the time of the maximum dynamic crush, the time of rebound and others.

The second data set provided was the filtered data shown in Table 4.2 using a third order low-pass Butterworth filter design. This data is generated from the raw unfiltered data by making use of CFC-60 and CFC-180 method according to the ISO-6487:1987 standard. The two channel classes use different cut off frequency that are 100 Hz for CFC-60 and 300 Hz for the CFC-180. The cut off frequency is a boundary condition for allowing low frequencies to pass through and attenuates the high ones. This is due to high disturbances and noise from a full scale vehicle crash which might cause bad signal processing. Th

Parameters	Explanation
X	From sensor 1, Acceleration in X direction
Y	From sensor 1, Acceleration in Y direction
Z	From sensor 1, Acceleration in Z direction
X1	From sensor 2, Acceleration in X direction
Y1	From sensor 2, Acceleration in Y direction
Z1	From sensor 2, Acceleration in Z direction
Angular velocity	Angular velocity in deg/s
Yaw rate	Degree of rotation from the gyro sensor

TABLE 4.1: *Data gathered from the mounted car sensors .*

Parameters	Explanation
Xcfc60	From sensor 1, Filtered acceleration in X direction
Ycfc60	From sensor 1, Filtered Acceleration in Y direction
Zcfc60	From sensor 1, Filtered Acceleration in Z direction
Xcfc180	From sensor 2, Filtered Acceleration in X direction
Ycfc180	From sensor 2, Filtered Acceleration in Y direction
Zcfc180	From sensor 2, Filtered Acceleration in Z direction
Angular velocity cfc60	Filtered Angular velocity in deg/s
Angular velocity cfc180	Filtered Angular velocity in deg/s

TABLE 4.2: *Filtered data set.*

4.2 Raw Data Analysis

4.2.1 Acceleration data from Accelerometer

The first part for analysis work is for the collected raw data from each accelerometers. This is unfiltered data for the crash scenario. The time range on the x-axis of the graph have been limited to 180ms after observing that this time range is sufficient to include the necessary points of discussion about the crash. The graph in Figure 4.1 shows the collected raw data of accelerometer from the first sensor in the X-axis direction. The deceleration is depicted for only the time range of 0s to 0.18s. Similarly, the graph in Figure 4.2 illustrate the collected raw data of accelerometer from the sensor in the Y-axis direction and the graph in Figure 4.3 shows the collected raw data from the sensor in the Z-axis direction.

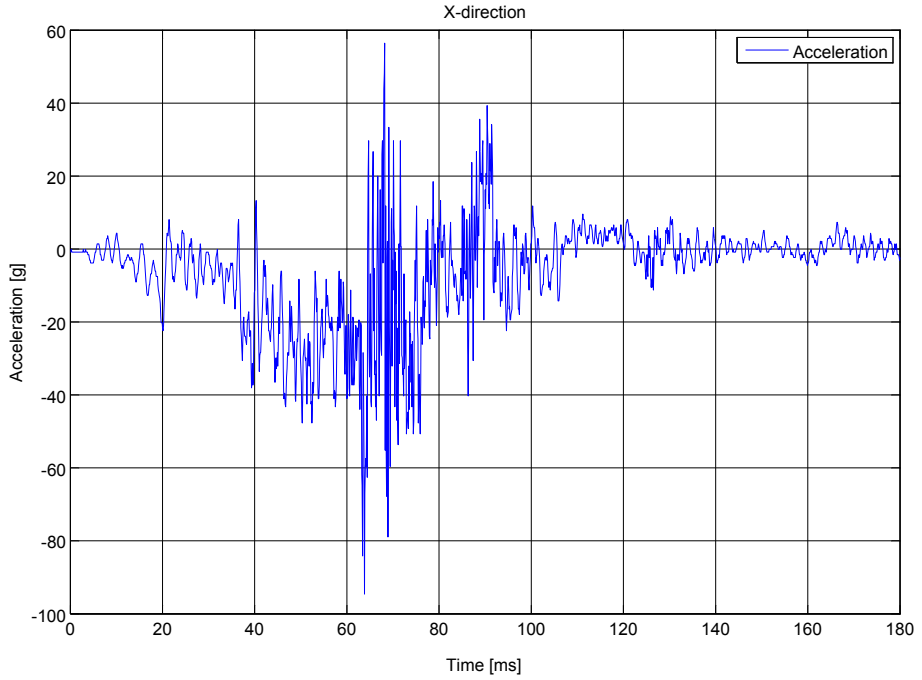

FIGURE 4.1: *Unfiltered acceleration in X-axis direction .*

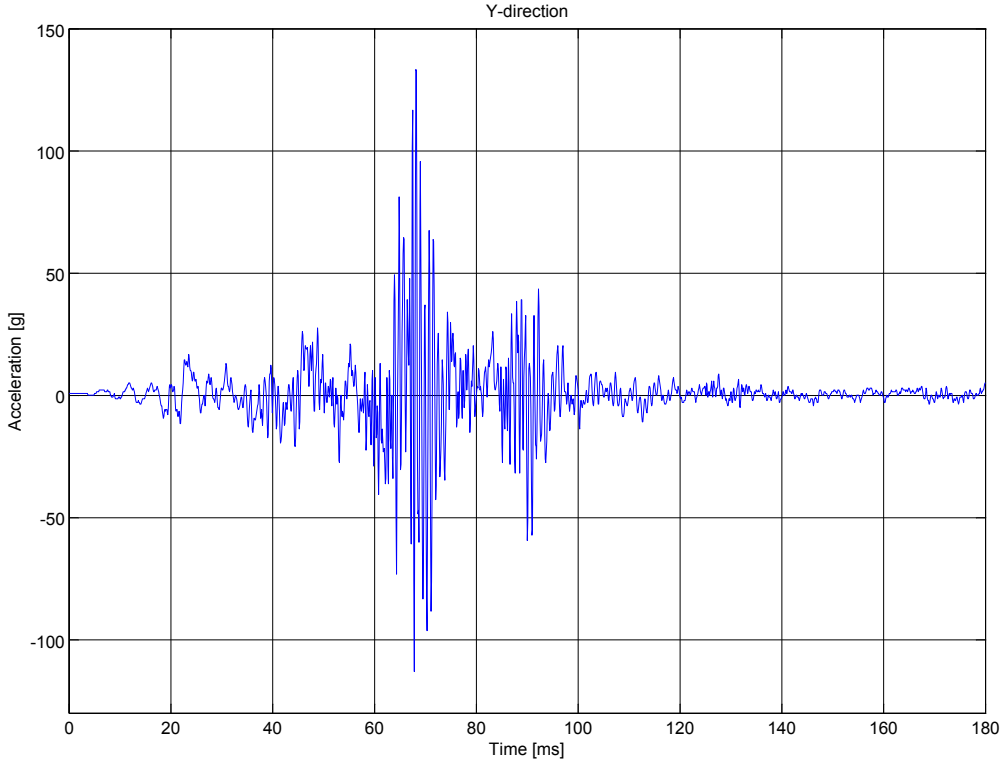

FIGURE 4.2: *Unfiltered acceleration in Y- axis direction .*

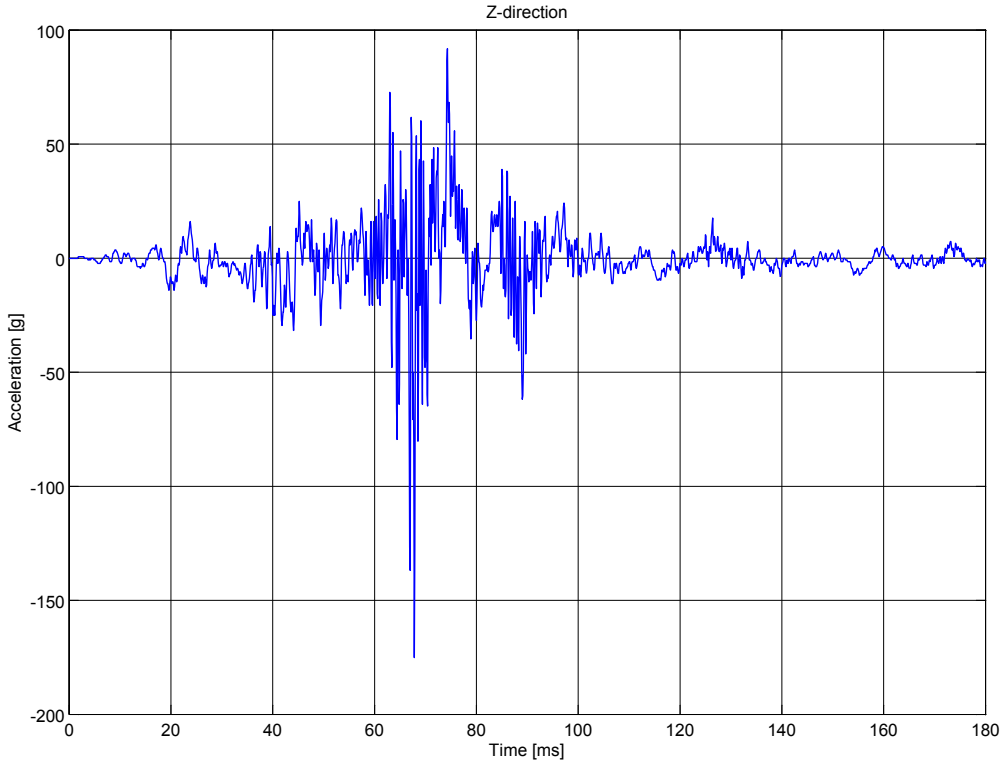

FIGURE 4.3: *Unfiltered acceleration in Z- axis direction* .

4.2.2 Yaw rate and yaw angle

A vehicle yaw rotation is the change of a vehicle movement around the Z-axis that changes the direction the vehicle is facing, to sideways of its direction of motion. A gyroscope was used to measure the yaw rate of the vehicle during the crash. A yaw rate or yaw velocity measured was the change of degree per second of the yaw rotation. The graph Figure 4.4 shows the measured yaw rate of the vehicle. The yaw angle is found by integrating the yaw rate with respect to the sampling time. The graph Figure 4.5 shows the yaw angle change of the vehicle for the time from 0ms to 180ms.

4.2.3 Velocity and dynamic crush from raw data

The raw data is difficult to analyze due to high frequencies, noises or some misalignment within the acquired data points. By using the curve fitting method one can achieve a more practical and feasible approximated crash pulse for further study. The Curve Fitting Toolbox in Matlab provides the mathematical function of fitting curves and surfaces to reference data. The solutions generated from the toolbox can be linear or nonlinear. The generated solution will follow the best possible path for the reference data. The Gaussian method with eight terms is observed to be the best method for creating a fitted curve in this case. The curve Fitting was used to approximate the

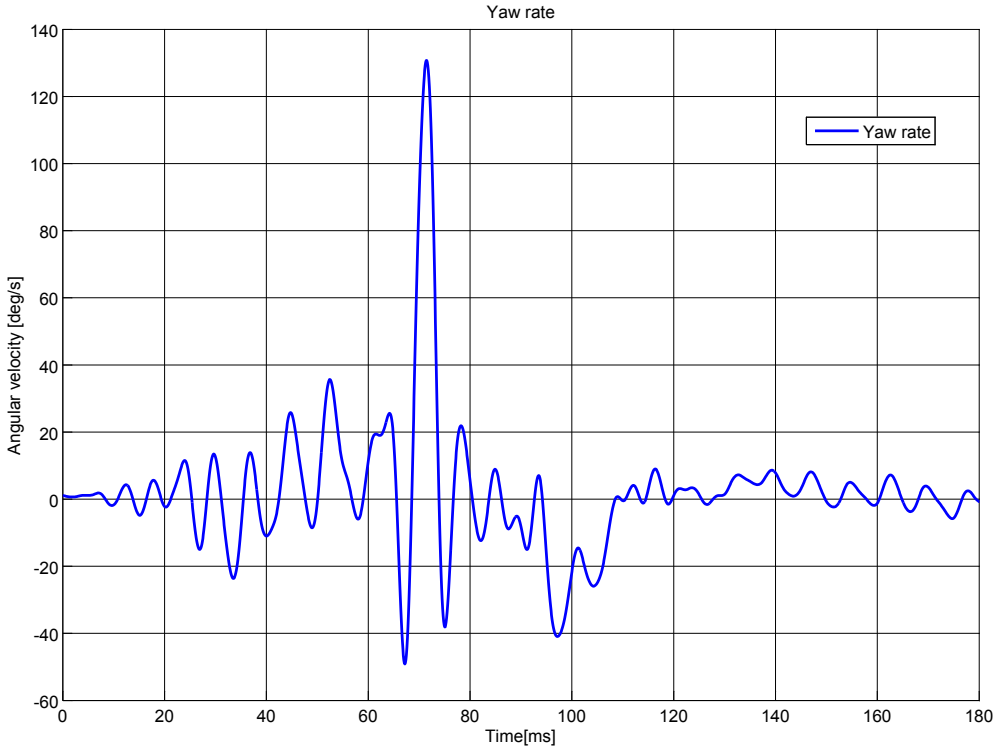

FIGURE 4.4: *Yaw rate of the vehicle.*

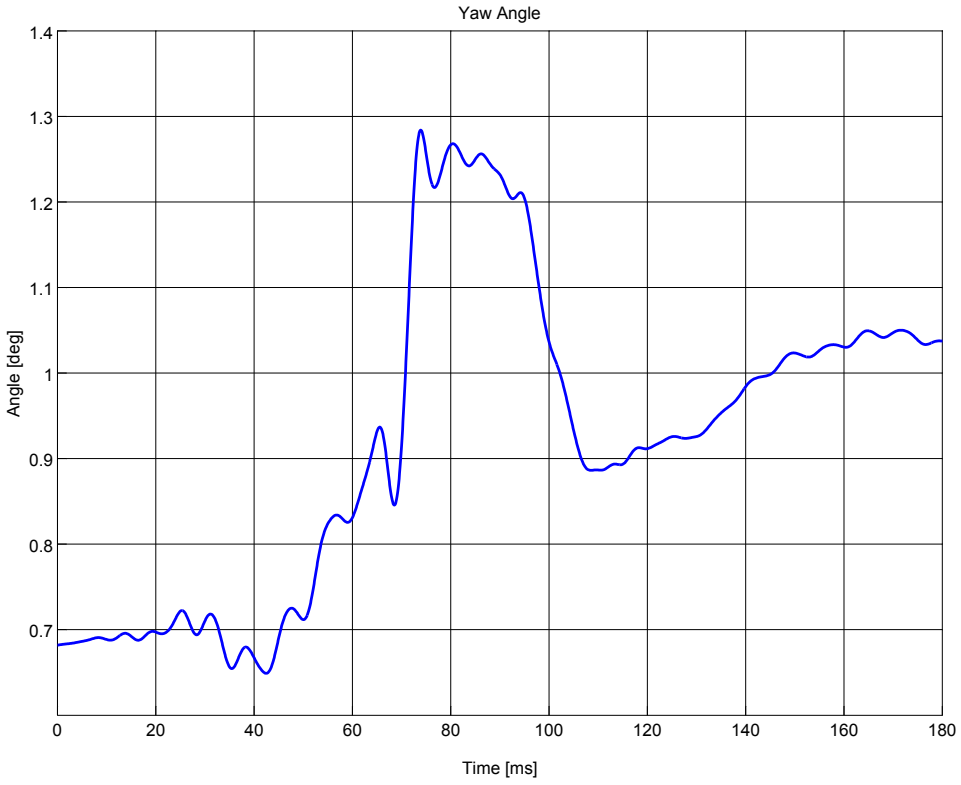

FIGURE 4.5: *Yaw angle of the vehicle.*

crash pulse and the car kinematics that include the velocity and dynamic crush. The velocity and the displacement of the vehicle impact is obtained by integrating the approximated crash pulse.

One of the facts to be considered here is that the experimental setup was for a front impact and the most relevant graph was the one in X direction, however the accelerometers recorded some crash pulse in Y and Z directions that needs to be taken into account. The acceleration data was input into the Curve Fitting Toolbox and Gaussian approximation was used as it is shown in Figure 4.6 and polynomial function curve fitting is used for comparison which is shown in Figure 4.7. These graphs show the accelerations, velocities and dynamic crushes of the vehicle during the impact in the X-axis direction(all the graphs are of high resolution, for a better view, zoom to see the specified area of target). It can be seen in both figures that the initial velocity is not equal to 35km/h as stated in the experiment description. The speed shows to be about 3km/h higher. This discrepancy is a result of using raw data - without filtering. On the same graphs the maximum dynamic crush and the time of occurrence are also shown. At time zero the front panel of the car was in contact with the rigid obstacle at 35 km/h. The velocity of the car decrease rapidly and the displacement viewed from the X-axis increased. The maximum dynamic crush happens at the point where the decreasing velocity of the vehicle reaches zero value from the initial velocity. The vehicle is shown to have maximum dynamic crush of 59.11 cm. The maximum dynamic crush occurred at time of 86.11 ms. After the maximum crush occurrence the car started to slowly rebound.

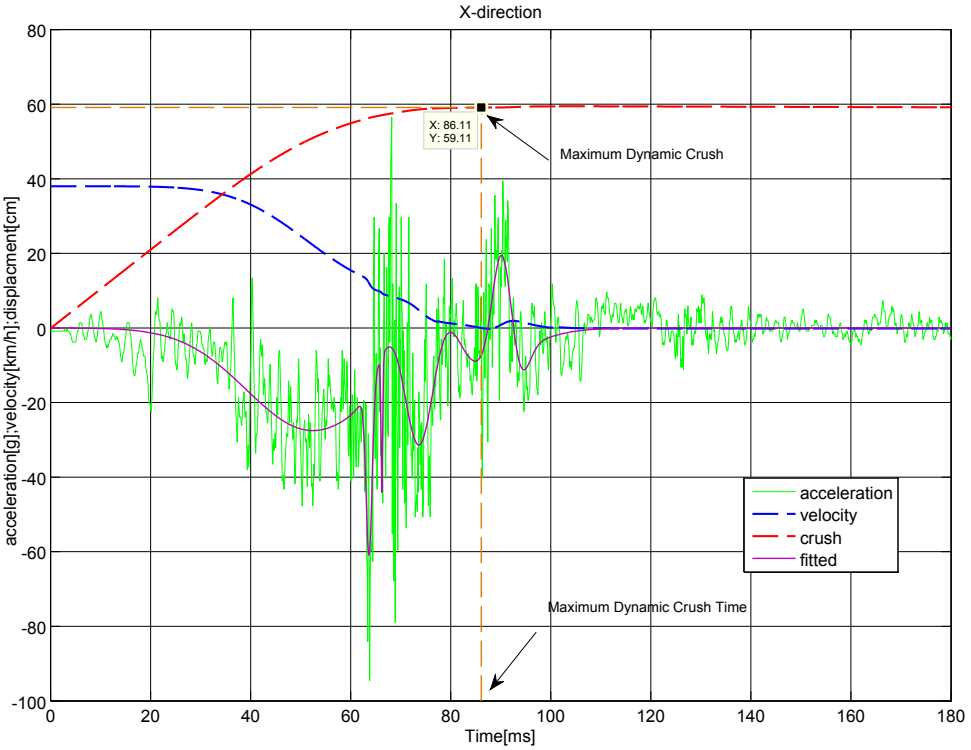

FIGURE 4.6: *Gaussian curve fitted acceleration, velocity and displacement in X- axis direction .*

To approximate the crash pulse in the Y-axis direction similar procedure of curve fitting in the X-axis direction is used. Then the approximated crash pulse is integrated to obtain the graph for

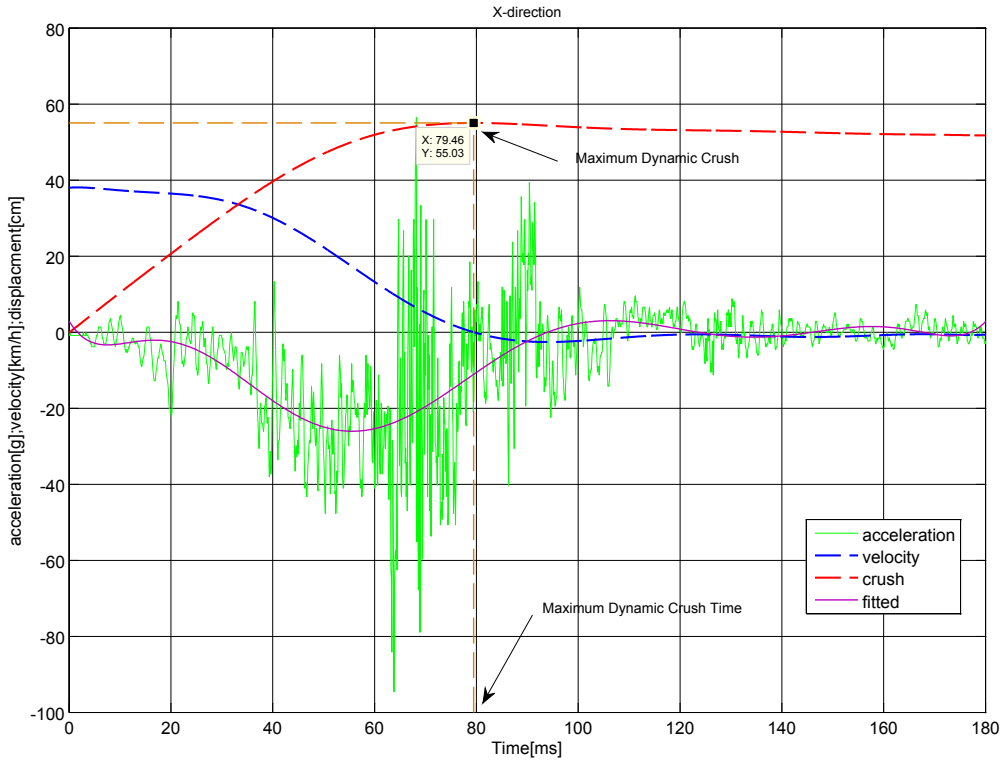

FIGURE 4.7: *Polynomial function curve fitted acceleration, velocity and displacement in X- axis direction .*

the velocity and by further integration the dynamic crush is obtained as shown in the Figure 4.8. The value of the dynamic crush on this graph is made in millimeter for a better display.

The crash pulse in the Z-axis direction as shown in the Figure 4.9 is obtained by utilizing the curve fitting procedure similar to the previous work. After the curve fitting the crash pulse was integrated to obtain the velocity and dynamic crush as shown on the plot. The value of the dynamic crash on this graph is also made in millimeter for a better display.

4.2.4 Fast Fourier Transform of the acceleration signal of raw data

Signal analysis can be carried out in time-domain or frequency-domain of data. The fast Fourier transform is a mathematical method for transforming a function of time into a function of frequency. Sometimes it is described as transforming from the time domain to the frequency domain. Frequency information is a powerful way of characterizing a signal. Using the fast Fourier transform it is possible to see if the frequency is periodic and what frequency is dominant. The Frequency analysis of crash pulses in linear scale looks like as in the Figure 4.10 for the X-axis direction. The same graph from Figure 4.10 for frequency analysis is shown in the Figure 4.11 with more clarity changing the frequency range from 0 to 1000Hz. It can clearly be spotted from both Figure 4.10 and Figure 4.11 that the lower frequencies have higher amplitudes.

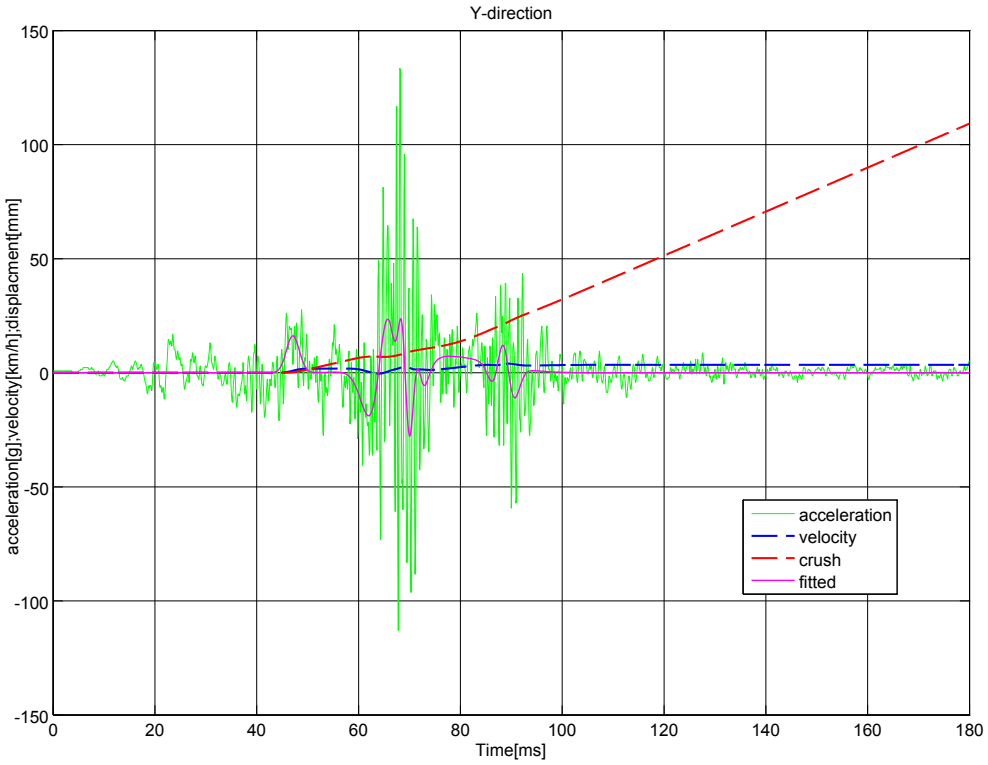

FIGURE 4.8: *Fitted model acceleration, velocity and displacement in Y- axis direction .*

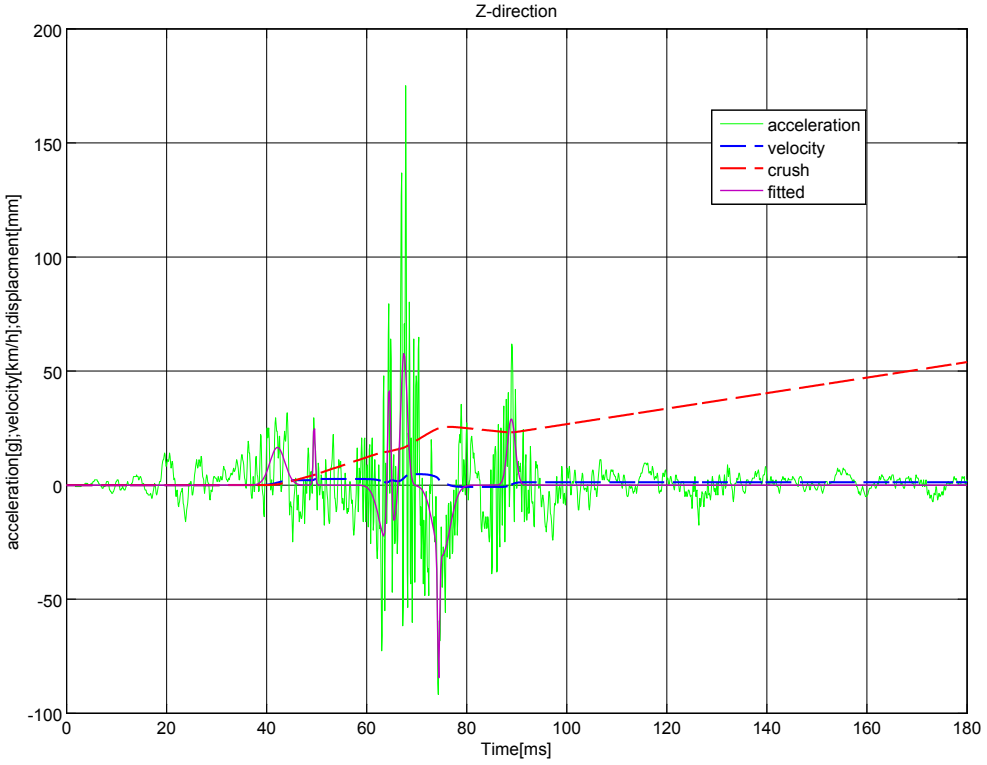

FIGURE 4.9: *Fitted model acceleration, velocity and displacement in Z- axis direction .*

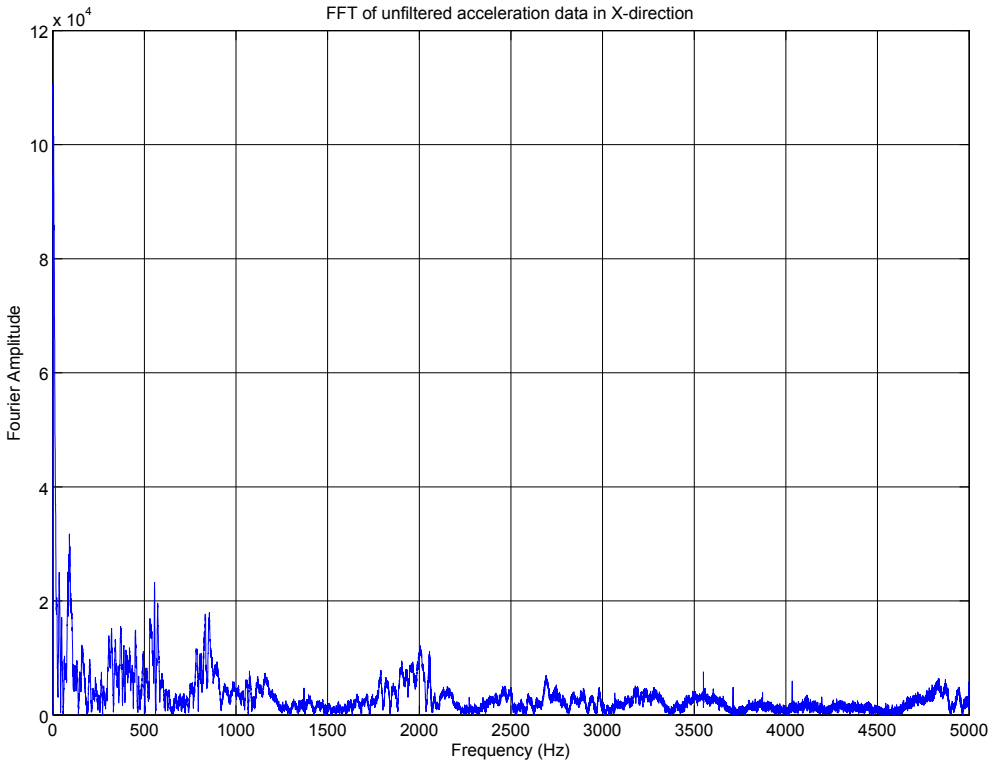

FIGURE 4.10: *The whole spectrum frequency analysis of X-axis crash pulses in linear scale .*

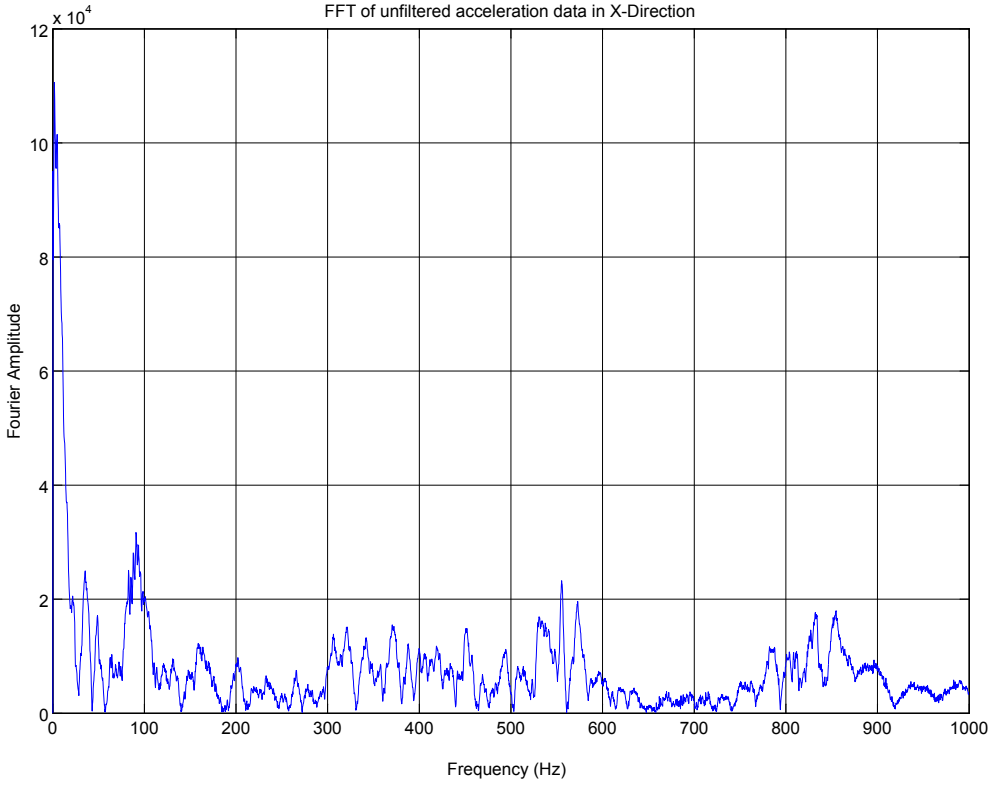

FIGURE 4.11: *A cut-off frequency analysis of X-axis crash pulses in linear scale .*

The next two figures shows the frequency domain analysis of the crash pulse in the Y-axis or lateral direction of the vehicle crash. The whole spectrum frequency analysis of crash pulses in linear scale for the Y-axis direction is shown in Figure 4.12 and the a part of frequency analysis of crash pulse is shown in the Figure 4.13.

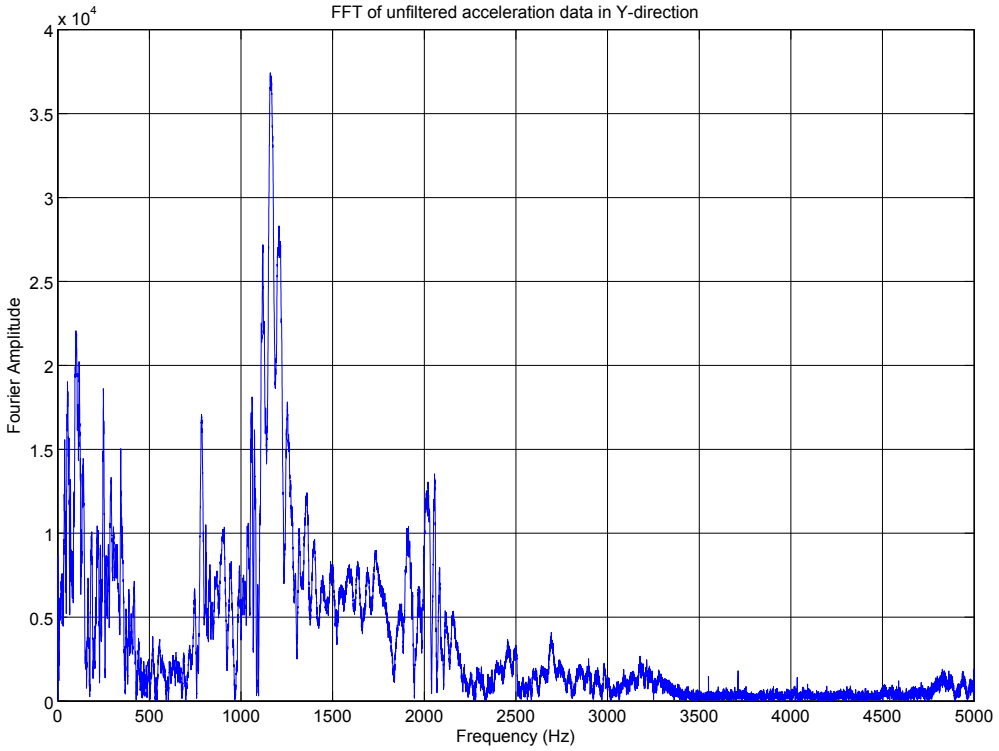

FIGURE 4.12: *The whole spectrum frequency analysis of Y-axis crash pulses in linear scale.*

The frequency domain analysis for the Z-axis or the vertical axis to the crash plane is also shown next. The FFT graph in Figure 4.14 shows the whole spectrum frequency analysis of Z-axis crash pulses in linear scale and the graph in Figure 4.15 shows a part of frequency analysis of Z-axis crash pulses in linear scale.

4.3 Signal Filtering

The raw data sometimes referred to as wideband data is the signal that can be obtained from the impact stress recorded by an accelerometer. Digital filtering technique should be used to obtain the signal in its useful frequency range. A filtering process is used to remove or suppress unwanted feature of the sample data. The filtering technique selection should be made in such a way as to satisfy the frequency response corridor specified by SAE J211 (Society of Automotive Engineers Recommended Practice on the "Instrumentation for Impact Tests") or ISO 6487 (the International Organization for Standardization).

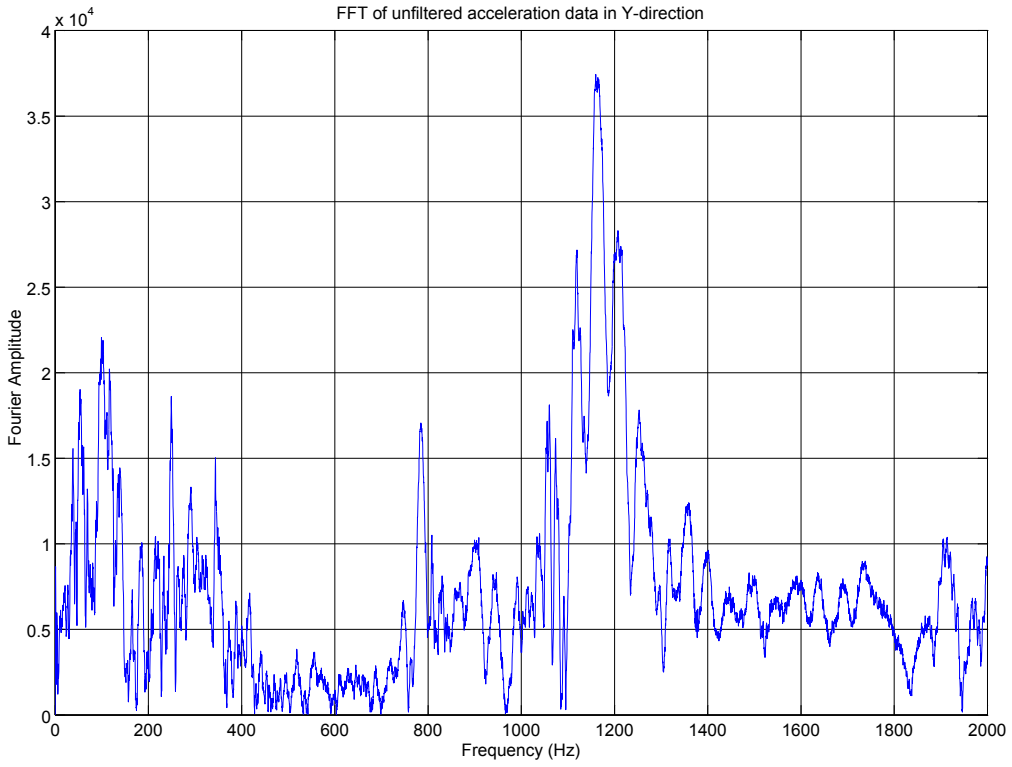

FIGURE 4.13: *A cut-off frequency analysis of crash pulses in linear scale.*

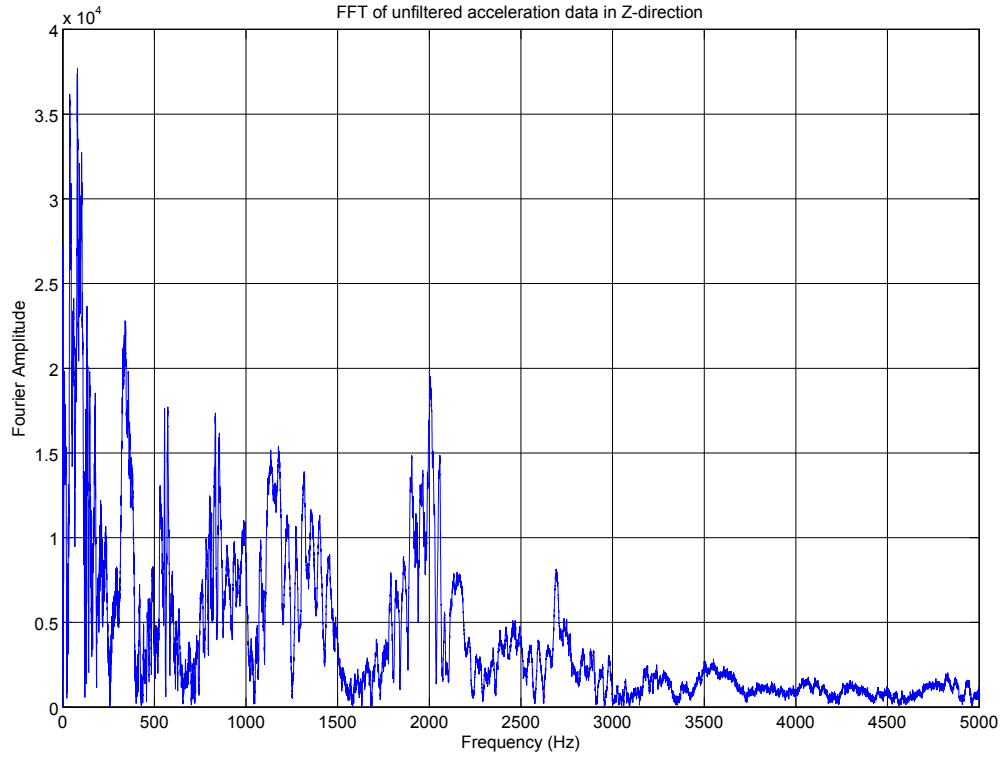

FIGURE 4.14: *The whole spectrum frequency analysis of Z-axis crash pulses in linear scale.*

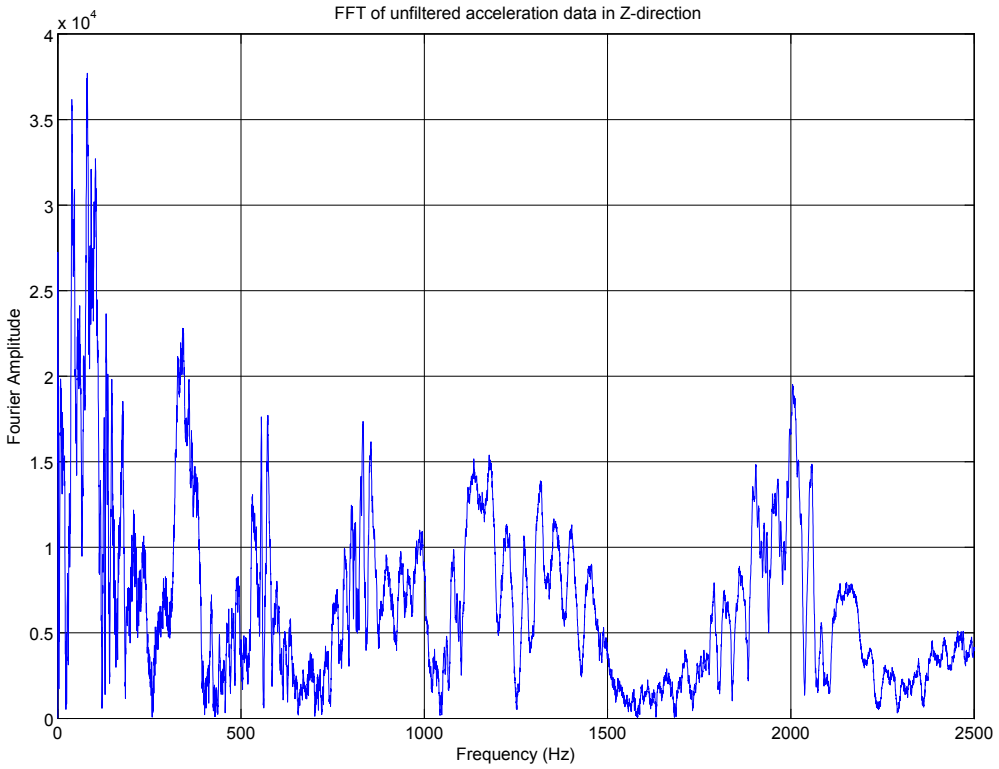

FIGURE 4.15: *A cut-off frequency analysis of Z-axis crash pulses in linear scale.*

The target of these organizations is providing guidelines for filtering specifications and the selection of a class of frequency response. The ISO 6487 protocol is used for filtering the raw data in this project. This technique was issued on May 1, 2000 as the third edition with a title Road Vehicles Measurement Techniques in Impact Tests Instrumentation [34]. The standard is basically the same as SAE J211, which was issued in March 1995.

According to ISO-6487:2002(E), which is attached in Appendix B, the frequency response of a data channel should lie within the limits for curves of CFCs 1000 and 600 that is specified as shown in the Figure 4.16. A number is indicating the frequency channel for designation of frequency class. The value of frequency F_H (in hertz) and the number are numerically equal. The table shown in Table 4.3 explains what the parameters in the Figure 4.16 indicates for the frequency response corridor given.

In the ISO-6487 standard indicated above frequency response values are specified for the passband, transition band, and stop band for four specific channel classes. Both SAE J211 and ISO 6487 use the same specfication for the channel classes CFC-60 and CFC-180 [5]. The channel class selected for a particular application is shown in Appendix C.

The filtering effect of three of these four channel classes with the wideband or unfiltered data are shown in the Figure 4.17. It can easily be observed in the figure that the bigger the designation number used for filtering the more similar the filtered data becomes to the unfiltered data.

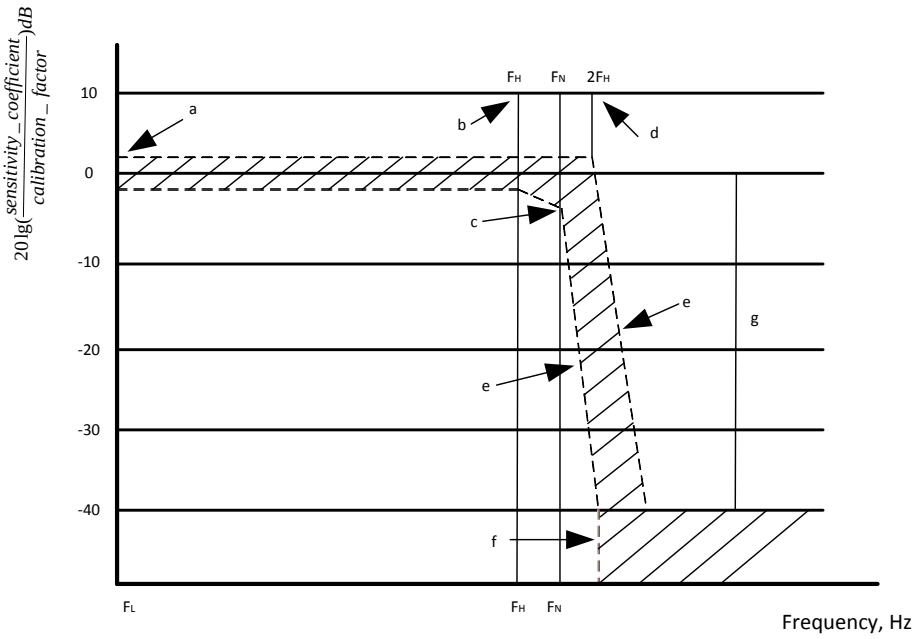

FIGURE 4.16: *Frequency Response Corridor Appendix B.*

Logarithmic scale	
a	±0,5 dB
b	±0,5 dB – 1 dB
c	±0,5 dB – 4 dB
d	±0,5 dB
e	-24 dB/octave
f	- ∞
g	- 40 dB

CFC	F_L *Hz*	F_H *Hz*	F_N *Hz*	*g*
1000	≤ 0,1	1000	1650	-40 dB
600	≤ 0,1	600	1000	-40 dB
180	≤ 0,1	180	300	- 30 dB
60	≤ 0,1	60	100	-30 dB

TABLE 4.3: *Parameter values in the Figure 4.16 .*

There are two types of digital filters used in processing vehicle crash test data. The two digital filters methods are commonly known as Chebyshev and Butterworth filters. The frequency response characteristics of Butterworth filters fall within the specified frequency response corridors specified in the ISO standard that make the filter type worth using. The amplitude response characteristic of Butterworth low-pass filters are designed to be as flat as possible at low frequency and decreases with increasing frequency [5].

The filter used for this project is Butterworth order lowpass digital filter with cut - off frequency $F_N = 300Hz$. It is called a channel class CFC-180 that is selected for the analysis of the crush pulse for finding the velocity and displacement from the integration of the acceleration data. The

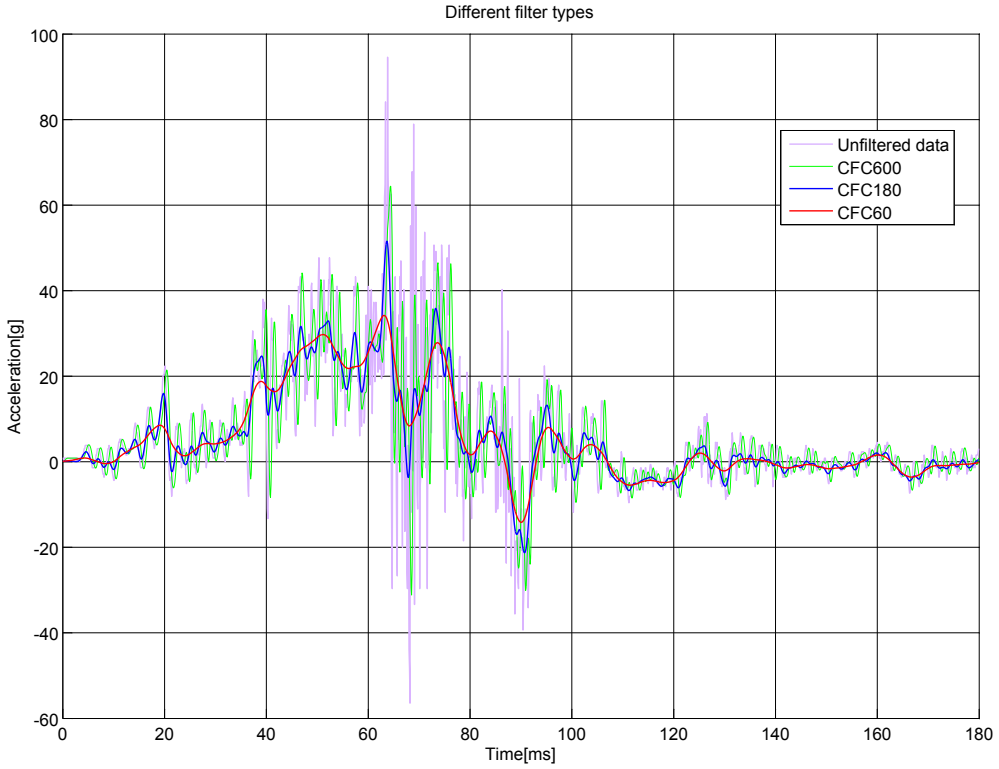

FIGURE 4.17: *The effect of three filtering channel frequency classes with unfiltered data .*

filter is described by its frequency response characteristic from the standard. The use of this filter is to get rid of the high frequency components of the crash pulse. The comparison between the deceleration from the filtered data with CFC-180 method and the wideband data in the X-axis direction is shown in the Figure 4.18.

The CFC-60 is used for filtering crash pulse to be used in the collision simulation input for vehicle structural acceleration. The comparison between the deceleration from the filtered data with CFC 60 method and the wideband data in the X-axis direction is shown in the Figure 4.19. Similarly, the comparison between the deceleration from the filtered data with CFC180 method and the wideband data in the Y-axis direction is shown in the Figure 4.20. The comparison between the deceleration from the filtered data with CFC60 method and the wideband data in the Y-axis direction is shown in Figure 4.21. The comparison between the deceleration from the filtered data with CFC180 method and the wideband data in the Z-axis direction is shown in the Figure 4.22.

Lastly, the comparison between the deceleration from the filtered data with CFC60 method and the wideband data in the Z-axis direction is shown in the Figure 4.23.

4.3.1 Time-domain analysis

The difference between the filtered data versus the unfiltered data using CFC-180 and CFC-60 for frontal impact cases(refering to the ISO-6487 standard) are shown in the graphs above. The

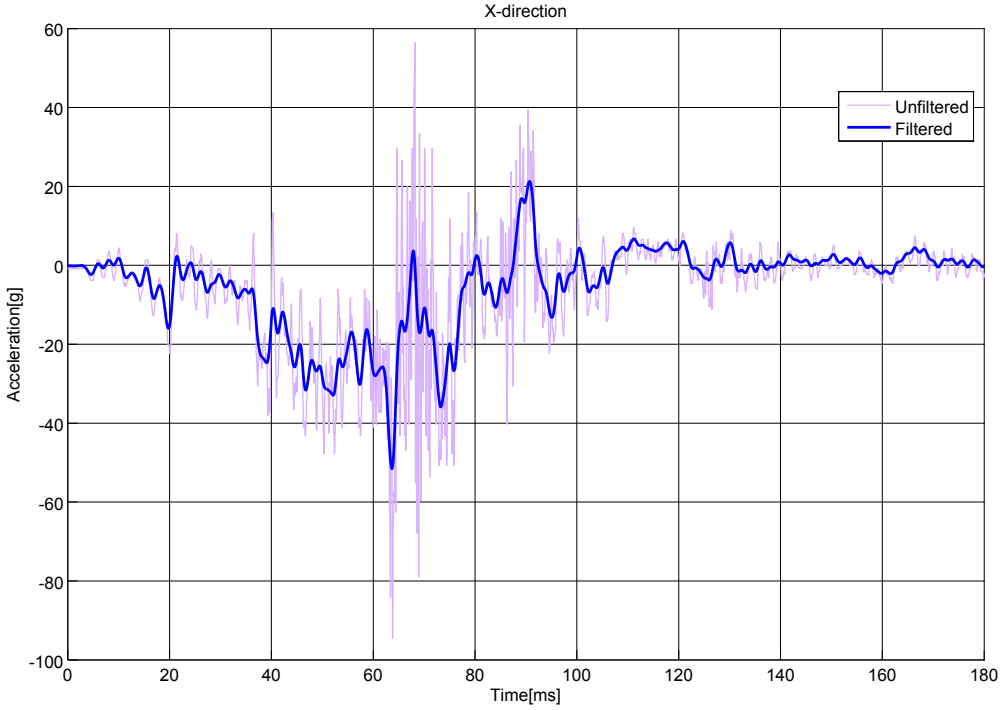

FIGURE 4.18: *The crash pulse from the impact measurement for CFC 180 filtered vs unfiltered data in X-axis direction .*

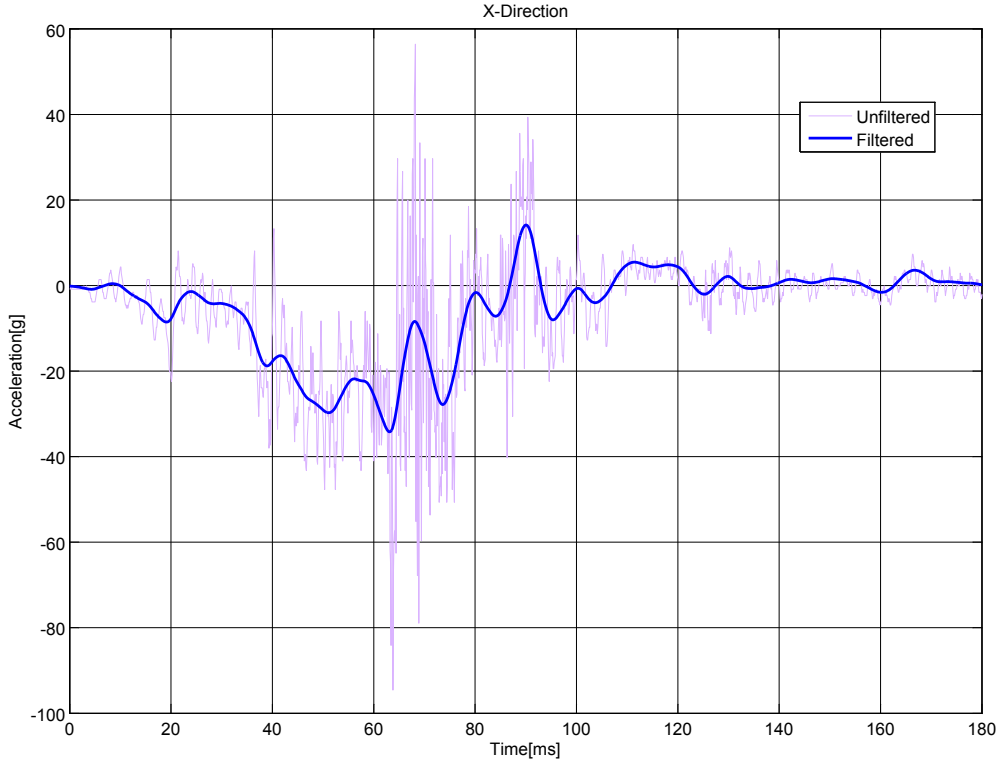

FIGURE 4.19: *The crash pulse from the impact measurement for CFC 60 filtered vs unfiltered data in X-axis direction .*

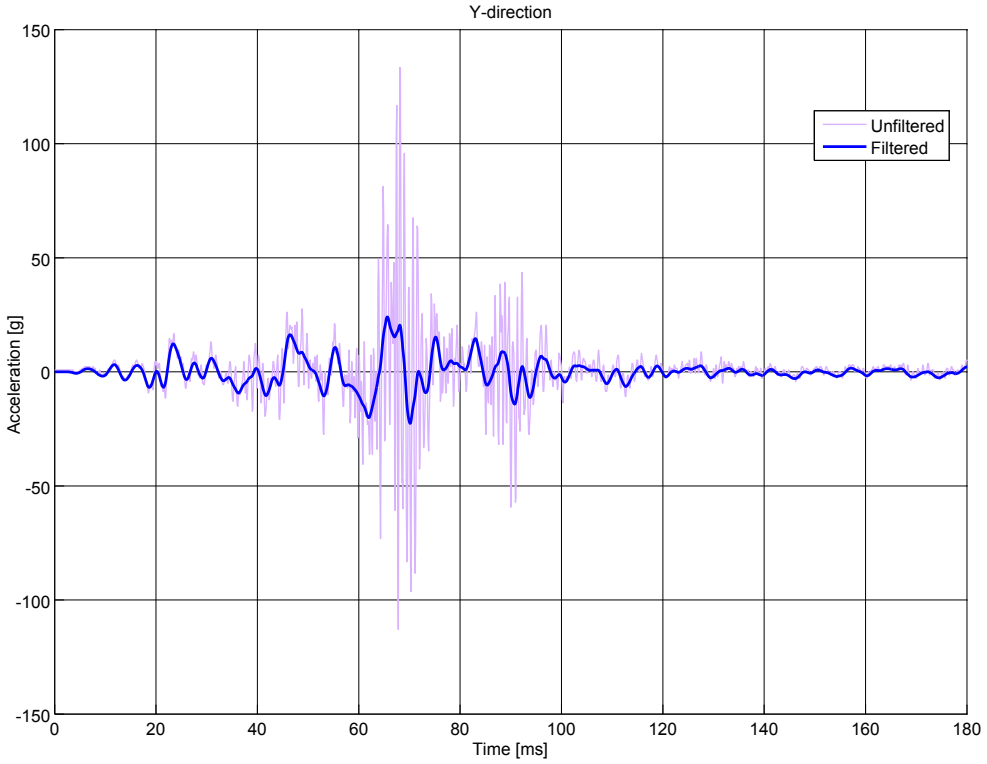

FIGURE 4.20: *The crash pulse from the impact measurement for filtered with CFC180 vs unfiltered data in Y-axis direction .*

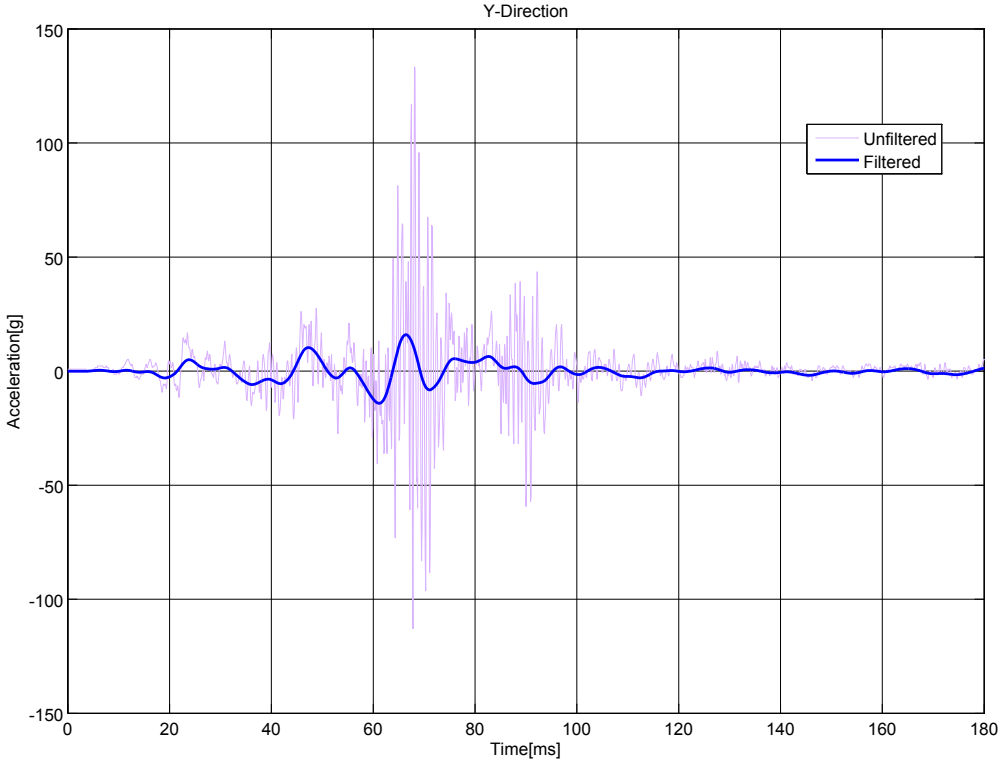

FIGURE 4.21: *The crash pulse from the impact measurement for filtered with CFC60 vs unfiltered data in Y-axis direction .*

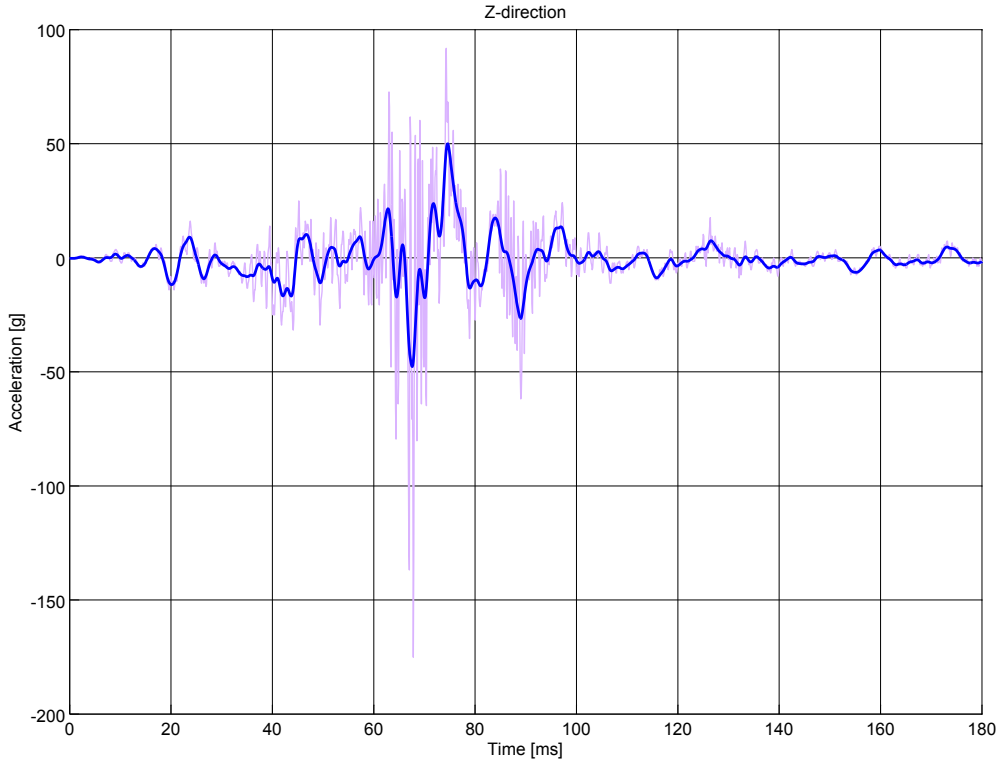

FIGURE 4.22: *The crash pulse from the impact measurement for filtered with CFC180 vs unfiltered data in Z-axis direction .*

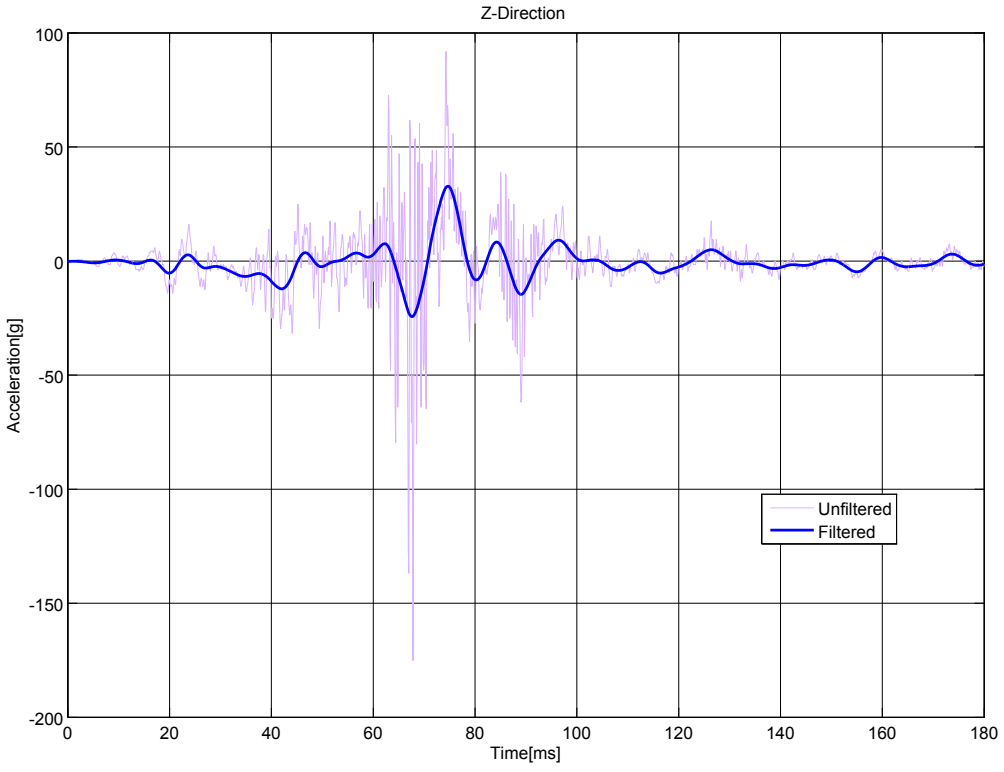

FIGURE 4.23: *The crash pulse from the impact measurement for filtered with CFC60 vs unfiltered data in Z-axis direction .*

filtering process is carried out by using Matlab software. The software does have a built-in method to calculate the filtered frequency using a Butterworth code.

Even though the whole time for the vehicle impact was recorded for more than 3seconds the dynamic crush can be clearly analyzed for the time range between 0 ms to 180 ms that has been used in this part of analysis. By making comparison between the filtered and unfiltered data it is easy to observe the filtered data is better in representing the real case scenario than the raw data. The initial velocity for the filtered graph is 35km/h compared to the fitted which was seen to be approximately 38km/h which is shown in Figure 4.6. The filtered data shows a smaller value of maximum dynamic crush of 50,17cm and a maximum dynamic crush time of 74,6ms which is shown in the Figure 4.24. The rebound can also be clearly spotted after the dynamic crush and continues to rebound to a certain limit where the deceleration becomes zero.

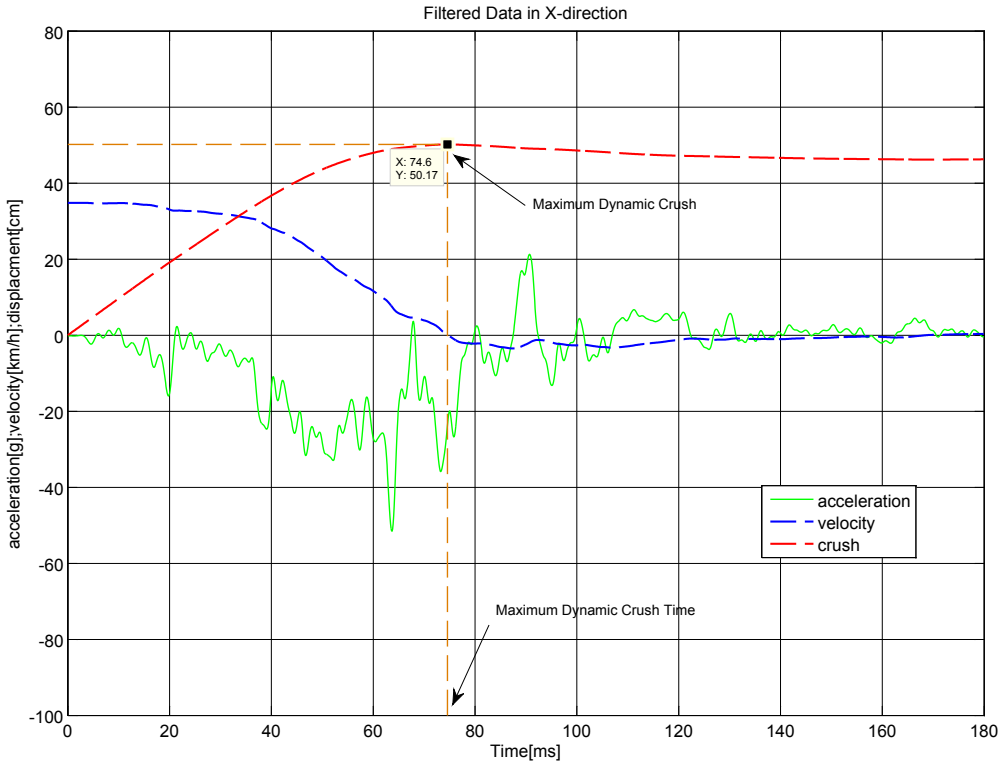

FIGURE 4.24: *Filtered data acceleration,velocity and displacement in X- axis direction.*

As described previous in the unfiltered fitted curves the Y and Z axis are not very crucial part of the information as the X-axis, since the experiment is a frontal impact. However, the sensors gave some readings and the filtered results are shown below. The acceleration-velocity-displacement graph for the Y-axis is shown in the Figure 4.25. For the Y and Z axis there is some unexpected attributes for the vehicle crash, as seen from the graphs. The velocity never reaches the value zero so the displacement look to increase over time.

There are some assumption made here to make the analysis simpler. For example, the velocity at the impact is assumed to be zero for both Y and Z axis since the frontal collision velocity is in

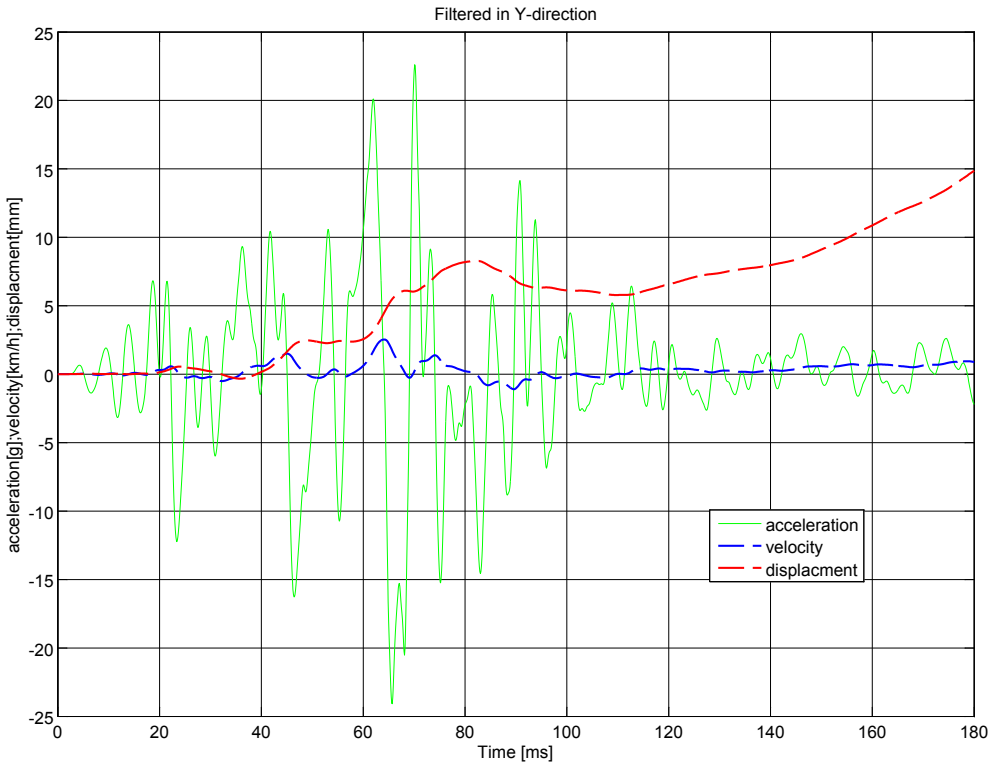

FIGURE 4.25: *Filtered data acceleration,velocity and displacement in Y- axis direction.*

X direction. The Y and Z axis could have had some initial velocity in practical sense but when creating the mathematical model this theory was left out due to the assumption of all velocity was generated in the X-direction. Another assumption is that the measurement picked up by the sensors for the Y-axis and Z-axis are due to the impact effect from the X-axis direction. This are important concept that could be utilized in the mathematical modeling representation of the vehicle-crash. The acceleration-velocity-displacement graph for the Y-axis is shown in the Figure 4.26. The measurement for the displacements in the Y and Z-axis are made to be in millimeter for a good display on the graphs.

4.3.2 Frequency-domain analysis

In the discussion above it is clearly described that the raw data obtained from the sensors reading should be prepared for signal analysis by using different types of digital filters. The filtering process will help to obtain a useful frequency range. It is stated above the digital filter CFC-180 type is used for the filtering of data in the integration for the displacement or velocity in the signal analysis of vehicle structural acceleration. The result after filtering process are shown in Figure 4.24 for the X-axis direction. Similar output is shown in Figure 4.25 for the Y-axis, and Figure 4.26 for the Z-axis.

The CFC-180 filter is a Butterworth third order lowpass digital filter with cutoff frequency $F_N = 300Hz$ and this is clearly seen from the graph of FFT below. The frequency beyond 300 Hz has no

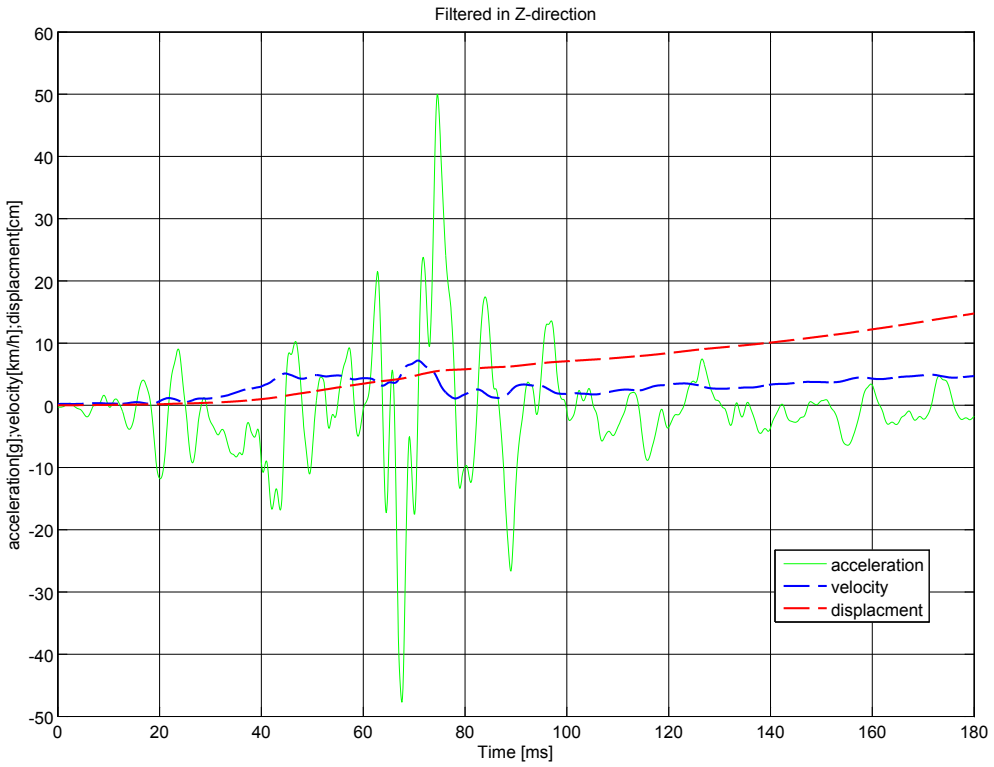

FIGURE 4.26: *Filtered data acceleration,velocity and displacement in Z- axis direction.*

amplitude values after applying the CFC-180 filter as shown in Figure 4.27 for the X-axis direction signal. The full frequency spectrum can be observed in the unfiltered FFT analysis section in the Figure 4.10. The higher amplitude for the crash signal is observed in both graphs at lower frequency which is the dominant frequency part that need to be considered in the simulation analysis.

Another digital filter type used in the signal analysis is CFC-60 that uses cutoff frequency $F_N = 100Hz$. The CFC-60 is used in the collision simulation input for vehicle structural acceleration. The filtered data FFT graph is shown in the Figure 4.28. It is clearly observed in this graph also that the frequency beyond 100Hz has no high amplitude.

The FFT graph is shown for Y-axis signal in the Figure 4.29 . The CFC-180 digital filter is also used for this case. The graph indicates larger amplitude values for lower frequency values than the previous signal(X-axis). Similar attribute can be observed here that the value of frequency above 300Hz has no high value.

Lastly, the Z-axis FFT graph for the signal in the Z-axis direction is shown Figure 4.30 after applying CFC-180 digital filter. Similar characteristics with previous discussion can also be observed for this data.

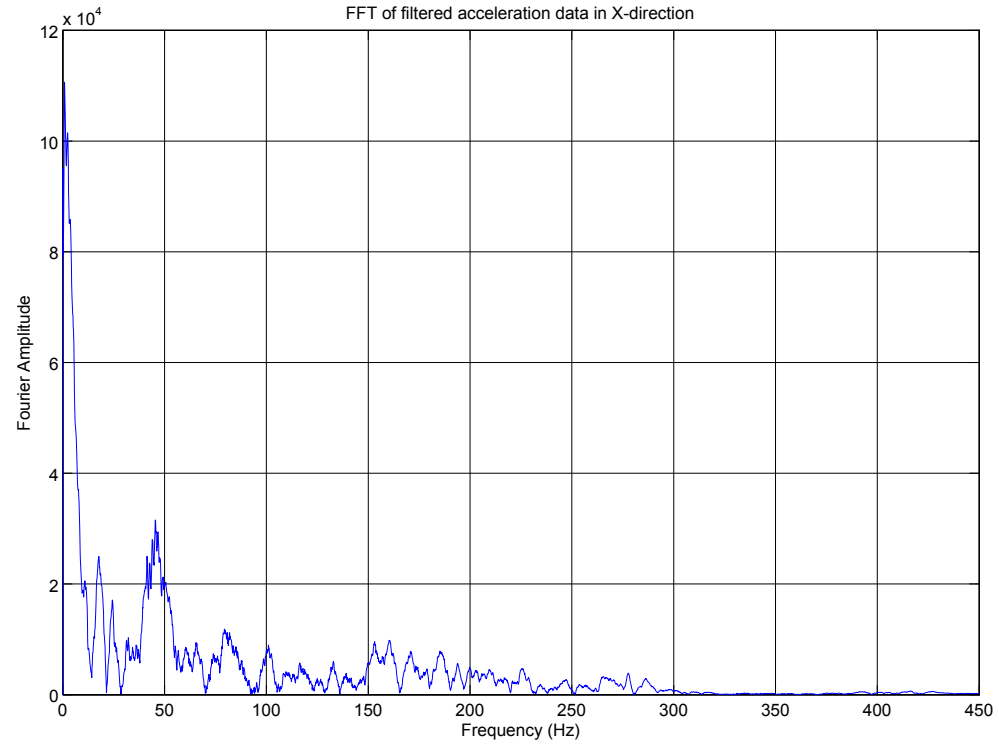

FIGURE 4.27: *Filtered data frequency analysis with CFC-180 of X-axis crash pulses in linear scale.*

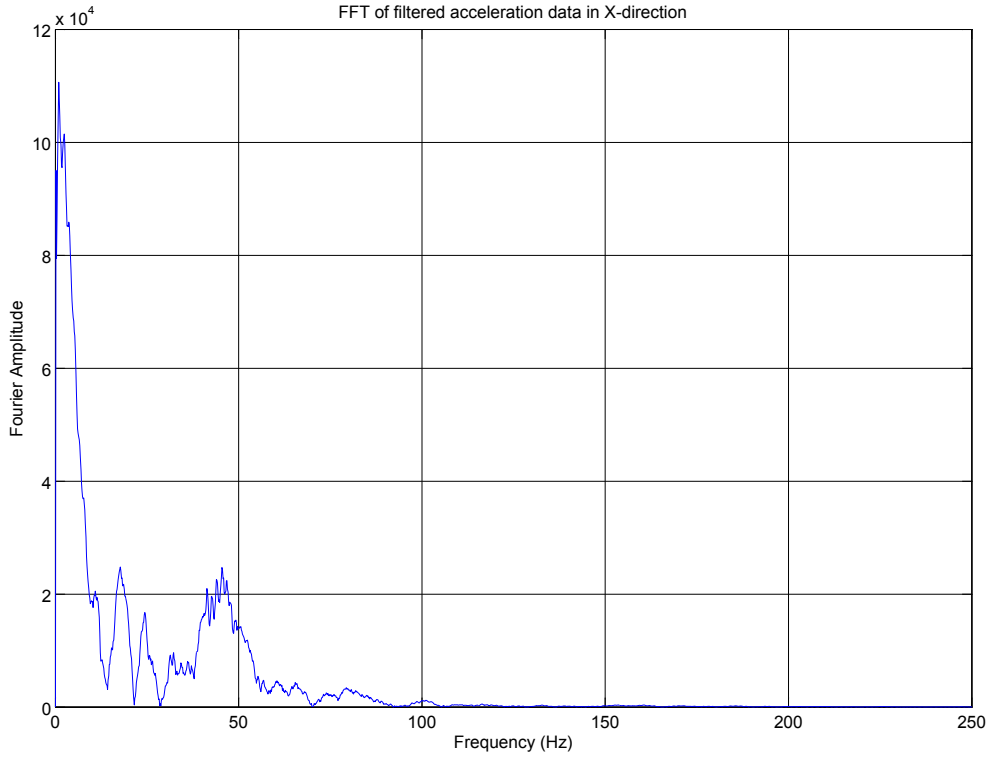

FIGURE 4.28: *Filtered data frequency analysis with CFC-60 of X-axis crash pulses in linear scale.*

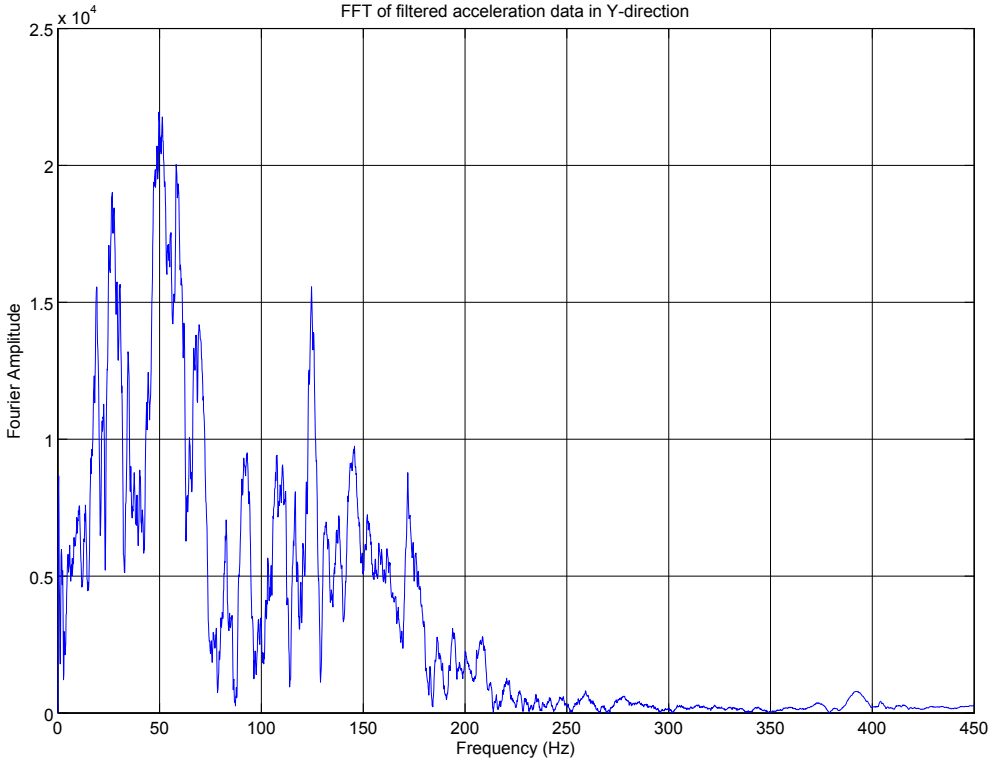

FIGURE 4.29: *Filtered data frequency analysis with CFC-180 of Y-axis crash pulses in linear scale.*

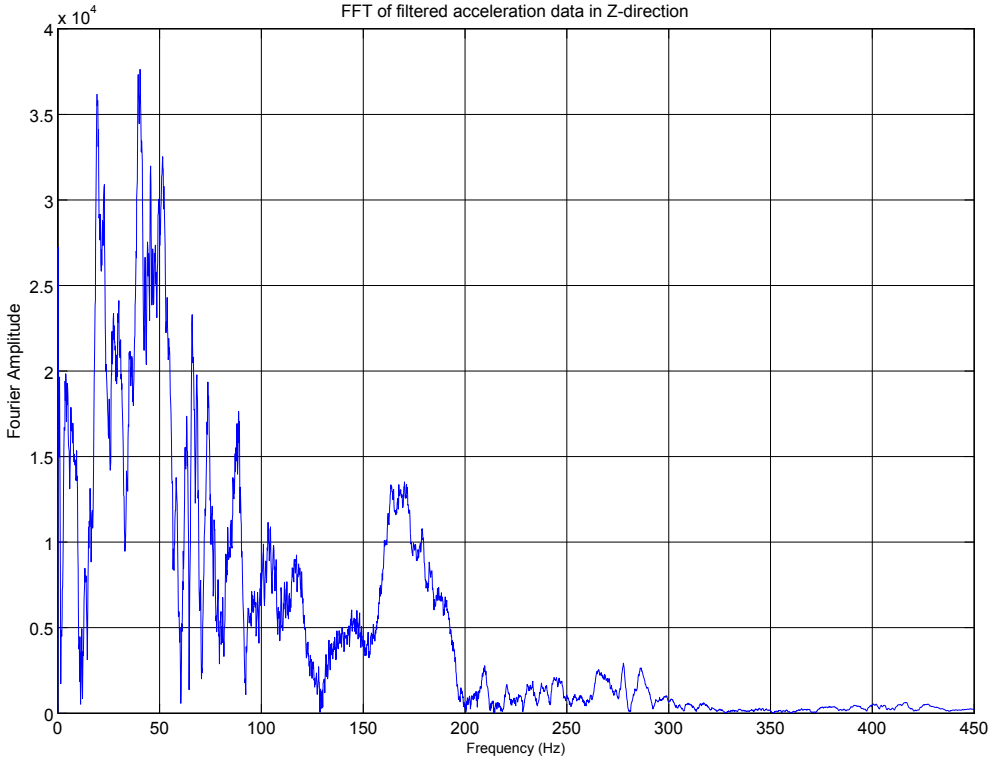

FIGURE 4.30: *Filtered data frequency analysis with CFC-180 of Z-axis crash pulses in linear scale.*

Chapter 5

Mathematical modeling of vehicle crash

5.1 2D Mathematical modeling of vehicle crash

5.1.1 Vehicle Planar Kinematics

A rigid vehicle can be assumed to act as a flat box moving on a horizontal surface as considered in a book by Jazar[7]. As shown in Figure 5.1 a flat box is attached with a local coordinate frame B(cxy) at its body mass center which moves in the X-Y plane of global reference frame. The unit vectors **i** and **j** are fixed in global coordinate frame G(OXY), while unit vectors $\mathbf{e_1}$ and $\mathbf{e_2}$ are fixed in reference local coordinate frame B(cxy). The unit vectors $\mathbf{e_1}$ and $\mathbf{e_2}$ share the motion with the body and change with respect to time.

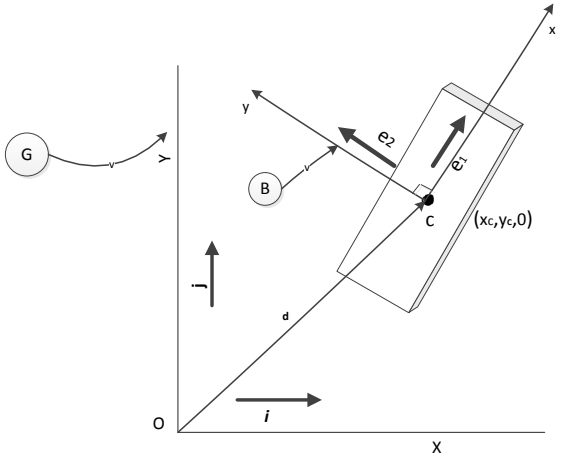

FIGURE 5.1: *Rigid Vehicle representation [6].*

A vehicle in a planar motion can be illustrated in more clarity as in the Figure 5.2. A global coordinate frame G is attached to the ground and a local coordinate frame B is attached to the vehicle at the mass center C. The Z and z-axes are parallel, and the orientation of the frame B is indicated by the heading angle Ψ between the X and x-axes. The global position vector of the mass center is denoted by d_G.

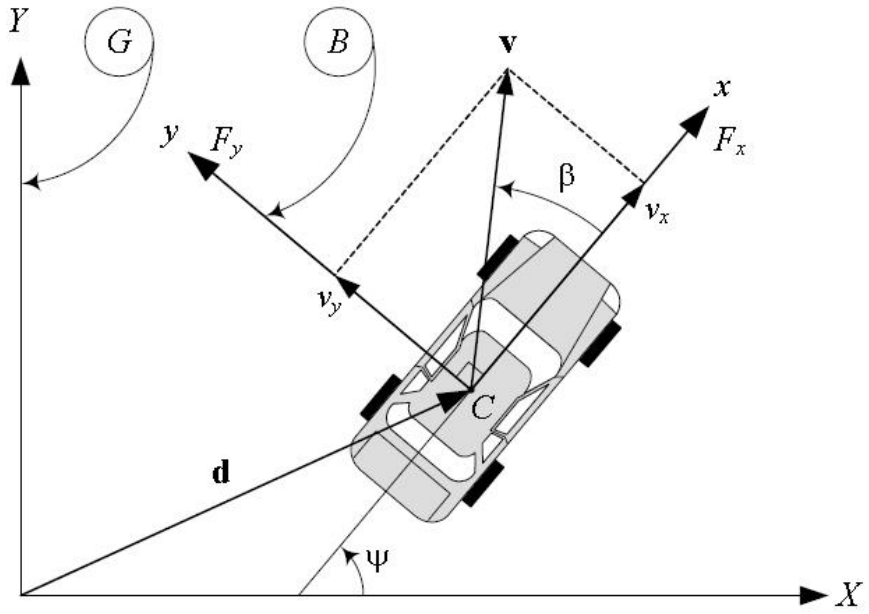

FIGURE 5.2: *A rigid vehicle in a planar motion[7].*

Transforming between local and global coordinate frames

A transformation matrix $\mathbf{R}_{\mathbf{B}}^{\mathbf{G}}$ which can be written as in the Equation 5.1 can be used to find the planar rigid vehicle's EOM(Equation of Motion) in the body coordinate frame by expressing the global EOM in the vehicle's body coordinate frame B. In the similar method it is possible to apply the transformation matrix to transform the vehicle's local frame coordinate into the global frame [9].

$$\mathbf{R}_{\mathbf{B}}^{\mathbf{G}} = \begin{bmatrix} cos\psi & -sin\psi & 0 \\ sin\psi & cos\psi & 0 \\ 0 & 0 & 1 \end{bmatrix} \tag{5.1}$$

where:

- $\mathbf{R}_{\mathbf{B}}^{\mathbf{G}}$-the transformation matrix.
- ψ-the yaw angle or rotational angle about an axis perpendicular to the plane.

Planar global frame velocity of a rigid vehicle

The velocity of the center of mass of the rigid vehicle with respect to the point O of global coordinate frame can be determined by Equation 5.2[6].

$$\mathbf{G_{vB}} = \dot{\mathbf{x}}_\mathbf{B}\mathbf{i} + \dot{\mathbf{y}}_\mathbf{B}\mathbf{j} \tag{5.2}$$

where:

- $\mathbf{G_{vB}}$- the velocity of the body with respect to point O of global coordinate frame.
- $\dot{\mathbf{x}}_\mathbf{B}$-the velocity of of the body in x-axis direction of local coordinate frame.
- $\dot{\mathbf{y}}_\mathbf{B}$- the velocity of the body in y-axis direction of local coordinate frame.
- $\mathbf{i}$-unit vector along the global X-axis direction.
- $\mathbf{j}$-unit vector along the global Y-axis direction.

Using the transformation matrix(Equation 5.1) the vehicle's local frame velocity can be transformed into the global velocity. The global velocity of the center of mass of the rigid vehicle with respect to the point O of the global frame can be written as Equation 5.3 which further can be expressed as Equation 5.4 for planar motion .

$$\mathbf{v}_\mathbf{C}^\mathbf{G} = \mathbf{R}_\mathbf{B}^\mathbf{G}\mathbf{v}_\mathbf{C}^\mathbf{B} \tag{5.3}$$

where:

- $\mathbf{v}_\mathbf{C}^\mathbf{G}$-the global frame velocity vector of the rigid vehicle.
- $\mathbf{R}_\mathbf{B}^\mathbf{G}$-the transformation matrix.
- $\mathbf{v}_\mathbf{C}^\mathbf{B}$-the local frame velocity vector of the rigid vehicle.

$$\begin{bmatrix} \mathbf{v_X} \\ \mathbf{v_Y} \\ 0 \end{bmatrix} = \begin{bmatrix} cos\psi & -sin\psi & 0 \\ sin\psi & cos\psi & 0 \\ 0 & 0 & 1 \end{bmatrix} \begin{bmatrix} v_x \\ v_y \\ 0 \end{bmatrix} \tag{5.4}$$

where:

- $\mathbf{v_X}$-global velocity of the rigid vehicle in the X-axis direction.

- $\mathbf{v_Y}$-global velocity of the rigid vehicle in the Y-axis direction.
- ψ- the yaw angle or rotational angle about an axis perpendicular to the plane.
- v_x- velocity of the rigid vehicle in the x-axis direction of local frame.
- v_y- velocity of the rigid vehicle in the y-axis direction of local frame.

Planar global frame acceleration of a rigid vehicle

The acceleration of the center of mass of the rigid body with respect to the point O of global reference frame is determined by Equation 5.5 [6] which can be further expressed as Equation 5.6 for planar motion. The angular velocity ω of the rigid body should be considered to determine the acceleration of the body with respect to the point O. The motion of the body is confined to the plane and the angular velocity vector is about the z-axis that points outward direction perpendicular to X-Y plane.

$$\mathbf{G_{aB}} = \ddot{\mathbf{x}}_\mathbf{B}\mathbf{i} + \ddot{\mathbf{y}}_\mathbf{B}\mathbf{j} \tag{5.5}$$

where:

- $\mathbf{G_{aB}}$- the acceleration of the body with respect to point O of global coordinate frame.
- $\ddot{\mathbf{x}}_\mathbf{B}$-the acceleration of the body in x-axis direction of local coordinate frame.
- $\ddot{\mathbf{y}}_\mathbf{B}$-the acceleration of the body in y-axis direction of local coordinate frame.
- **i**-unit vector along the global X-axis direction.
- **j**-unit vector along the global Y-axis direction.

According to Jazar([7]), the global acceleration of the center of mass of the rigid vehicle with respect to the point O of the global frame can be expressed in the vector form as the Equation 5.6 using the transformation matrix.

$$\begin{bmatrix} \dot{\mathbf{v}}_\mathbf{X} \\ \dot{\mathbf{v}}_\mathbf{Y} \\ 0 \end{bmatrix} = \begin{bmatrix} (\dot{v}_x - \dot{\psi}v_y)cos\psi - (\dot{v}_y + \dot{\psi}v_x)sin\psi \\ (\dot{v}_y + \dot{\psi}v_x)cos\psi + (\dot{v}_x - \dot{\psi}v_y)sin\psi \\ 0 \end{bmatrix} \tag{5.6}$$

where:

- $\dot{\mathbf{v}}_\mathbf{X}$-global acceleration of the rigid vehicle in the X-axis direction of global frame.

- $\dot{\mathbf{v}}_{\mathbf{Y}}$-global acceleration of the rigid vehicle in the Y-axis direction of global frame.
- $\dot{v}_x$-local coordinate acceleration of the rigid vehicle in the x-axis direction of the local frame.
- $\dot{v}_y$-local coordinate acceleration of the rigid vehicle in the y-axis direction of the local frame.
- ψ-the yaw angle or rotational angle about an axis perpendicular to the plane.
- $\dot{\psi}$=ω_z-the yaw rate or the angular velocity of the rigid vehicle about z-axis which is perpendicular to the planar motion.

5.1.2 Vehicle Planar Dynamics

To express the vehicle planar dynamics, a vehicle coordinate frame B(Cxyz) can be assumed to be attached to the vehicle at the mass center C to express the EOM for the vehicle. This is shown in Figure 5.3 which indicates the x-axis is directed forward and it is a longitudinal axis passing through C. The y-axis is directed laterally to the left from the driver's viewpoint. The z-axis makes the coordinate system a right hand triad. The z-axis is perpendicular to horizontal flat ground and opposite to the gravitational acceleration(g) according to Jazar[7]. For this vehicle coordinate frame representation of the EOM is presented using Newton-Euler law's of motion as in Equation 5.7, Equation 5.8 and Equation 5.9:

$$F_x = m\dot{v}_x - m\omega_z v_y \tag{5.7}$$

$$F_y = m\dot{v}_y + m\omega_z v_x \tag{5.8}$$

$$M_z = \dot{\omega}_z I_z \tag{5.9}$$

The transformation matrix can also be used here to transform the force vector from the local coordinate frame to the global frame. The global Newton's EOM can be written as Equation 5.10 which can be further expressed as in Equation 5.11 for planar motion.

$$\mathbf{F}_{\mathbf{C}}^{\mathbf{G}} = \mathbf{R}_{\mathbf{B}}^{\mathbf{G}}\mathbf{F}_{\mathbf{C}}^{\mathbf{B}} \tag{5.10}$$

where:

- $\mathbf{F}_{\mathbf{C}}^{\mathbf{G}}$-global force vector.
- $\mathbf{R}_{\mathbf{B}}^{\mathbf{G}}$-the transformation matrix.
- $\mathbf{F}_{\mathbf{C}}^{\mathbf{B}}$-local frame force vector which is written in Equation 5.7, Equation 5.8 and Equation 5.9.

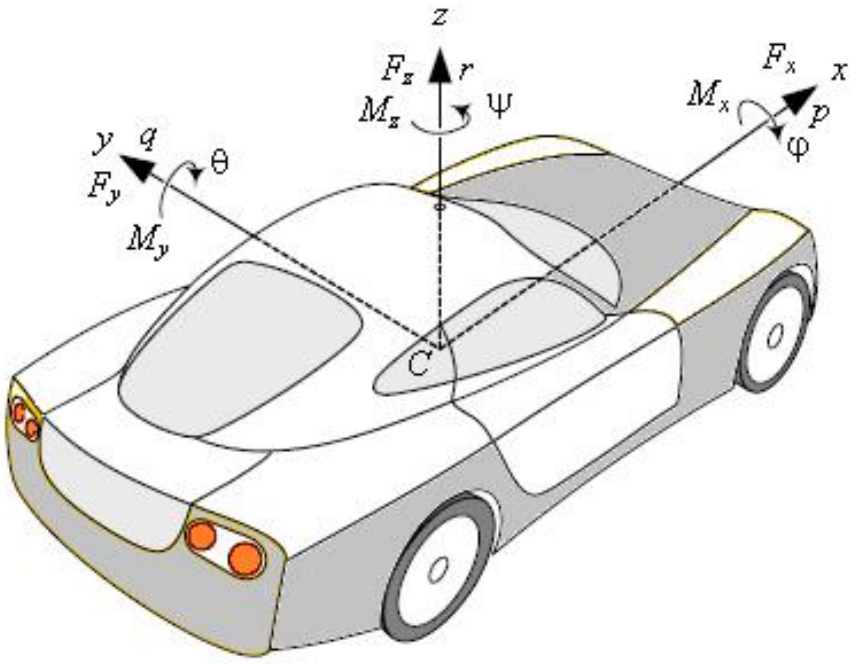

FIGURE 5.3: *Vehicle body coordinate frame B(Cxyz)*[7].

$$\begin{bmatrix} \mathbf{F_X} \\ \mathbf{F_Y} \\ 0 \end{bmatrix} = m * \begin{bmatrix} \dot{\mathbf{v}}_\mathbf{X} \\ \dot{\mathbf{v}}_\mathbf{Y} \\ 0 \end{bmatrix} = m * \begin{bmatrix} (\dot{v}_x - \dot{\psi} v_y)cos\psi - (\dot{v}_y + \dot{\psi} v_x)sin\psi \\ (\dot{v}_y + \dot{\psi} v_x)cos\psi + (\dot{v}_x - \dot{\psi} v_y)sin\psi \\ 0 \end{bmatrix} \tag{5.11}$$

where:

- $\mathbf{F_X}$-global force vector of the rigid vehicle in the X-axis direction of global frame.
- $\mathbf{F_Y}$-global force vector of the rigid vehicle in the Y-axis direction of global frame.
- m-mass of the rigid vehicle.
- $\dot{v}_X$-Global coordinate acceleration of the rigid vehicle in the x-axis direction of the global frame.
- $\dot{v}_Y$-globalcoordinate acceleration of the rigid vehicle in the y-axis direction of the global frame.
- $\dot{v}_x$-lolcal coordinate acceleration of the rigid vehicle in the x-axis direction of the local frame.
- $\dot{v}_y$-lolcal coordinate acceleration of the rigid vehicle in the y-axis direction of the local frame.
- ψ-the yaw angle or rotational angle about an axis perpendicular to the plane.
- $\dot{\psi}$=ω_z-the yaw rate or the angular velocity of the rigid vehicle about z-axis which is perpendicular to the planar motion.

By applying the same procedure for the moment transformation, the yaw moment of the rigid vehicle about global Z-axis can be obtained as shown in Equation 5.12 which can be further expressed as in Equation 5.13 for planar motion.

$$\mathbf{M_C^G} = \mathbf{R_B^G M_C^B} \tag{5.12}$$

$$\mathbf{M_C^G} = \begin{bmatrix} cos\psi & -sin\psi & 0 \\ sin\psi & cos\psi & 0 \\ 0 & 0 & 1 \end{bmatrix} \begin{bmatrix} 0 \\ 0 \\ M_z \end{bmatrix} = \begin{bmatrix} 0 \\ 0 \\ M_z \end{bmatrix} \tag{5.13}$$

where:

- $\mathbf{M_C^G}$-global yaw moment about global Z-axis.
- $\mathbf{R_B^G}$-the transformation matrix.
- $\mathbf{M_C^B}$-local yaw moment about local z-axis.
- ψ-the yaw angle or rotational angle about an axis perpendicular to the plane.
- $\mathbf{M_z}$-local yaw moment about local z-axis.

5.1.3 2D Mass-spring-damper Model

In this section a dynamic model with three degrees of freedom is developed for a rigid vehicle in a planar motion based on [7],[6] and [9]. A planar dynamic model can be applied when the forward, lateral and yaw velocities are important and are enough to examine the behavior of a vehicle [7].

A simple 2D mass-spring-damper Model is shown in the Figure 5.4. It consist of a spring of elastic coefficient value $k_x[N/m]$, which is in parallel connection with a damper of damping coefficient value C_x[Ns/m] to a mass with $m[kg]$ in the x-axis direction. Another spring of elastic coefficient value $K_y[N/m]$ is parallel connected with a damper of damping coefficient value C_y[Ns/m] in the y-axis direction to the center of gravity of the mass m. This simple model can be used to represent the vehicle to barrier or vehicle to vehicle collisions.

To include the yaw motion of the mass this system is redrawn to represent the vehicle model in 2D as shown in Figure 5.5. A point mass m with two degrees of freedom and its motion is described by the coordinates x and y in the horizontal plane and rotational motion(yaw motion) about the vertical axis. For modeling purposes, a spring with stiffness K_x, and a viscous damper with a damping coefficient C_x are used to constrain motions along the x-axis direction attached the center of mass m. Another spring-damper combination is used to constrain motions along the y-axis direction attached to the center of mass m. The vehicle model has initial velocity in the X-axis direction as represented in the Figure 5.5.

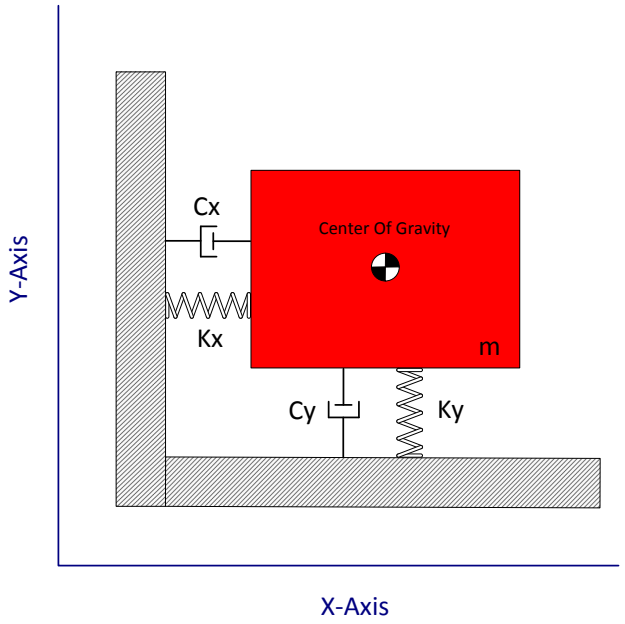

FIGURE 5.4: *Mass-spring-damper Model in 2-D for Vehicle to Barrier collision.*

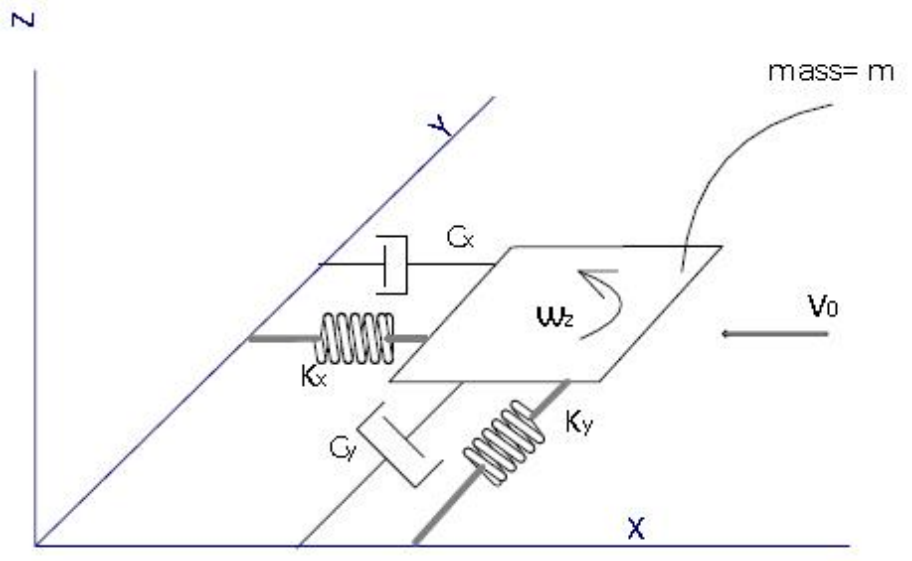

FIGURE 5.5: *Mass-spring-damper Model for Vehicle to Barrier Collision in 2D.*[6]

Equation of Motion

To obtain the governing equations, force balance is considered along the X-axis and Y-axis directions. Making use of the diagram shown in Figure 5.5 and assuming X-axis component of the resultant F_x acting on the mass(m) in the X-axis direction, and the Y-axis component of the resultant force F_y acting on the mass(m) in the Y-axis direction, it is possible to obtain the relations shown in Equation 5.14 and Equation 5.15 [9].

$$F_X = -C_x v_x - K_x x \tag{5.14}$$

$$F_Y = -C_y v_y - K_y x \tag{5.15}$$

Where:

- x and y are the respective displacements along the X-axis and Y-axis directions of the model.
- v_x and v_y are the respective velocities along the X-axis and Y-axis directions of the model.
- F_X and F_Y are the components of the resultant force acting on the mass(m) along the X-axis and X-axis directions of the model respectively.
- $Vx_0 = 35km/h = 9.72m/s$ and $Vy_0 = 0km/h$ are initial velocity in the X and Y directions respectively.
- K_x and K_y are the respective spring stiffness along the X-axis and Y-axis directions respectively.
- C_x and C_y are the respective damping coefficient along the X-axis and Y-axis directions respectively.

Using the Equation 5.11 of planar vehicle dynamics for a rigid vehicle in combination with the Equation 5.14 and Equation 5.15 for force balance it is possible to arrive at the Equation 5.16 and Equation 5.17.

$$m((\dot{v}_x - \dot{\psi} v_y)cos\psi - (\dot{v}_y + \dot{\psi} v_x)sin\psi) = -C_x v_x - K_x x \tag{5.16}$$

$$m((\dot{v}_y + \dot{\psi} v_x)cos\psi + (\dot{v}_x - \dot{\psi} v_y)sin\psi) = -C_y v_x - K_y x \tag{5.17}$$

The Equation 5.16 and Equation 5.17 can be rearranged in matrix form as in Equation 5.18

$$[M]\begin{bmatrix} \ddot{x} \\ \ddot{y} \end{bmatrix} + [C]\begin{bmatrix} \dot{x} \\ \dot{y} \end{bmatrix} + [G]\begin{bmatrix} \dot{x} \\ \dot{y} \end{bmatrix} + [K]\begin{bmatrix} x \\ y \end{bmatrix} = \begin{bmatrix} 0 \\ 0 \end{bmatrix} \tag{5.18}$$

where:

$$[M] = \begin{bmatrix} mcos\psi & -msin\psi \\ msin\psi & mcos\psi \end{bmatrix},$$

$$[C] = \begin{bmatrix} C_x & 0 \\ 0 & C_y \end{bmatrix},$$

$$[G] = \begin{bmatrix} -m\omega_z sin\psi & -m\omega_z cos\psi \\ m\omega_z cos\psi & -m\omega_z sin\psi \end{bmatrix},$$

$$[K] = \begin{bmatrix} K_x & 0 \\ 0 & K_y \end{bmatrix},$$

- m-mass
- K_x-stiffness constant of spring in X-axis direction.
- K_y-stiffness constant of spring in Y-axis direction.
- C_x-damping coefficient constant of spring in X-axis direction.
- C_y-damping coefficient constant of spring in Y-axis direction.
- ω_z-yaw rate about the vertical Z-axis direction perpendicular to the vehicle plane.
- ψ-yaw angle about the vertical Z-axis direction perpendicular to the vehicle plane.

5.1.4 Parameter Estimation and Model Establishment

A. Solving systems of linear equations

The differential equations derived for the 2D dynamic model of the vehicle in this project looks like a system of linear equations, and a solution finding method of linear system can be applied for the estimation of the parameters for the model.

The concept of linear system is the basis for a subject of linear algebra that is used in most parts of modern mathematics. The method of finding the solutions to a linear system or computational algorithms for finding the solutions is an important part of numerical linear algebra, and play a prominent role in engineering, physics, chemistry, computer science, and economics. Non-linear equations can often be represented with linear equations. The process is called linearization and it is used when making a mathematical model or computer simulation of a relatively complex system [35].

According to [36], a linear equation in unknown variables $x_1, x_2, ..., x_n$ is an equation of the form $a_1x_1 + a_2x_2 + ... + a_nx_n = b$. where, $a_1; a_2; ...; a_n$ and b are constant real or complex numbers which are called the coefficients of x_i variables; and b is called the constant term of the equation.

A system of linear equations is a set or collection of equations that can be dealt all at once. For example, a linear system of m equations in n variables $x_1, x_2, ..., x_n$ can be written as

$$\begin{cases} a_{11}x_1 + a_{12}x_2 + ... + a_{1n}x_n = b_1 \\ a_{21}x_1 + a_{22}x_2 + ... + a_{2n}x_n = b_2 \\ \qquad\qquad . \\ \qquad\qquad . \\ a_{m1}x_1 + a_{m2}x_2 + ... + a_{mn}x_n = b_m \end{cases} \tag{5.19}$$

To find the solution of systems of simultaneous linear equations is to make an assignment of numbers to the variables such that all the equations are simultaneously satisfied. A linear system may behave in any one of three possible ways:

1. The system has infinitely many solutions.
2. The system has a single unique solution.
3. The system has no solution

The general form of linear equations(see Equation 5.19) can be represented in vector form as in Equation 5.20.

$$x_1 \begin{bmatrix} a_{11} \\ a_{21} \\ . \\ . \\ . \\ a_{m1} \end{bmatrix} + x_2 \begin{bmatrix} a_{12} \\ a_{22} \\ . \\ . \\ . \\ a_{m2} \end{bmatrix} + ... + x_n \begin{bmatrix} a_{1n} \\ a_{2n} \\ . \\ . \\ . \\ a_{mn} \end{bmatrix} = \begin{bmatrix} b_1 \\ b_2 \\ . \\ . \\ . \\ b_m \end{bmatrix} \tag{5.20}$$

The vector equation can further be written in the form of matrix equation for $\mathbf{Ax} = \mathbf{b}$ where A is an $m \times n$ matrix, x is a column vector with n entries, and b is a column vector with m entries.

$$\mathbf{A} = \begin{bmatrix} a_{11} & a_{12} & . & . & . & a_{1n} \\ a_{21} & a_{22} & . & . & . & a_{2n} \\ . & . & . & & & . \\ . & . & & . & & . \\ . & . & & & . & . \\ a_{m1} & a_{m2} & . & . & . & a_{mn} \end{bmatrix}$$

$$\mathbf{X} = \begin{bmatrix} x_1 \\ x_2 \\ . \\ . \\ . \\ x_n \end{bmatrix}$$

$$\mathbf{b} = \begin{bmatrix} b_1 \\ b_2 \\ . \\ . \\ . \\ b_m \end{bmatrix}$$

B. Total Least Squares method

Total least squares is also known as error-in-variables method or orthogonal regression method [37]. It is an extension of the usual Least Squares method data modeling technique [38] that was introduced by Golub and Van Loan [[39],[40]]. It is a generalization of Deming regression, and can be applied to both linear and non-linear models.

Total least square was introduced as a solution for an overdetermined linear system of equations $Ax \approx B$ that represents many problems in data estimation, where $A \epsilon \mathbb{R}^{m \times n}$ and $B \epsilon \mathbb{R}^{m \times d}$ are the given data and $X \epsilon \mathbb{R}^{n \times d}$ is unknown. An approximated solution for X is what should be searched with $m > n$, since there is no typically exact solution for X [41]. In the classical least squares approach all errors are coined to the observation vector b, and the system matrix A is assumed to be free from error. In real engineering application this assumption often does not hold true. For example, if both the right-hand side b and the matrix A are obtained by measurements or if the matrix A is an approximation of the true operator, then there is some noise in both elements of the system equation [8].

An appropriate approach to this problem is the total least squares (TLS) method which is a natural generalization of the least-squares approximation method when the data in both A and B is perturbed [[41],[8]]. Distance is an optimal fitting criterion in the field of signal processing or image processing for applications such as shape recognition and curve detection and fitting. Numerical routine of minimization is used for orthogonal distance fitting. Some sort of iteration methods must be used for general curve fitting even in the case of orthogonal distance fitting.

The total least square method is a general curve fitting approach that can be used in n-dimensional space and it can be characterized by the orthogonal distance as it is depicted in the Figure 5.6. The total least square method can be expressed mathematically using an Equation 5.21.

$$R = \sum_{i=1}^{n} |d_i| \tag{5.21}$$

Where the target is to find minimum of R summing the orthogonal distance d.

Eigenvalue, Singular Value Decomposition (SVD) and Principal Component Analysis (PCA) are well-known mathematical tools that can be used for practical calculation with the TLS method. There are many areas of application of TLS method such as signal processing, in computer vision or image processing, speech and audio processing, modal and spectral analysis, linear system theory, system identification, economics or several possible open problems [37, 41].

C. The spring stiffness and the damping coefficient in X-axis direction

The numerical data of acceleration which was obtained from the experiment as discussed in the previous chapters is used for estimation of parameters in this subsection. First, analysis of the

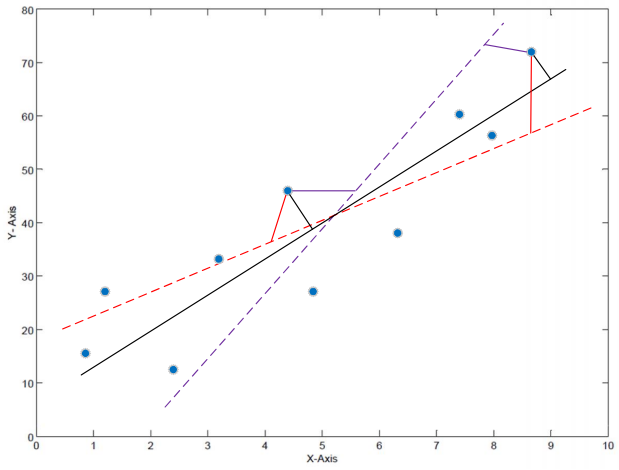

FIGURE 5.6: *Principle of the TLS method.*[8]

kinematics of the impacting vehicle is made. The velocity for the vehicle in the global frame is obtained from integration of the global acceleration data and considering also the initial vehicle velocity which is 35km/h. Further, the velocity is integrated to obtain the displacement data. The next step is considering the planar dynamic EOM for the vehicle and making parameter estimation using a matlab code. Planar dynamic EOM in the global frame X-axis direction is considered as Equation 5.22. The following is coded into matlab that helps to calculate the spring stiffness and damping coefficient of the model in the x-axis direction.

$$m((\dot{v}_x - \dot{\psi}v_y)cos\psi - (\dot{v}_y + \dot{\psi}v_x)sin\psi) = -K_x x - C_x\dot{x} \tag{5.22}$$

Re-arranging the Equation 5.22 will result in the Equation 5.23. The equation can be treated as a linear system equation and finding the solution for the spring stiffness and damping coefficient of the model in the x-axis direction.

$$\begin{bmatrix} C_x \\ K_x \end{bmatrix} \begin{bmatrix} \dot{x} & x \end{bmatrix} = -m((\dot{v}_x - \dot{\psi}v_y)cos\psi - (\dot{v}_y + \dot{\psi}v_x)sin\psi) \tag{5.23}$$

Letting the left hand side part of the equation represented by $\begin{bmatrix} C_x \\ K_x \end{bmatrix} * A_x$, where, $A_x = \begin{bmatrix} \dot{x} & x \end{bmatrix}$ and representing the right hand side of the equation by bx as shown in Equation 5.24 the and using linear equation solving method the operation of linear system shown in the Equation 5.25 can be performed.

$$bx = -m\ cos\psi\ \ddot{x} + m\ \dot{\psi}\ cos\psi\ \dot{y} + m\ \ddot{y}\ sin\psi + m\ \dot{\psi}\ sin\psi\ \dot{x} \tag{5.24}$$

Following the steps the value of spring stiffness and the damping coefficient in the X-axis direction is calculated from Equation 5.25.

$$\begin{bmatrix} C_x \\ K_x \end{bmatrix} = A_x \backslash bx \tag{5.25}$$

For more robust solution a total least square method can be used to obtain the parameters values and the equation in Matlab is coded as a combination of equations A_x , Equation 5.24, and Equation 5.26 to find the output as in Equation 5.27.

$$[U, S, V] = svd([Ax, bx], 0) \tag{5.26}$$

$$\begin{bmatrix} C_x \\ K_x \end{bmatrix} = -V(1:2, 3)/V(3, 3) \tag{5.27}$$

D. The spring stiffness and the damping coefficient in Y-axis direction

A similar method of finding the parameter values in the X-axis direction can be applied in the Y-axis direction. Following the same steps as in X-axis in previous section, the planar dynamics EOM can be written as Equation 5.28. The velocity for the vehicle in the global frame is obtained from integration of the global acceleration data and considering also the initial vehicle velocity which is 0km/h in the Y-axis direction. Further, the velocity can be integrated to obtain the displacement data. The estimation technique is coded into matlab that helps to calculate the spring stiffness and damping coefficient of the model in the Y-axis direction.

$$m((\dot{v}_y + \dot{\psi} v_x) cos\psi + (\dot{v}_x - \dot{\psi} v_y) sin\psi) = -K_y y - C_y \dot{y} \tag{5.28}$$

Similar to X-axis direction parameter estimation the rearrangement of Equation 5.28 will result in the Equation 5.30. The equation here can also be treated as a linear system equation to find the solution for the spring stiffness and damping coefficient of the model in the Y-axis direction. For more robust solution a total least square method can be be applied here also to obtain the parameter values.

$$\begin{bmatrix} C_y \\ K_y \end{bmatrix} \begin{bmatrix} \dot{y} & y \end{bmatrix} = -m\ cos\psi\ \ddot{y} - m\ \dot{\psi}\ cos\psi\ \dot{x} - m\ \ddot{x}\ sin\psi + m\ \dot{\psi}\ sin\psi\ \dot{y} \tag{5.29}$$

Letting the left hand side part of the equation represented by $\begin{bmatrix} C_y \\ K_y \end{bmatrix} * A_y$, where, $A_y = \begin{bmatrix} \dot{y} & y \end{bmatrix}$ and representing the right hand side of the equation by *by* as shown in the Equation 5.30 and using

linear equation solving method the operation of linear system shown in the Equation 5.31 can be performed.

$$by = -m\ cos\psi\ \ddot{y} - m\ \dot{\psi}\ cos\psi\ \dot{x} - m\ \ddot{x}\ sin\psi + m\ \dot{\psi}\ sin\psi\ \dot{y} \tag{5.30}$$

Following the above steps the value of spring stiffness and the damping coefficient in the Y-axis direction is calculated from Equation 5.31.

$$\begin{bmatrix} C_y \\ K_y \end{bmatrix} = A_y \backslash by \tag{5.31}$$

For more robust solution a total least square method can be used to obtain the parameters values in Y-axis also and the equation in Matlab is coded as a combination of equations A_y, Equation 5.30, and Equation 5.32 to find the output as in Equation 5.33.

$$[U, S, V] = svd([Ay, by], 0) \tag{5.32}$$

$$\begin{bmatrix} C_y \\ K_y \end{bmatrix} = -V(1:2, 3)/V(3, 3) \tag{5.33}$$

5.2 3D Mathematical modeling of vehicle crash

5.2.1 3D Vehicle Kinematics

Position and orientation of rigid vehicle in X-Y-Z directions

A vehicle can be considered as a rigid body with an attached Cartesian coordinate frame B(oxyz) fixed to the rigid body B and the rigid body is further attached to the ground G(OXYZ) at the origin point O that is shown in the Figure 5.7[7].

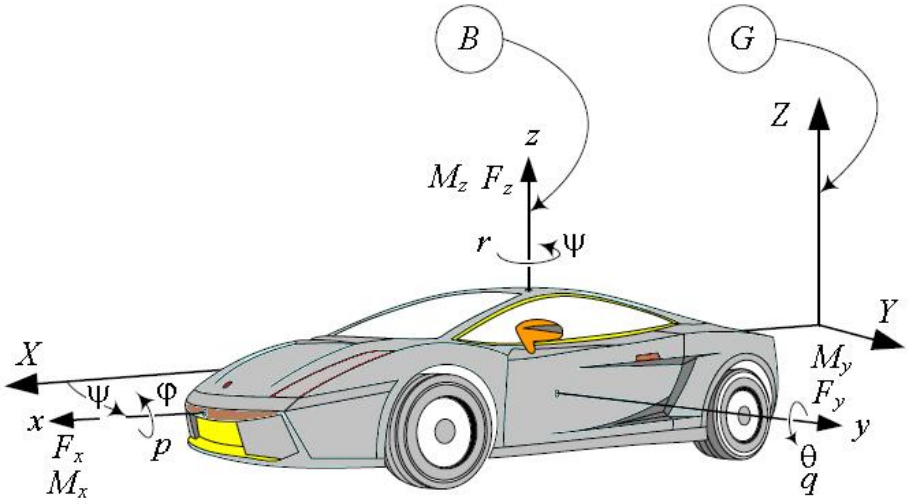

FIGURE 5.7: *3D Rigid Vehicle representation [7].*

The rigid body can move freely in the fixed global coordinate frame so that it can rotate freely in the global frame and the origin of the body frame can be assumed to translate relative to the origin of G as shown in Figure 5.8. A point P on the rigid body coordinate can be expressed in global frames as in Equation 5.34.

$$G_{r_P} = G_{R_B} B_{r_P} + G_{d_B} \tag{5.34}$$

where:

G_{r_P}-global coordinate of a point P on a body B

G_{R_B}-rotational transformation matrix

B_{r_P}-local coordinate of a point P on a body B

G_{d_B}-the position of the moving origin o relative to the fixed origin O.

Transformation between local and global coordinate frames

Similar to the planar dynamics the transformation matrix G_{R_B} which can be written as in the Equation 5.35 can be used to find the planar rigid vehicle's EOM in the body coordinate frame

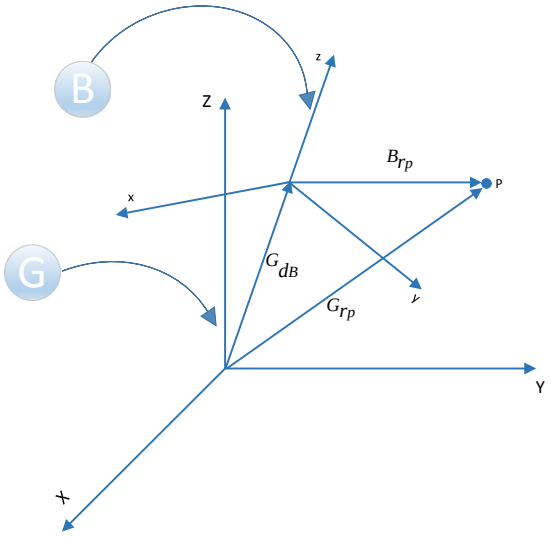

FIGURE 5.8: *A rigid body with an attached coordinate frame B(oxyz) moving freely in a global coordinate frame G(OXYZ)*[7].

by expressing the global EOM in the vehicle's body coordinate frame B. In the same manner it is possible to apply the transformation matrix to transform the vehicle's local frame coordinate into the global frame.

$$R_{G_B} = \begin{bmatrix} cos\psi & -sin\psi & 0 \\ sin\psi & cos\psi & 0 \\ 0 & 0 & 1 \end{bmatrix} \begin{bmatrix} cos\theta & 0 & sin\theta \\ 0 & 1 & 0 \\ -sin\theta & 0 & cos\theta \end{bmatrix} \begin{bmatrix} 1 & 0 & 0 \\ 0 & cos\varphi & -sin\varphi \\ 0 & sin\varphi & cos\varphi \end{bmatrix} \tag{5.35}$$

where:

- ψ-yaw angle
- θ-pitch angle
- φ-roll angle

Velocity of a rigid vehicle in X-Y-Z directions

The velocity of the point P of the rigid body shown in the Figure 5.8 that is attached to global coordinate can be expressed as in Equation 5.36.

$$G_{VP} = G\omega_B \times (G_{r_P} - G_{d_B}) + G_{\dot{d}_B} \tag{5.36}$$

where:

- G_{VP}-the velocity of the point P in Global coordinate.
- $G\omega_B$-angular velocity of the body B relative to the fixed origin O.
- G_{r_P}- a global coordinate of a point P on a body B .
- G_{d_B}-the position of the moving origin o relative to the fixed origin O.
- $G_{\dot{d}_B}$-the velocity of the moving origin o relative to the fixed origin O.

The velocity of the center of mass of the rigid vehicle with respect to the point O of global reference frame can be determined by Equation 5.37 by using a transformation matrices.

$$\begin{bmatrix} v_X \\ v_Y \\ v_Z \end{bmatrix} = \begin{bmatrix} cos\psi & -sin\psi & 0 \\ sin\psi & cos\psi & 0 \\ 0 & 0 & 1 \end{bmatrix} \begin{bmatrix} cos\theta & 0 & sin\theta \\ 0 & 1 & 0 \\ -sin\theta & 0 & cos\theta \end{bmatrix} \begin{bmatrix} 1 & 0 & 0 \\ 0 & cos\varphi & -sin\varphi \\ 0 & sin\varphi & cos\varphi \end{bmatrix} \begin{bmatrix} v_x \\ v_y \\ v_z \end{bmatrix} \tag{5.37}$$

where:

- v_X-rigid vehicle global coordinate velocity in X-axis direction.
- v_Y-rigid vehicle global coordinate velocity in Y-axis direction.
- v_Z-rigid vehicle global coordinate velocity in Z-axis direction.
- ψ-yaw
- θ-pitch
- φ-roll
- v_x-rigid vehicle local coordinate velocity in x-axis direction.
- v_y-rigid vehicle local coordinate velocity in y-axis direction.
- v_z-rigid vehicle local coordinate velocity in z-axis direction.

Acceleration of a rigid vehicle in X-Y-Z directions

The acceleration formula for a rigid body moving freely in a fixed global coordinate frame G(OXYZ) and that has an attached coordinate frame B (oxyz) is shown Equation 5.38. The origin of the body frame B can translate relative to the origin of G, while rigid body can rotate in the global frame. The coordinates of a body point P is shown as in Figure 5.9 [7].

$$G_{a_P} = G_{\alpha B} \times (G_{r_P} - G_{d_B}) + G\omega_B \times (G\omega_B \times (G_{r_P} - G_{d_B})) + G_{\ddot{d}_{BP}} \tag{5.38}$$

Where:

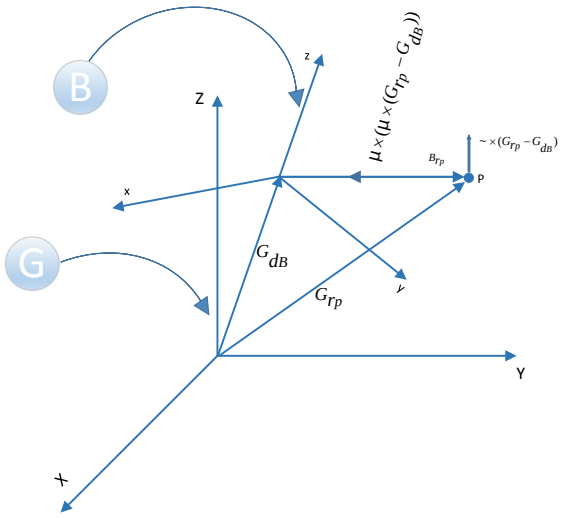

FIGURE 5.9: *Vehicle body coordinate frame B(Cxyz)*[7].

- G_{a_P}-acceleration of the point P in Global coordinate.
- $G_{\alpha B}$-angular acceleration of the point P in Global coordinate.
- G_{r_P}- a global coordinate of a point P on a body B .
- G_{d_B}-the velocity of the moving origin o relative to the fixed origin O.
- $G\omega_B$-angular velocity of the body B relative to the fixed origin O.
- $G_{\ddot{d}_B}$-the acceleration of the moving origin o relative to the fixed origin O.

The acceleration of the center of mass of the rigid vehicle with respect to the point O of the global frame can be expressed in the matrix form as in Equation 5.41 using the transformation matrices.

$$R_{G_B} = \begin{bmatrix} cos\psi cos\theta & (cos\psi sin\theta sin\varphi - sin\psi cos\varphi) & (sin\psi sin\varphi + cos\psi sin\theta cos\varphi) \\ sin\psi cos\theta & v_y cos\psi cos\varphi + sin\psi sin\theta sin\varphi & sin\psi sin\theta cos\varphi - cos\psi sin\varphi \\ sin\theta & cos\theta sin\varphi & cos\theta cos\varphi \end{bmatrix} \tag{5.39}$$

$$\dot{v}_{B_C} = \begin{bmatrix} \dot{v}_x + (\omega_y v_z - \omega_z v_y) \\ \dot{v}_y - (\omega_x v_z - \omega_z v_x) \\ \dot{v}_z + (\omega_x v_y - \omega_y v_x) \end{bmatrix} \tag{5.40}$$

$$\begin{bmatrix} \dot{v}_X \\ \dot{v}_Y \\ \dot{v}_Z \end{bmatrix} = R_{G_B} \star \dot{v}_{B_C} = R_{z,\psi} R_{y,\theta} R_{x,\varphi} \star \dot{v}_{B_C} \tag{5.41}$$

where:

- R_{G_B}-The global roll-pitch-yaw rotation matrix.
- ψ-yaw angle.
- θ-pitch angle.
- φ-roll angle.
- $\dot{v}_{B_C}$-acceleration of the rigid vehicle in body coordinate frame.
- $\dot{v}_x$-rigid vehicle local coordinate acceleration in x-axis direction.
- $\dot{v}_y$-rigid vehicle local coordinate acceleration in y-axis direction.
- $\dot{v}_z$-rigid vehicle local coordinate acceleration in z-axis direction.
- ω_z-yaw rate.
- ω_y-pitch rate.
- ω_x-roll rate.
- $\dot{v}_X$-rigid vehicle global coordinate acceleration in X-axis direction.
- $\dot{v}_Y$-rigid vehicle global coordinate acceleration in Y-axis direction.
- $\dot{v}_Z$-rigid vehicle global coordinate acceleration in Z-axis direction.
- $R_{z,\psi}$-transformation matrix for rotation about Z-axis.
- $R_{y,\theta}$-transformation matrix for rotation about Y-axis.
- $R_{x,\varphi}$-transformation matrix for rotation about X-axis.

5.2.2 3D Rigid vehicle dynamics

A motion of a rigid body with respect to a fixed global coordinate frame can be used to represent dynamics of a rigid vehicle. The translational and rotational motion of the rigid vehicle can be described by the principles of Newton and Euler equations of motion. The Newton-Euler equation of motion for a rigid vehicle in the body coordinate frame B, attached to the vehicle at its mass center C, are [7]:

$$F_x = ma_x + m(\omega_y v_z - \omega_z v_y) \tag{5.42}$$

$$F_y = ma_y - m(\omega_x v_z - \omega_z v_x) \tag{5.43}$$

$$F_z = ma_z + m(\omega_x v_y - \omega_y v_x) \tag{5.44}$$

$$M_x = I_{xx}\dot{\omega}_x + I_{xy}\dot{\omega}_y + I_{xz}\dot{\omega}_z - (I_{yy} - I_{zz})\omega_y\omega_z - I_{yz}(\omega_z^2 - \omega_y^2) - \omega_x(\omega_z I_{xy} - \omega_y I_{xz}) \tag{5.45}$$

$$M_y = I_{yx}\dot{\omega}_x + I_{yy}\dot{\omega}_y + I_{yz}\dot{\omega}_z - (I_{zz} - I_{xx})\omega_z\omega_x - I_{xz}(\omega_x^2 - \omega_z^2) - \omega_y(\omega_x I_{yz} - \omega_z I_{xy}) \tag{5.46}$$

$$M_z = I_{zx}\dot{\omega}_x + I_{zy}\dot{\omega}_y + I_{zz}\dot{\omega}_z - (I_{xx} - I_{yy})\omega_x\omega_y - I_{xy}(\omega_y^2 - \omega_x^2) - \omega_z(\omega_y I_{xz} - \omega_x I_{yz}) \quad (5.47)$$

where:

- F_x-longitudinal force$[N]$
- F_y-lateral force$[N]$
- F_z-vertical force$[N]$
- m-mass of the vehicle$[kg]$
- v_x-longitudinal velocity component$[m/s]$
- v_y-lateral velocity component$[m/s]$
- v_z-vertical velocity component$[m/s]$.
- ω_x-angular velocity about longitudinal axis$[rad/s]$.
- ω_y-angular velocity about lateral axis$[rad/s]$.
- ω_z-angular velocity about vertical axis$[rad/s]$.
- M_x-Pitch moment$[Nm]$.
- M_y-Roll moment $[Nm]$.
- M_z- yaw moment $[Nm]$.
- $\dot{\omega}_x$-angular acceleration about longitudinal axis$[rad/s^2]$.
- $\dot{\omega}_y$-angular acceleration about lateral axis$[rad/s^2]$.
- $\dot{\omega}_z$-angular acceleration about vertical axis$[rad/s^2]$.
- I_{xx}-mass moment of inertia about longitudinal axis $[kg.m^2]$.
- I_{zz}-mass moment of inertia about lateral axis $[kg.m^2]$
- I_{yy}-mass moment of inertia about lateral axis $[kg.m^2]$
- I_{xy}=I_{yx}-the product of inertia about zx $[kg.m^2]$.
- I_{xz}=I_{zx}-the product of inertia about yz$[kg.m^2]$.
- I_{yz}=I_{zy}-the product of inertia about xy $[kg.m^2]$.

The transformation matrix can be used here also to transform the force vector from the local coordinate frame to the global frame. The global Newton's EOM can be written as Equation 5.48 which can be further expressed as in Equation 5.50 in 3D motion .

$$\mathbf{F_C^G} = \mathbf{R_B^G F_C^B} \tag{5.48}$$

where:

- $\mathbf{F_C^G}$-global force vector.
- $\mathbf{R_B^G}$-the transformation matrix.
- $\mathbf{F_C^B}$-local frame force vector which is written in Equation 5.42, Equation 5.43 and Equation 5.44.

$$R_{z,\psi}R_{y,\theta}R_{x,\varphi} = \begin{bmatrix} cos\psi cos\theta & (cos\psi sin\theta sin\varphi - sin\psi cos\varphi) & (sin\psi sin\varphi + cos\psi sin\theta cos\varphi) \\ sin\psi cos\theta & (cos\psi cos\varphi + sin\psi sin\theta sin\varphi) & (sin\psi sin\theta cos\varphi - cos\psi sin\varphi) \\ sin\theta & cos\theta sin\varphi & cos\theta cos\varphi \end{bmatrix} \tag{5.49}$$

$$\mathbf{F_C^G} = \mathbf{R_B^G F_C^B} = R_{z,\psi}R_{y,\theta}R_{x,\varphi} \begin{bmatrix} ma_x + m(\omega_y v_z - \omega_z v_y) \\ ma_y - m(\omega_x v_z - \omega_z v_x) \\ ma_z + m(\omega_x v_y - \omega_y v_x) \end{bmatrix} \tag{5.50}$$

The same procedure can be applied for the roll-pitch-yaw moments transformation of the rigid vehicle about the respective axes as shown in the previous discussion that can be expressed as in the Equation 5.51.

$$\mathbf{M_C^G} = \mathbf{R_B^G M_C^B} \tag{5.51}$$

Where:

- $\mathbf{M_C^G}$-global roll-pitch-yaw moments.
- $\mathbf{R_B^G}$-the transformation matrix.
- $\mathbf{M_C^B}$-local roll-pitch-yaw moments that are expressed in Equation 5.45, Equation 5.47 and Equation 5.47 .

.

5.2.3 3D Mass-spring-damper Model

A 3D Mass-spring-damper model is shown in the Figure 5.10. It consist of a spring of elastic coefficient value $K_x[N/m]$, which is in parallel connection with a damper of damping coefficient

value $C_x[Ns/m]$ to a mass with $m[kg]$ in the X-axis direction. Another pair of spring of elastic coefficient value $K_y[N/m]$, which is in parallel connection with a damper of damping coefficient value $C_y[Ns/m]$ to the mass with $m[kg]$ in the Y-axis direction. The third spring-damper pair is in the Z-axis direction connected in parallelt to the same mass. This simple model can be used to represent the vehicle to barrier or vehicle to vehicle collisions.

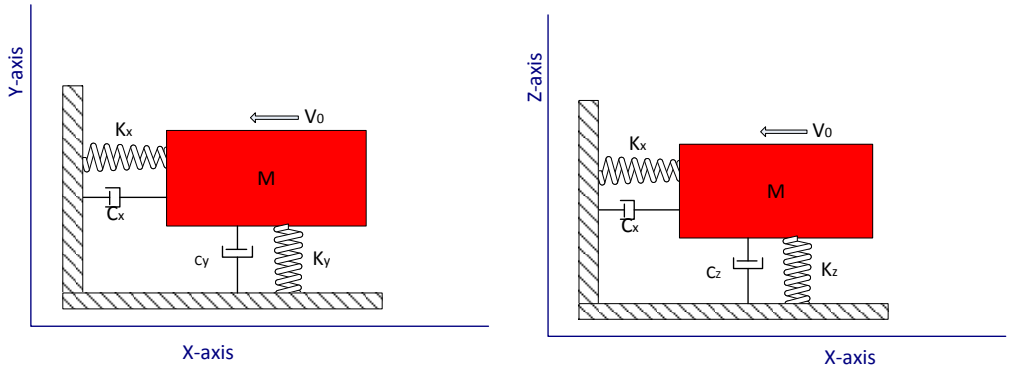

FIGURE 5.10: *3D Vehicle to barrier collision mass-spring-damper model .*

The mass-spring-damper model representation of the rigid vehicle will be accurate if all the motions and constraints are considered and applied properly. The mass-spring-damper (see Figure 5.10) system has six degree of freedom with its translational motion described by the coordinates X and Y in the horizontal plane and vertical Z-axis as well as the three rotational degrees of freedom about the longitudinal (X-axis), lateral (Y-axis) and vertical (Z-axis). The vehicle model has initial velocity in the X-axis direction as represented.

Equation of Motion

The governing equations of motion can be obtained by considering the force balance along the respective axis motions. A good knowledge of the resultant force components can be obtained from Figure 5.7. Making use of the mass-spring-damper model in the Figure 5.10 and assuming the component of the resultant force acting on the mass in the X-axis direction (F_X), the relationship shown in Equation 5.52 can be presented. Similarly, assuming the component of the resultant force acting on the mass(m) in the Y-axis direction (F_Y), the relationship in shown Equation 5.53 can also be presented. Lastly, assuming the component of the resultant force acting on the mass in the Z-axis direction (F_Z), the relationship in shown Equation 5.54 can be presented.

$$F_X = -C_x\dot{x} - K_x x \tag{5.52}$$

$$F_Y = -C_y\dot{y} - K_y y \tag{5.53}$$

$$F_Z = -C_z\dot{z} - K_z z \tag{5.54}$$

Where:

- F_X ,F_Y, and F_Z are the components of the respective resultant force components acting on the mass(m) along the X-axis, Y-axis and z-axis directions of the model.
- x , y and z are the respective displacements along the X-axis,Y-axis and Z-axis directions of the model.
- $\dot{x}$, $\dot{y}$ and $\dot{z}$ are the respective velocities along the X-axis, Y-axis and Z-axis directions of the model.
- The initial velocity in the X, Y and Z directions of global reference frame are $Vx_0 = 35km/h = 9.72m/s$, $Vy_0 = 0km/h$ and $Vz_0 = 0km/h$.
- K_x , K_y and K_z are the respective spring stiffness along the X-axis, Y-axis and Z-axis directions.
- C_x , C_y and C_z are the respective damping coefficient along the X-axis, Y-axis and Z-axis directions.

Making use of the relationships in the Equation 5.41, Equation 5.50, Equation 5.52, Equation 5.53 and Equation 5.54 it is possible to derive a relationship below shown in Equation 5.55. All of the equations parameters below are described in previous equations.

$$\mathbf{F_C^G} = \mathbf{R_B^G F_C^B} = R_{z,\psi}R_{y,\theta}R_{x,\varphi}\begin{bmatrix} ma_x + m(\omega_y v_z - \omega_z v_y) \\ ma_y - m(\omega_x v_z - \omega_z v_x) \\ ma_z + m(\omega_x v_y - \omega_y v_x) \end{bmatrix} = \begin{bmatrix} -C_x v_x - K_x x \\ -C_y v_y - K_y y \\ -C_z v_z - K_x z \end{bmatrix} \tag{5.55}$$

where:

$$R_{z,\psi}R_{y,\theta}R_{x,\varphi} = \begin{bmatrix} cos\psi cos\theta & (cos\psi sin\theta sin\varphi - sin\psi cos\varphi) & (sin\psi sin\varphi + cos\psi sin\theta cos\varphi) \\ sin\psi cos\theta & (cos\psi cos\varphi + sin\psi sin\theta sin\varphi) & (sin\psi sin\theta cos\varphi - cos\psi sin\varphi) \\ sin\theta & cos\theta sin\varphi & cos\theta cos\varphi \end{bmatrix} \tag{5.56}$$

The equations can be rewritten for the X-axis direction as in Equation 5.57, for the Y-axis direction as in Equation 5.58 ,and for the Z-axis direction as in Equation 5.59.

$$\begin{aligned} &cos\psi cos\theta(ma_x + m(\omega_y v_z - \omega_z v_y)) + (cos\psi sin\theta sin\varphi - sin\psi cos\varphi)(ma_y - m(\omega_x v_z \\ &-\omega_z v_x)) + (sin\psi sin\varphi + cos\psi sin\theta cos\varphi)(ma_z + m(\omega_x v_y - \omega_y v_x)) + C_x v_x + K_x x = 0 \end{aligned} \tag{5.57}$$

$$sin\psi cos\theta(ma_x + m(\omega_y v_z - \omega_z v_y)) + (cos\psi cos\varphi + sin\psi sin\theta sin\varphi)(ma_y - m(\omega_x v_z - \omega_z v_x)) + (sin\psi sin\varphi + cos\psi sin\theta cos\varphi)(ma_z + m(\omega_x v_y - \omega_y v_x)) + Cv_y + Ky = 0 \tag{5.58}$$

$$sin\theta(ma_x + m(\omega_y v_z - \omega_z v_y)) + cos\theta sin\varphi(ma_y - m(\omega_x v_z - \omega_z v_x) + cos\theta cos\varphi(ma_z + m(\omega_x v_y - \omega_y v_x)) + C_z v_z + K_x z = 0 \tag{5.59}$$

5.2.4 Parameter Estimation and Model Establishment

Parameter identification is a critical part of mathematical modeling to represent the crash scenario. The spring stiffness and viscous damping coefficients should be systematically identified to use the lumped parameter modeling (LPM) and make simulations for comparison between the real data and the model established.

The parameters identification for the 3D is similar to identification of parameter for the planar dynamics model. To make correct estimation of parameters the data acquired from the experiment should be complete to apply the solution method. The Linear Equations System Method or Total Least Square method can be used if the all the necessary data are acquired from the experiment at the beginning or while making the vehicle crash test. However, there are missing data for roll rate or rotational speed about the X-axis(longitudinal axis of the car) that is represented by ω_x in the Equation 5.58 and Equation 5.59. The pitch rate or the rotational speed about the Y-axis(lateral-axis) that is represented by ω_y in the Equation 5.57 and Equation 5.57 is also missing from the obtained data. The measurements for these two angular speed are not taken during the experiment.

The hole in the provided data made it difficult to find the respective parameters and to make the complete analysis of the data for the 3D mathematical modeling without making a rough assumption. The complete and accurate 3D mathematical modeling can only be made by considering the missing data. The value for the roll-rate and pitch-rate measurments are made similar to the measured yaw-rate by minor modifications. The ptich-angle and yaw-angle measurments are found from the integration of the respective angular-rates.

Chapter 6

Simulation Results

6.1 2D Analysis of the kinematics of the impacting vehicle in the global frame

In the fourth chapter of this report an extensive signal analysis have been made for the vehicle in the local frame attached to the rigid vehicle at its center of gravity. In contrary for this section, the local frame kinematics is required to be transformed into global frame using the transformation matrix as explained in the planar dynamics subsection. The graph for the global representation of the vehicle kinematics are shown in Figure 6.2 for the data in the X-axis direction. The initial position of the center of gravity from the center of global frame is calculated to be $L = -1.54m$ in X-axis direction and $W = -0.026\ m$ in the Y-axis direction. The global reference frame is assumed to be at front part of the car as shown in the Figure 6.1. The graph in Figure 6.3 shows the global vehicle kinematics in the Y-axis direction. The calculation is performed for both coordinates using the global acceleration equation of motion of the vehicle which is expressed in Equation 5.6.

6.2 2D Model Simulation and Comparison of the Model and real data of Vehicle Crash

2D mathematical modeling of the vehicle to barrier collision has been carried out and it has been presented in section 5.1. The next step is to implement the model in MATLAB Simulink and making the simulation of the model for verification. The figure of Simulink model for 2D model of the vehicle crash looks like as depicted in Figure 6.4.

The acceleration data from the accelerometer in the longitudinal and lateral directions as well as the yaw rate are used in obtaining the values of spring stiffness and the damping coefficients. By integrating car's deceleration, we obtain plots of velocity and displacement respectively. The global reference kinematic analysis of the collision is shown in the Figure 6.2 and Figure 6.3. The

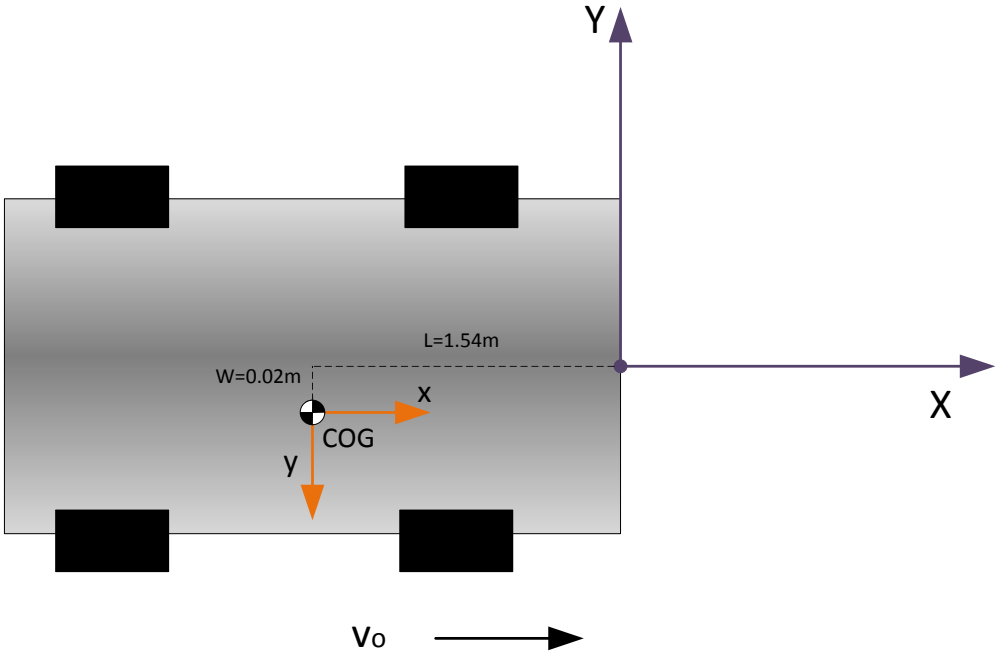

FIGURE 6.1: *Vehicle moving in the global reference frame.*

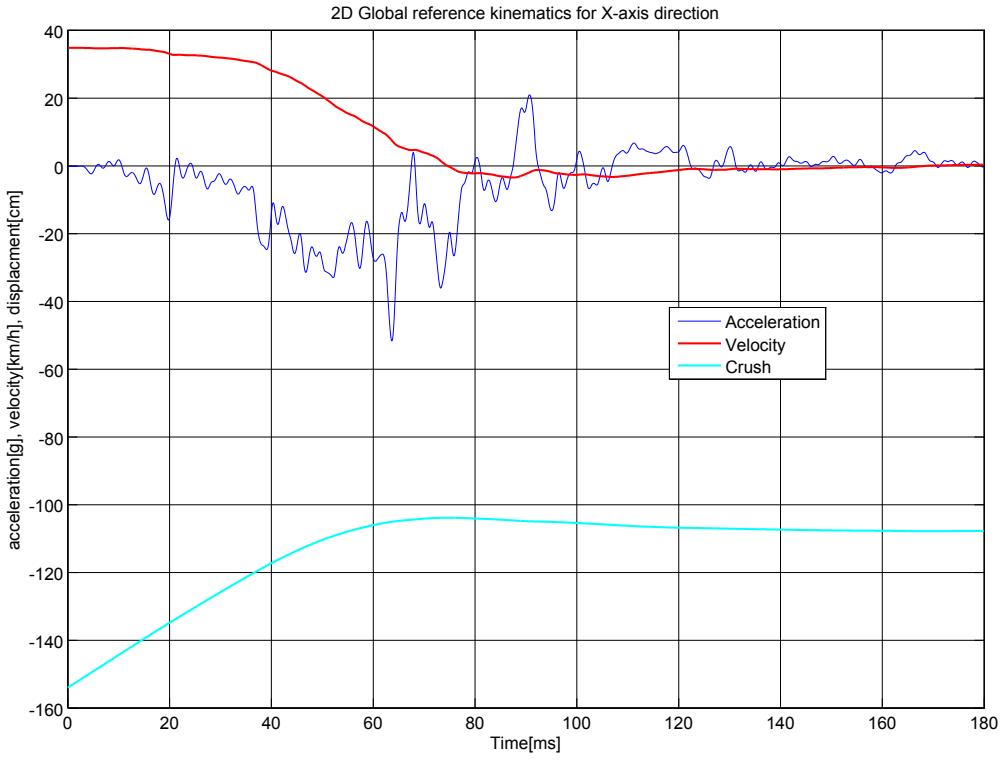

FIGURE 6.2: *2D Reference data in global frame for X-axis direction.*

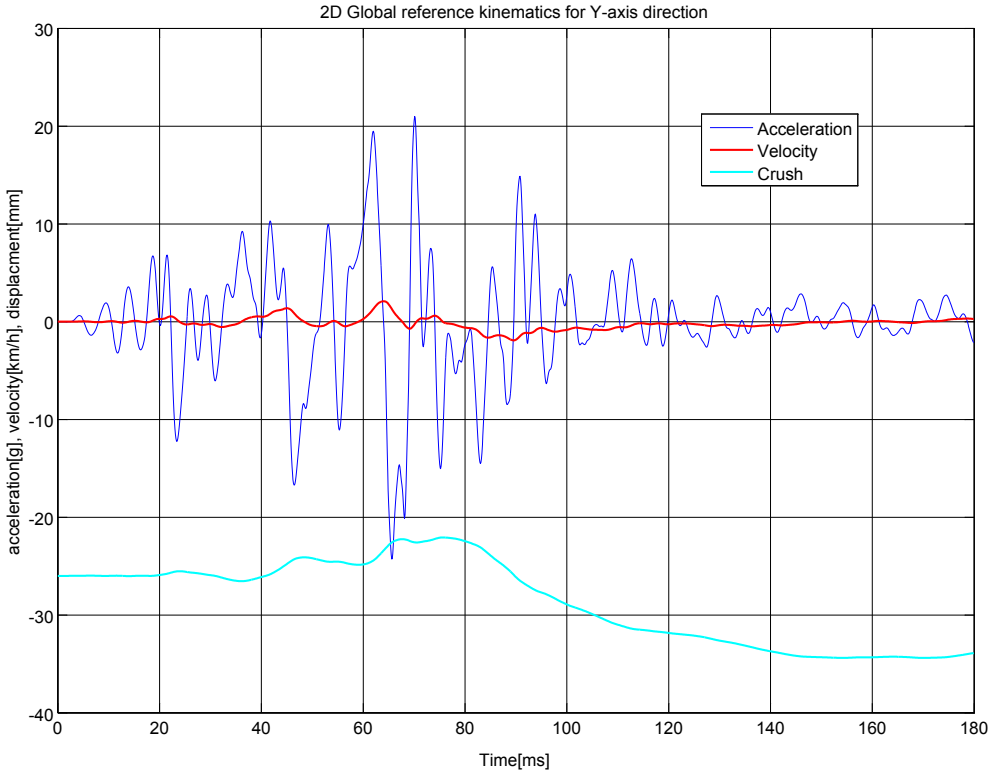

FIGURE 6.3: *2D Reference data in global frame for Y-axis direction.*

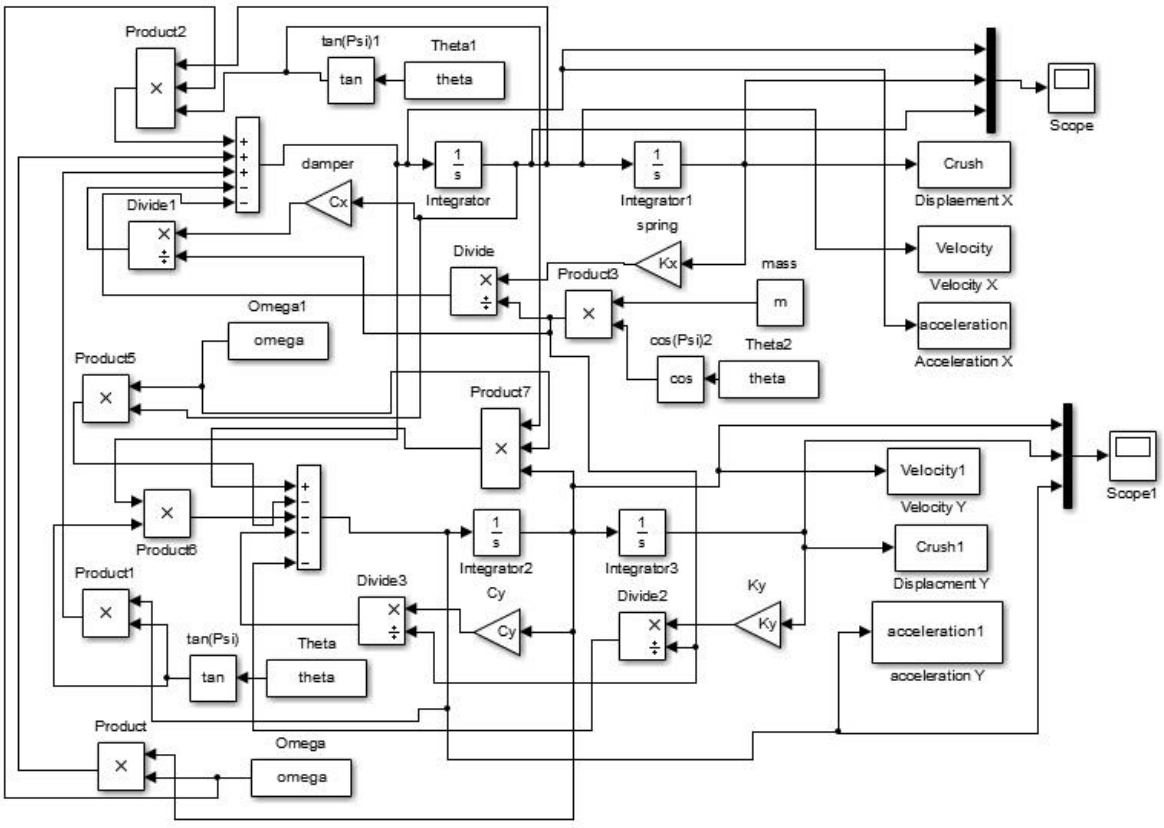

FIGURE 6.4: *2D Simulink Model for Vehicle to Barrier collision.*

calculation is performed using the global acceleration equation of motion of the vehicle which is expressed in Equation 5.6.

The complete two-dimensional model that is used to reproduce the described crash test was shown in the Figure 5.4. The center of gravity(COG) of the system model is assumed to be located at exactly the same position as the car's COG and the global coordinate system of the model is exactly the same as the global reference frame of the vehicle crash which is shown in Figure 6.1.

The known parameters of the model are: mass $m = 873[kg]$ -the same as the vehicle's mass, X-axis direction initial impact velocity component $V_x = 35$ $[km/h]$, and Y-direction initial impact velocity component $V_y = 0$ $[km/h]$. The unknown structural parameters: K_x, C_x, K_y, and C_y are all determined by using the techniques of identifying the parameter which was described in the parameter estimation subsection 5.1.4. The parameters values are determined to be:
X-direction spring stiffness:$K_x = 14,667$ $[N/m]$;
X-direction damping coefficient: $C_x = 1,930$ $[Ns/m]$;
Y-direction spring stiffness:$K_y = 469,750$ $[N/m]$;
Y-direction damping coefficient: $C_y = 254,000$ $[Ns/m]$;
A modified value from the measured yaw-rate is used in the model and integrated to find the value of yaw-angle which is also used in combination with other input parameters. The model response kinematics are drawn on the same graph with the reference kinematic plots (acceleration, velocity and displacement) for comparison as shown in the Figure 6.5 for the X-axis direction. For the Y-axis direction the acceleration, velocity and displacement are shown on separate graphs.

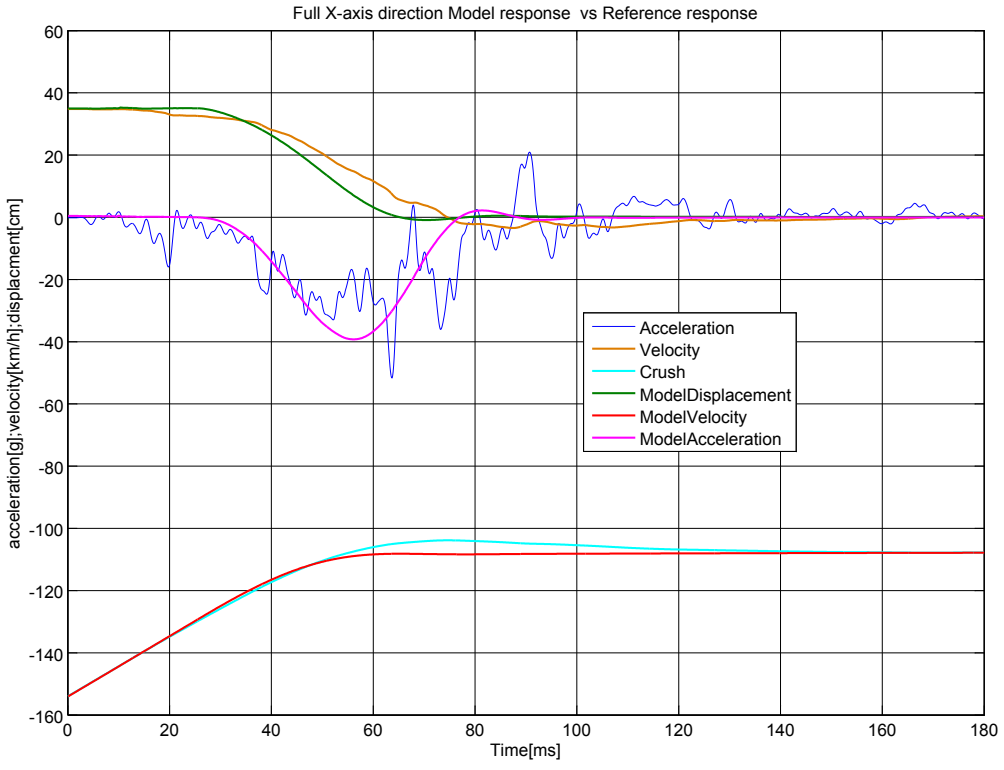

FIGURE 6.5: *2D Model response kinematics vs global frame kinematics in X-axis direction.*

For more clarity the model acceleration response vs the global reference data from vehicle crash acceleration are shown in the Figure 6.6 for the longitudinal direction, and another pair of acceleration is shown in the Figure 6.7 for the lateral direction.

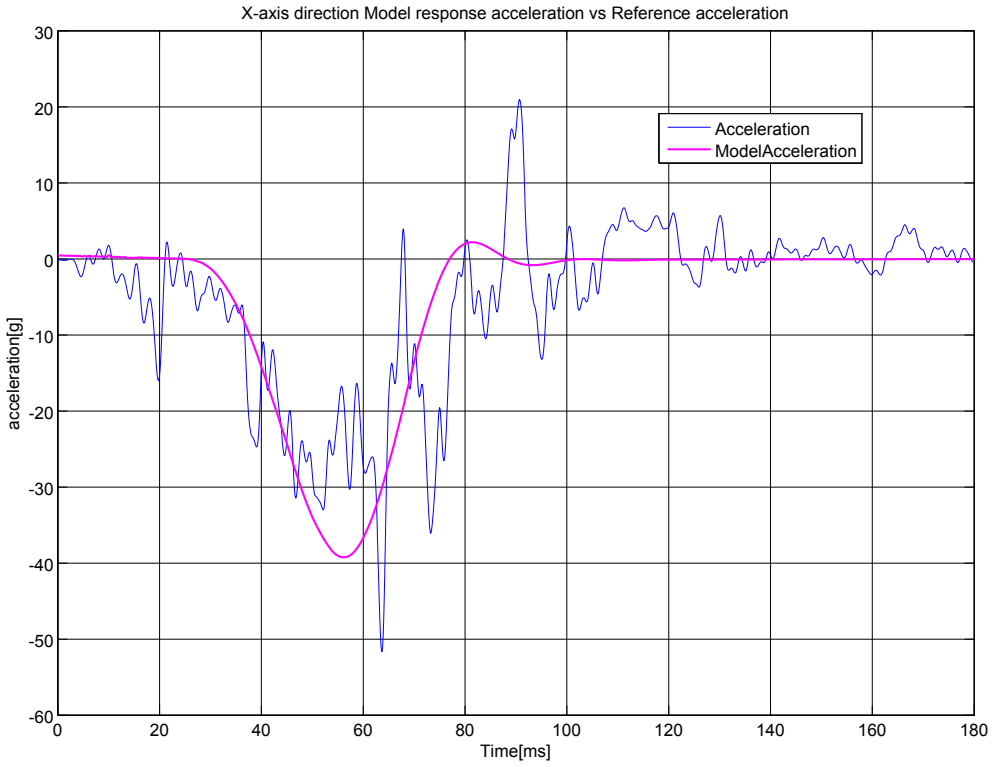

FIGURE 6.6: *2D Model response acceleration vs global frame reference acceleration in the X-axis direction.*

The velocity response of the model with the global frame velocity of the vehicle found by the integration of the global acceleration are also shown as in the Figure 6.8 for the longitudinal direction, and the other velocity pair are shown for lateral direction as in the Figure 6.9.

Lastly, the displacement response of the model and the global frame displacement or dynamic crush from real experiment are shown in the Figure 6.10 for longitudinal direction and as in the Figure 6.11 for lateral direction.

6.3 3D Model Simulation and Comparison of the Model and real data of Vehicle Crash

The derivation of mathematical model for 3D mass-spring-damper representation of the vehicle to barrier collision has been carried out and it has been presented in subsection 5.2.3. The mathematical model derived is implemented in MATLAB simulink and it looks like as shown in Figure 6.12. The subsystems in the figure has more detail model components.

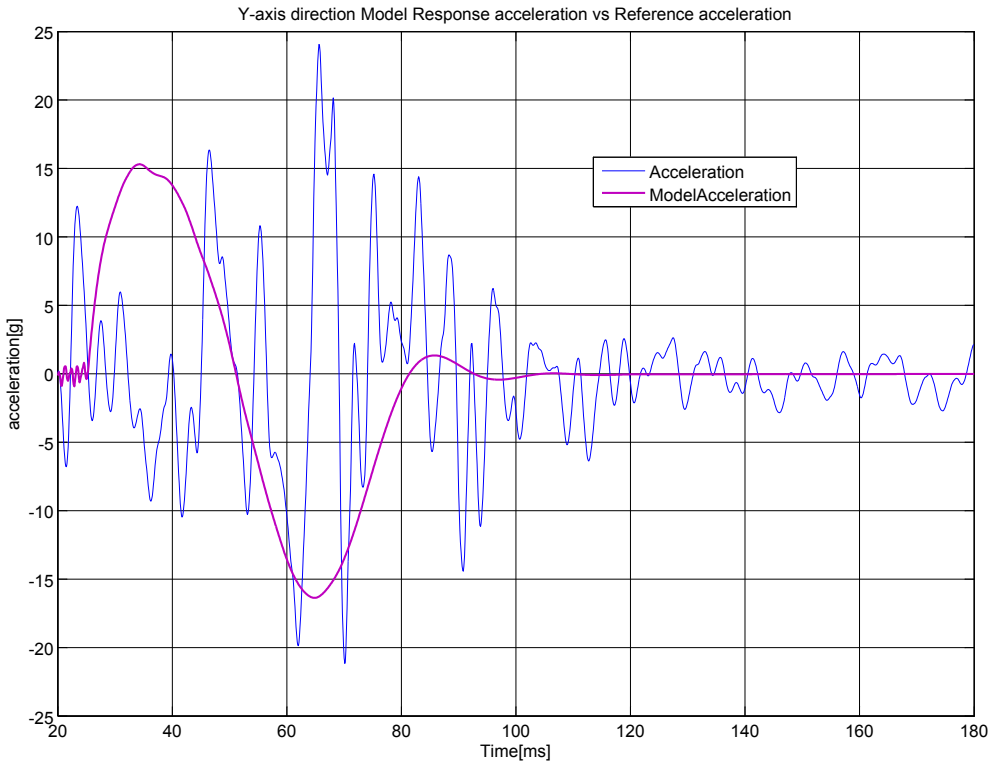

FIGURE 6.7: *2D Model response acceleration vs global frame reference acceleration in the Y-axis direction.*

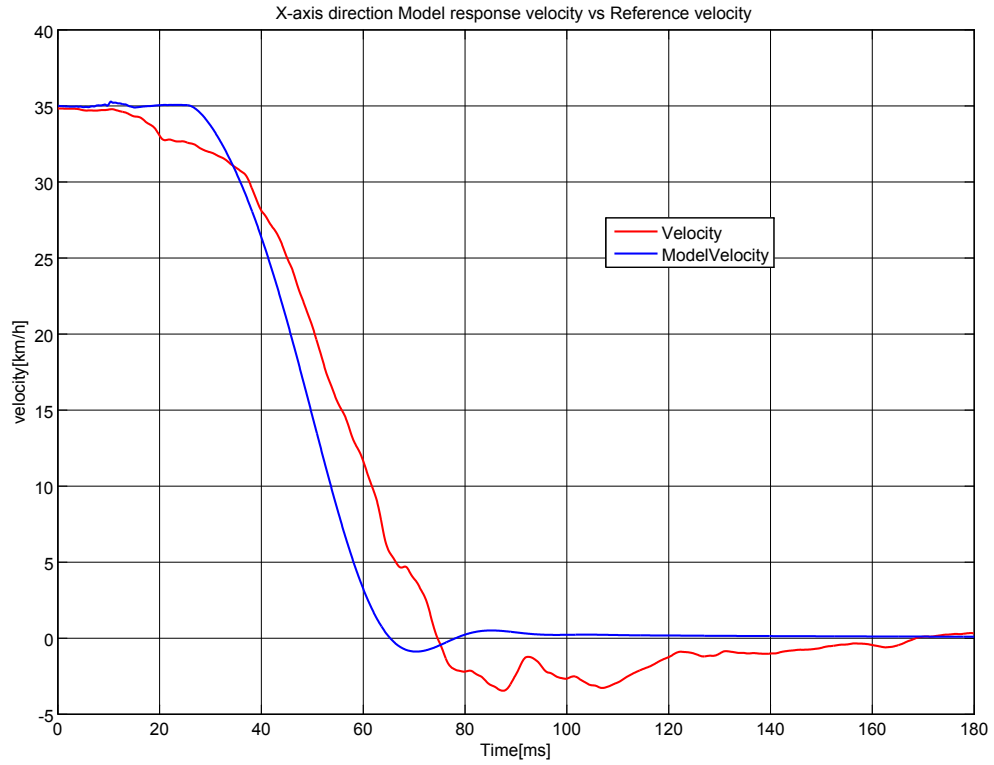

FIGURE 6.8: *2D Model response velocity vs global frame reference velocity in X-axis direction.*

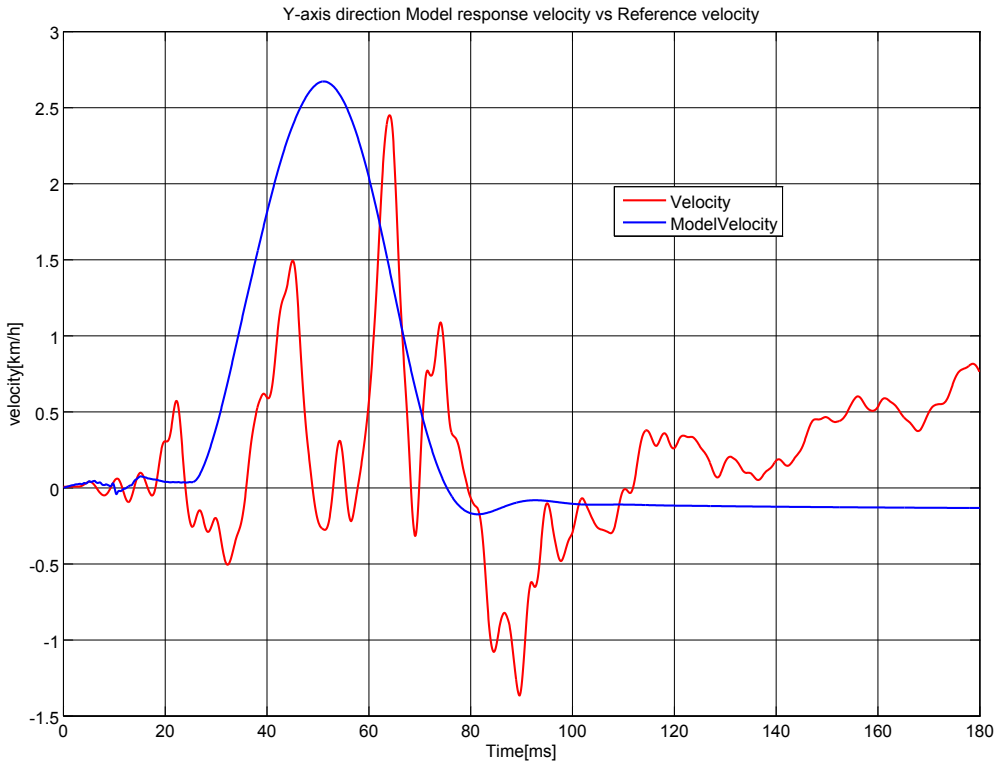

FIGURE 6.9: *2D Model velocity response vs global frame reference velocity in Y-axis direction.*

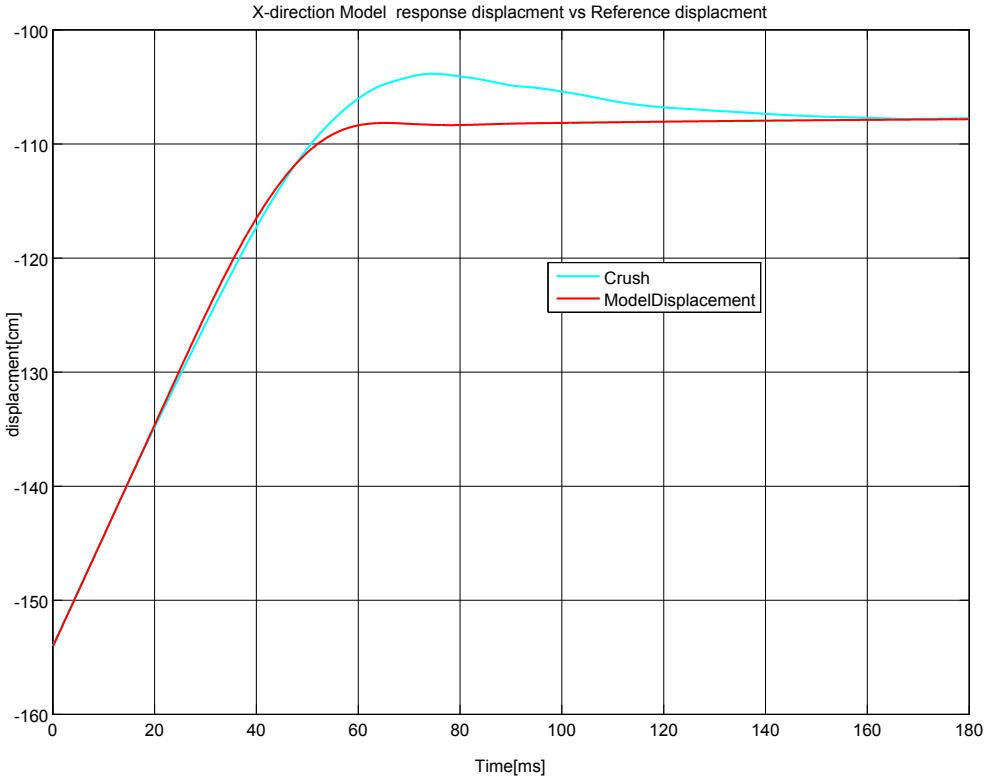

FIGURE 6.10: *2D Model response displacement vs global frame reference displacement in X-axis direction.*

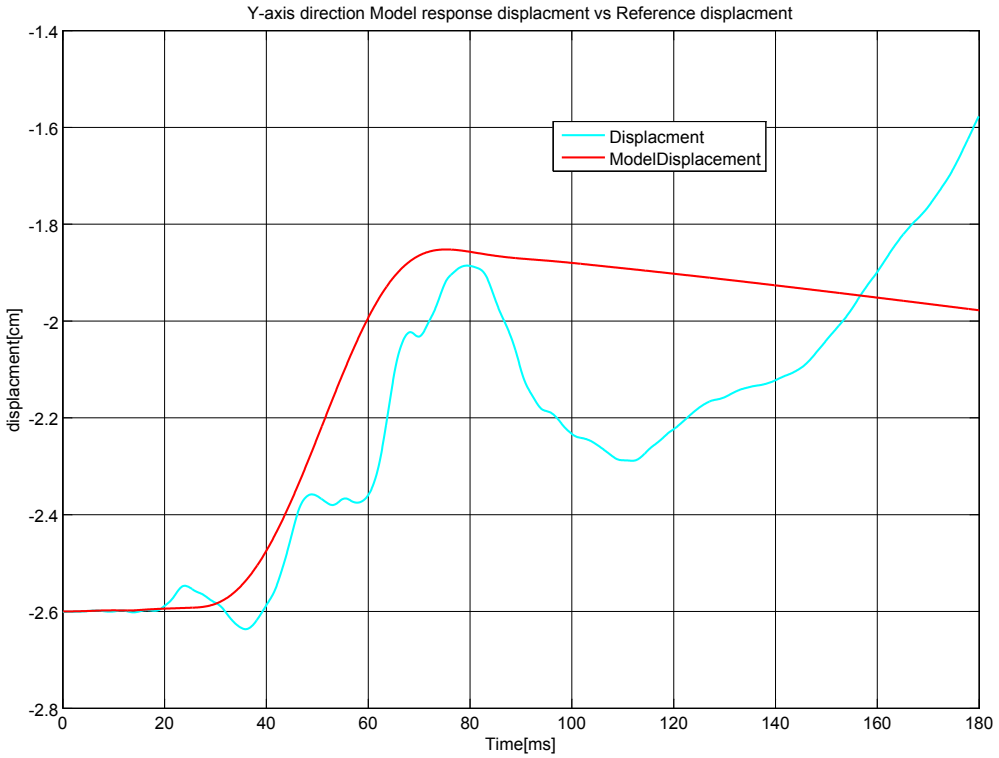

FIGURE 6.11: *2D Model response displacement vs global frame reference displacement in Y-axis direction.*

The establishment of the complete 3D model for the vehicle to barrier collision can only be made possible by considering all the angular rates (yaw-rate, pitch-rate and roll-rate), the three angular positions (yaw-angle, pitch-angle and roll-angle), the three accelerations in the X, Y and Z with the respective velocity and displacement about the longitudinal, lateral and vertical axes. However, the provided data from the vehicle crash include only the accelerations in the three axes (X, Y and Z) and yaw rate. The recorded acceleration pulses were measured in the coordinate frame associated with the car which is placed at its center of gravity. There are four missing data to make a fulfilled 3D model. The missing data are pitch-rate, pitch-angle, roll-rate and the roll-angle measurements. The measurements should have been collected during the impact test. In this section an assumption was made to estimate the missing data by making the pitch-rate and the roll-rate equivalent to the measured yaw-rate by making some minor modifications. Then the three angular position measurements are found by integrating the respective angular-rates.

After making the estimations for the missing data, the transformation matrices are used to calculate the global frame reference accelerations. The global frame reference velocity and displacement are also calculated. Then the comparison can be made between the calculated global reference kinematics and the model response kinematics to reproduce the crash event. The global coordinate frame is assumed to be at a position where the car make the first contact with the barrier as shown in Figure 6.13 for the 3D rigid vehicle. The center of gravity of the system model is assumed to be

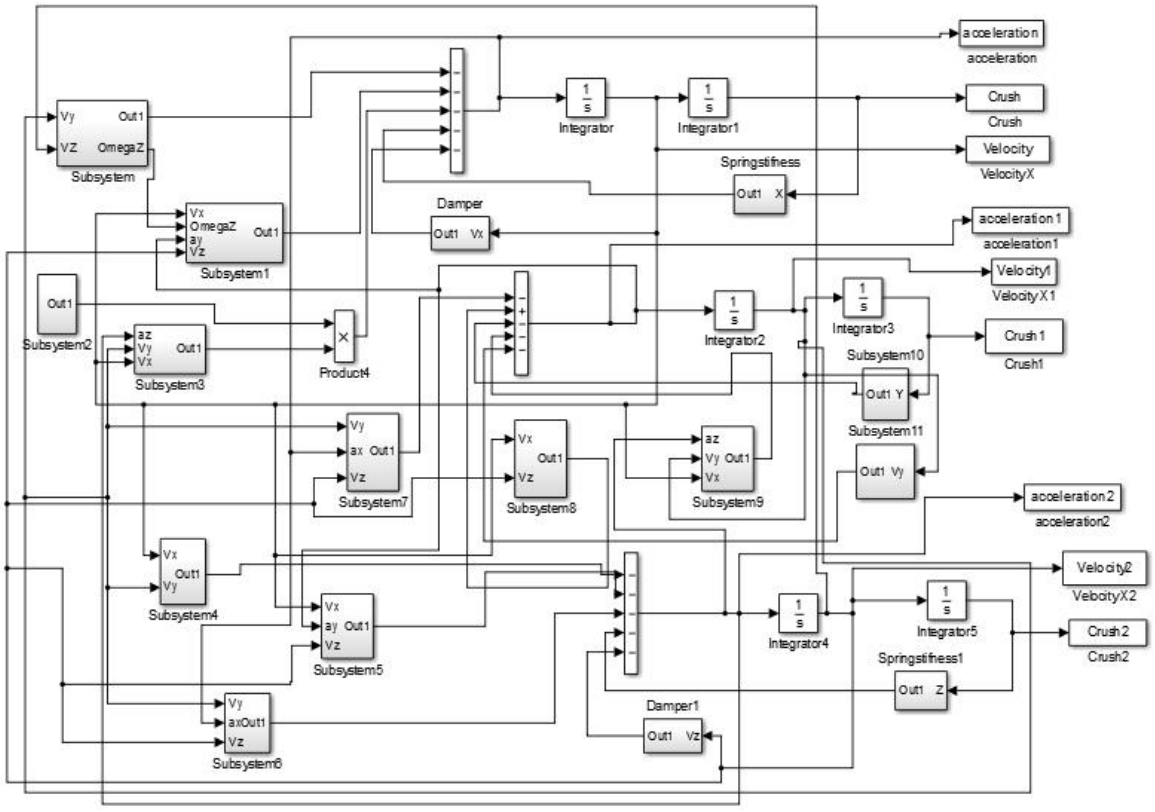

FIGURE 6.12: *Simulink model of 3D Model for Vehicle to Barrier collision.*

placed at the same position of the vehicles center of gravity. The global coordinate frame of the model is exactly the same as the global coordinate frame of the vehicle.

The known parameters of the model are: mass $m = 873[kg]$ - the same as the vehicle's mass, X-direction initial impact velocity component $V_x = 35$ $[km/h]$, Y-direction initial impact velocity component $V_y = 0$ $[km/h]$, Z-direction intial impact velocity component$V_z = 0$ $[km/h]$.

The unknown structural parameters: K_x, C_x, K_y, C_y, K_z,and C_z are all determined by using the techniques of identifying the parameter which was described in the parameter estimation subsection 5.1.4. The parameters values are determined to be:
X-direction spring stiffness:$K_x = 14,450$ $[N/m]$;
X-direction damping coefficient: $C_x = 2,672.5$ $[Ns/m]$;
Y-direction spring stiffness:$K_y = 1,560,100$ $[N/m]$;
Y-direction damping coefficient: $C_y = 5,145,600$ $[Ns/m]$;
Z-direction spring stiffness:$K_z = 11,328$ $[N/m]$;
Z-direction damping coefficient: $C_z = 158,070$ $[Ns/m]$.
The values for the roll-rate, pitch-rate are made similar value with the measured yaw-rate from the experiment to check the response of the system model. The roll-angle, pitch-angle and yaw-angle are obtained from the integration of the respective angular rates. All the six values are used in combination with the identified parameters as input to the model for obtaining the model response. The model's acceleration, velocity and displacement responses are drawn on the same graph with the reference kinematic plots (acceleration, velocity and displacement) for comparison as shown

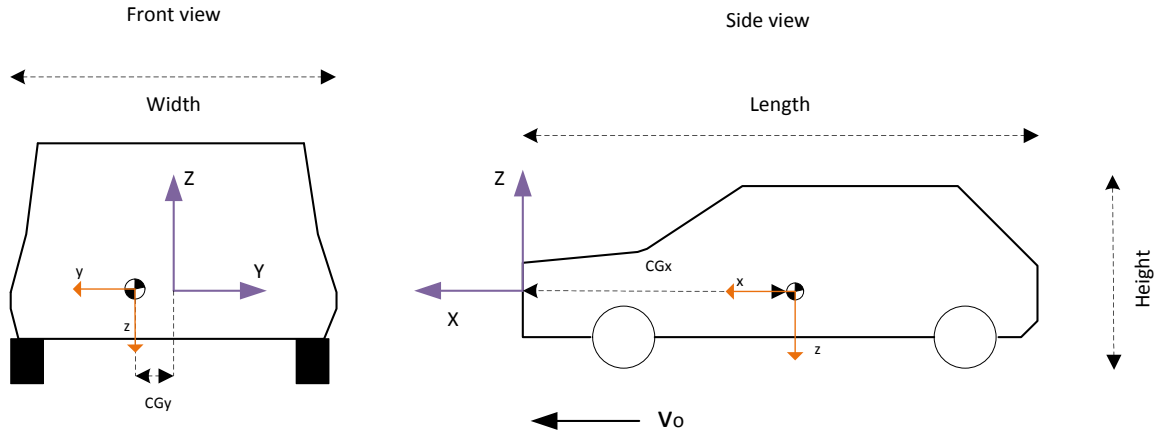

FIGURE 6.13: *The global coordinate of the vehicle in motion.*

in the Figure 6.14 for the X-axis direction. The comparison between the model response and the reference data(the acceleration, velocity and displacement) for the Y-axis and Z-axis direction are shown on separate graphs.

The acceleration response of the model and global acceleration of the reference data is shown in the Figure 6.15 for X-axis direction. The acceleration response of the model and global acceleration of the reference data is shown in the Figure 6.16 for Y-axis direction. The acceleration comparison for the model response and the real crash global acceleration is depicted in Figure 6.17 for Z-axis direction.

The velocity response of the model with the velocity from the integration of real crash acceleration are also shown as in the Figure 6.18 for the Y-axis direction. The velocity response of the model with the velocity from the integration of real crash acceleration are also shown as in the Figure 6.19 for the Y-axis direction and the other velocity pair are shown for Z-axis direction as in the Figure 6.20.

The displacement response of the model and the displacement or dynamic crush from real experiment are shown in the Figure 6.21 for X-axis direction.

Lastly,The displacement response of the model and the displacement or dynamic crush from real experiment are shown in the Figure 6.22 for Y-axis direction and as in the Figure 6.31 for Z-axis direction.

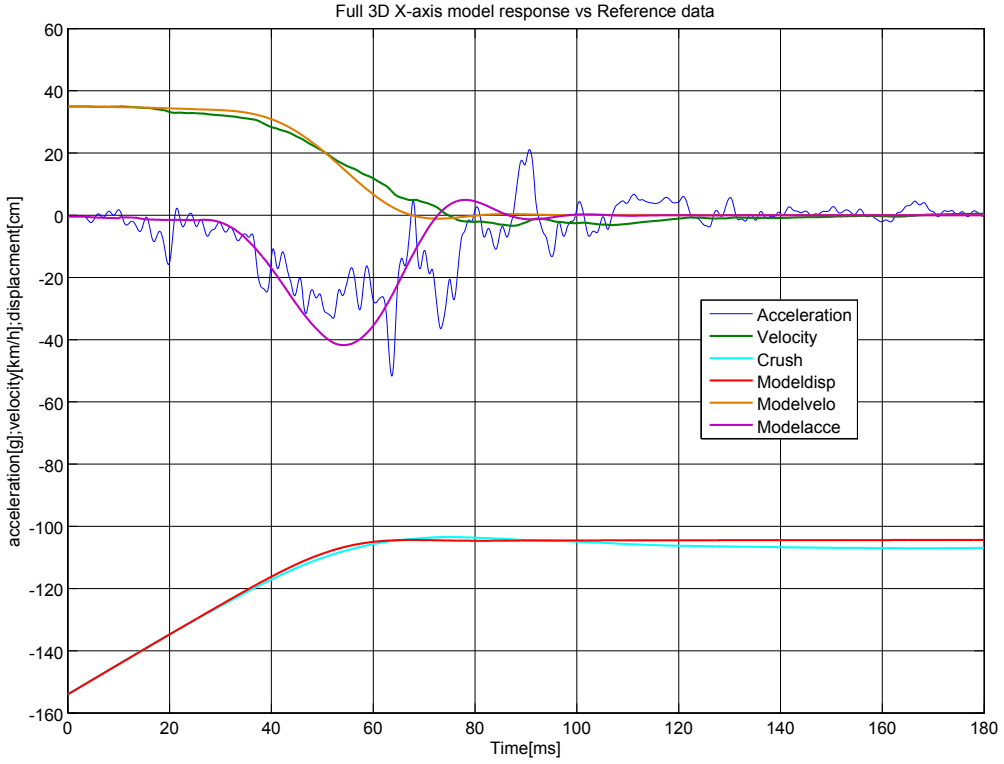

FIGURE 6.14: *3D Model response vs global frame reference kinematics in X-axis direction.*

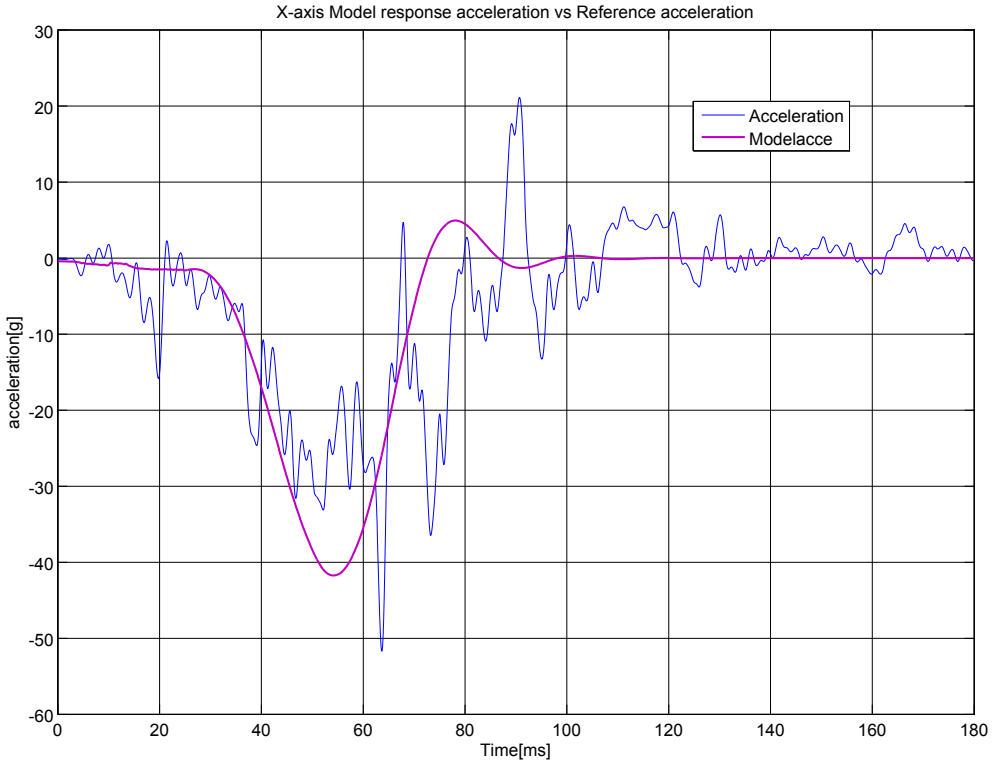

FIGURE 6.15: *3D Model acceleration response vs global frame reference acceleration in X-axis direction.*

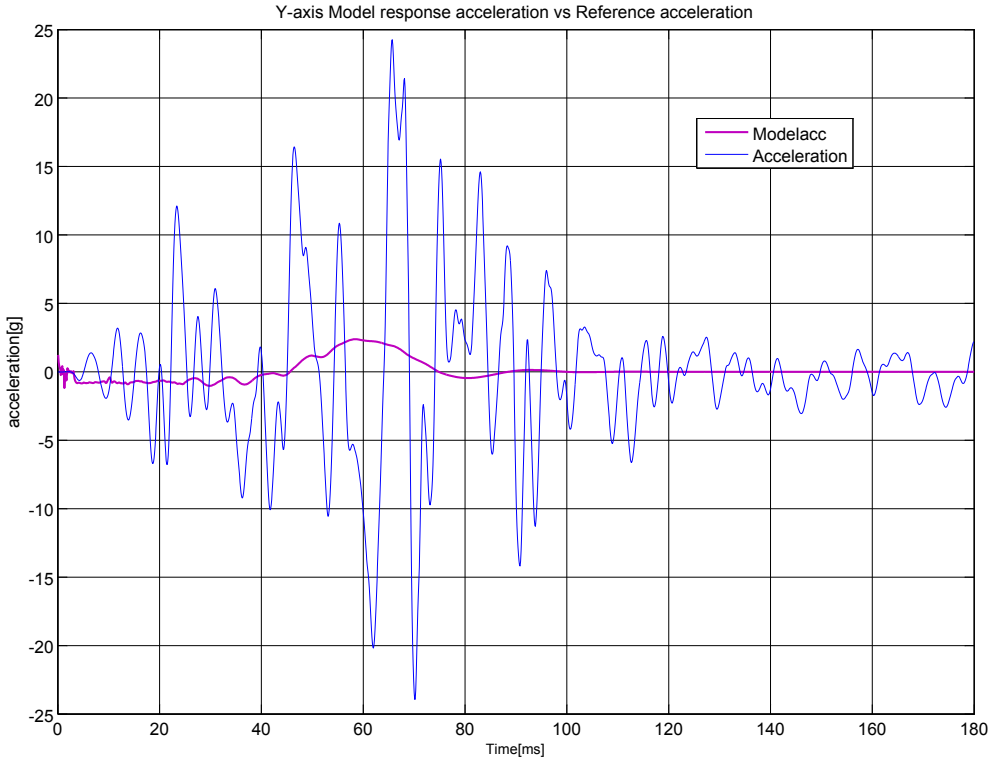

FIGURE 6.16: *3D Model acceleration response vs global frame reference acceleration in Y-axis direction.*

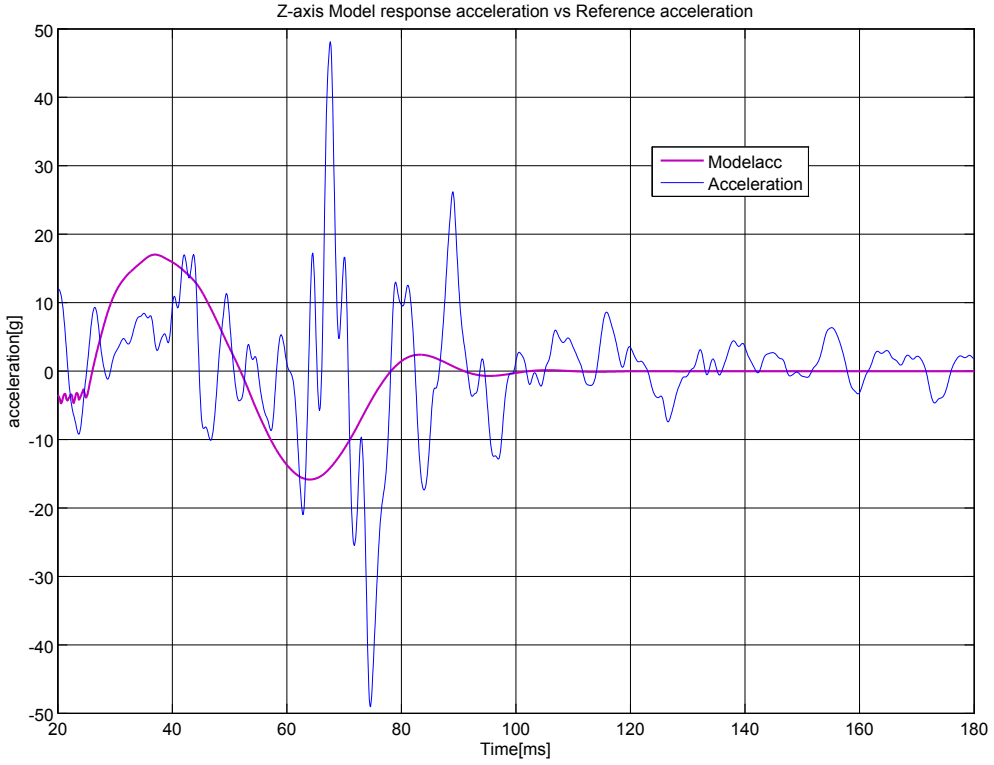

FIGURE 6.17: *3D Model acceleration response vs global frame reference acceleration in Z-axis direction.*

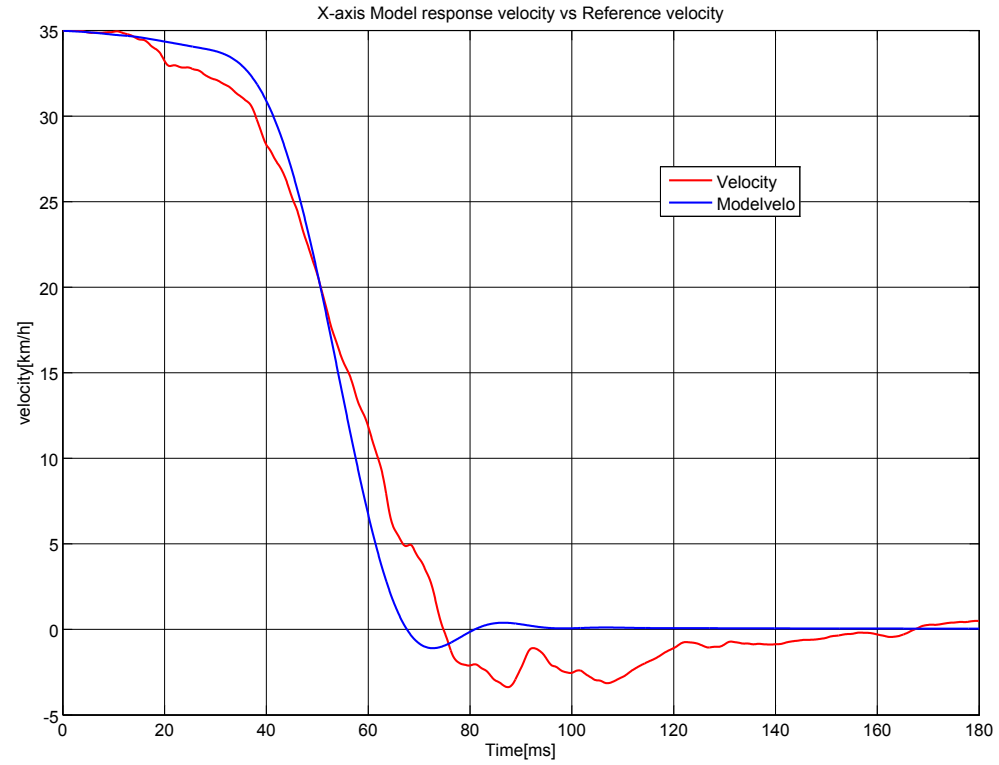

FIGURE 6.18: *3D Model velocity response vs global frame reference velocity in X-axis direction.*

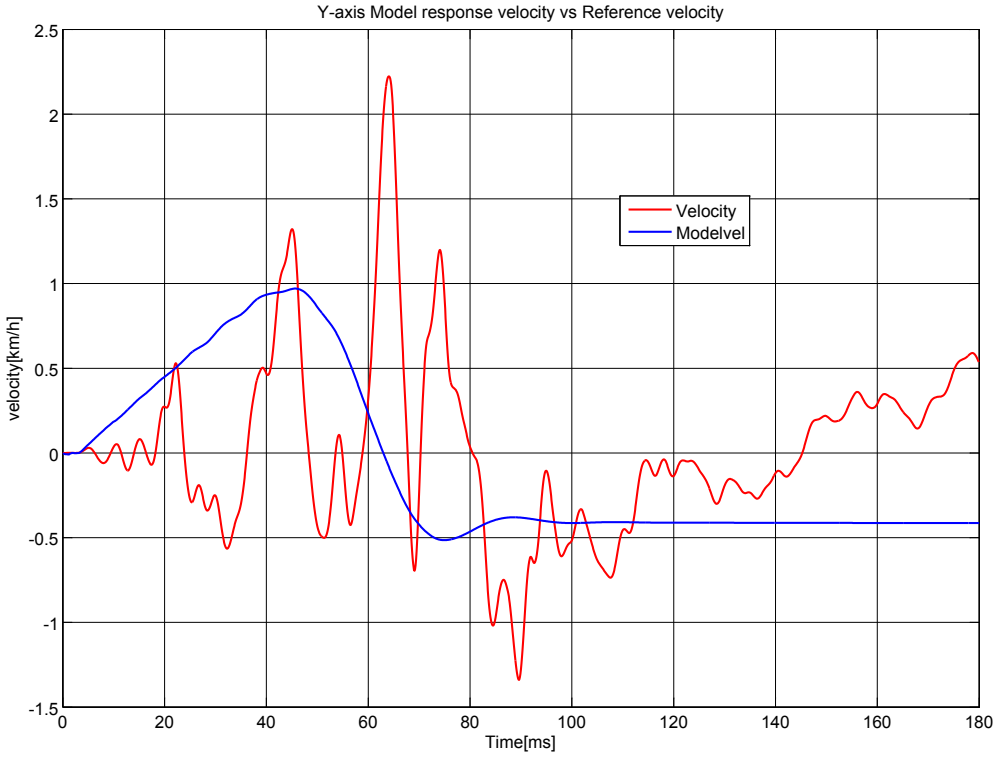

FIGURE 6.19: *3D Model velocity response vs global frame reference velocity in Y-axis direction.*

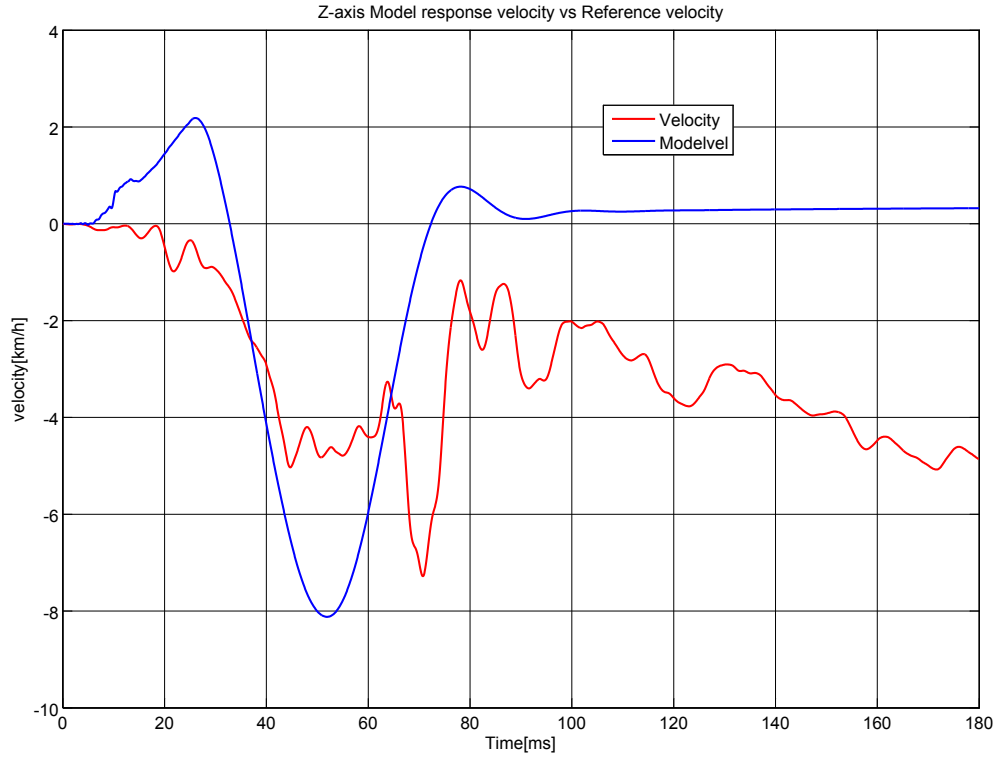

FIGURE 6.20: *3D model velocity response vs global frame reference velocity in Z-axis direction.*

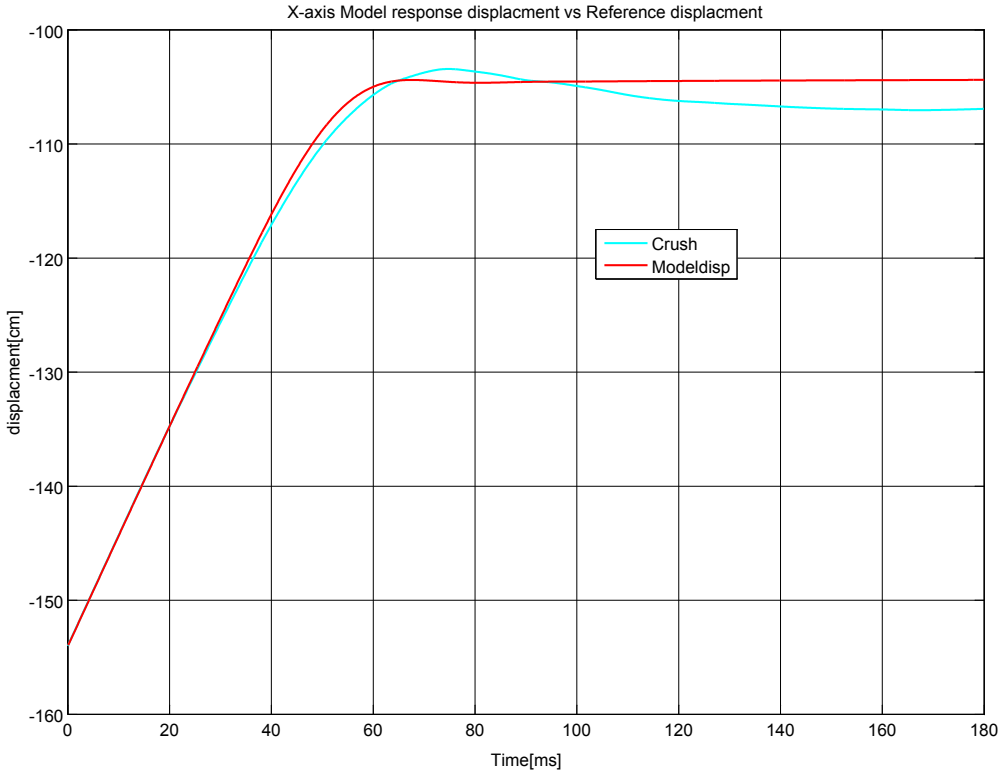

FIGURE 6.21: *3D Model displacement response vs global frame reference displacement in X-axis direction.*

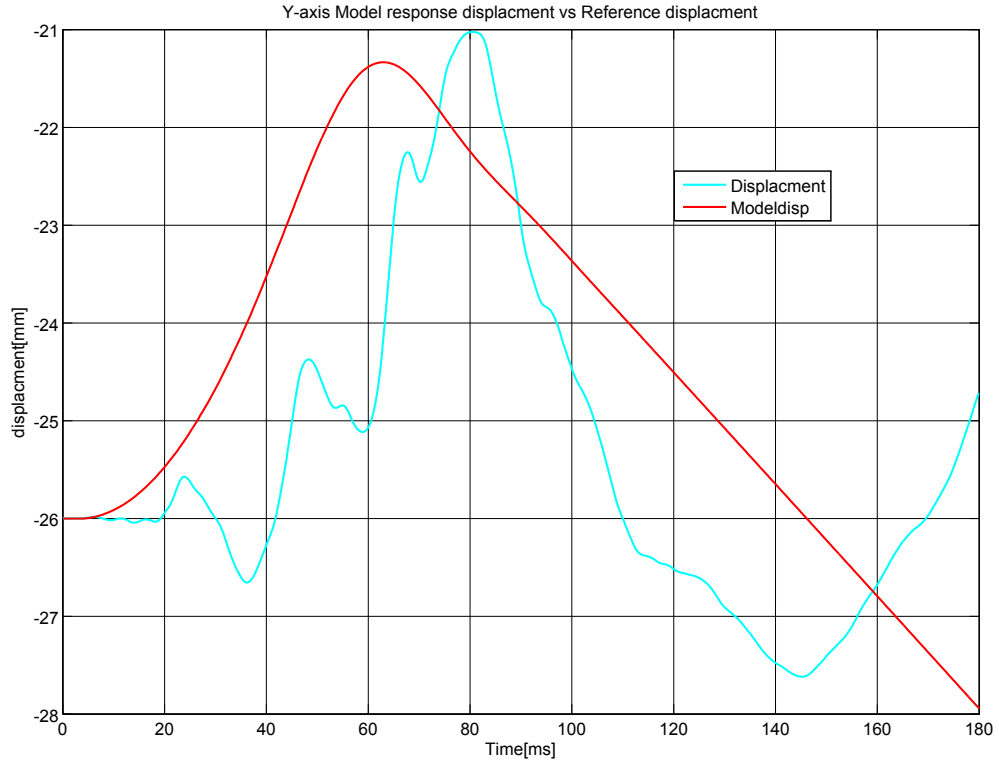

FIGURE 6.22: *3D Model displacement response vs global frame reference displacement in Y-axis direction.*

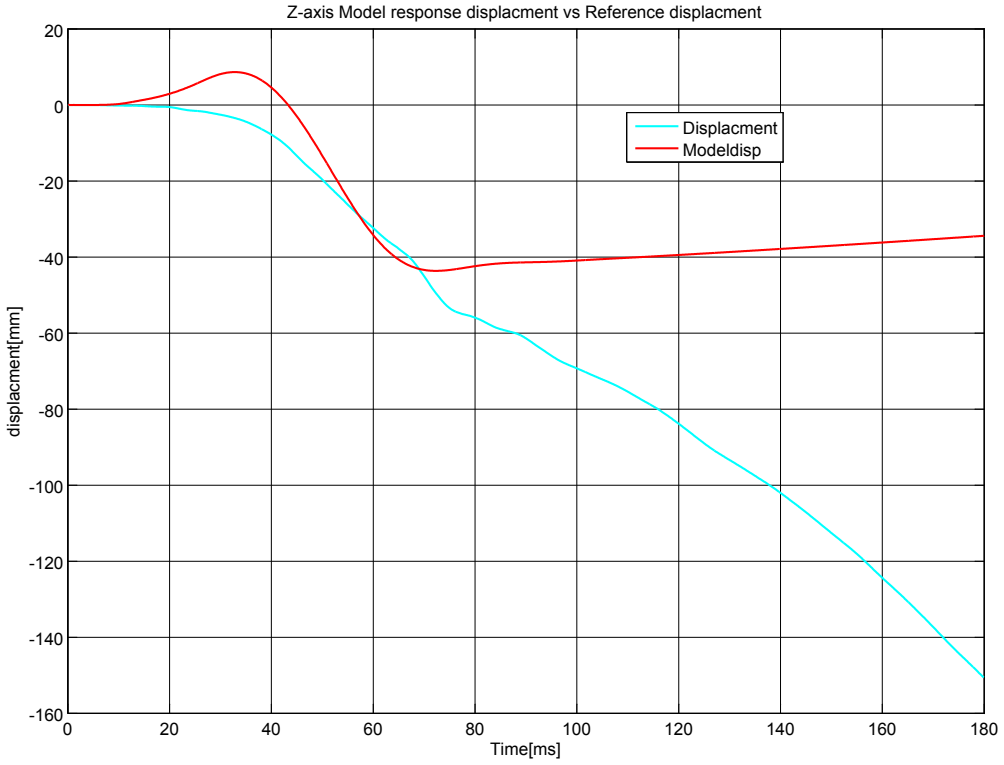

FIGURE 6.23: *3D Model displacement response vs global frame reference displacement in Z-axis direction.*

6.4 Simulation of vehicle to road safety barrier oblique collision for validation of 2D Model

6.4.1 Brief description of the experiment set-up and the vehicle information

A second vehicle to barrier collision experimental data set is provided to check the validation of the derived model. This new experiment data is from a typical high-speed vehicle to barrier oblique collision-scheme. The layout of the experimental setup is shown in the Figure 6.24. The angle of impact for the vehicle to the barrier was $\psi = 20^0$ and the initial vehicle velocity of impact was 104km/h. A belted dummy without fully loaded instrumentation was seated at driver seat and the total mass of the vehicle was determined to be 893kg including the dummy and the measuring equipments.

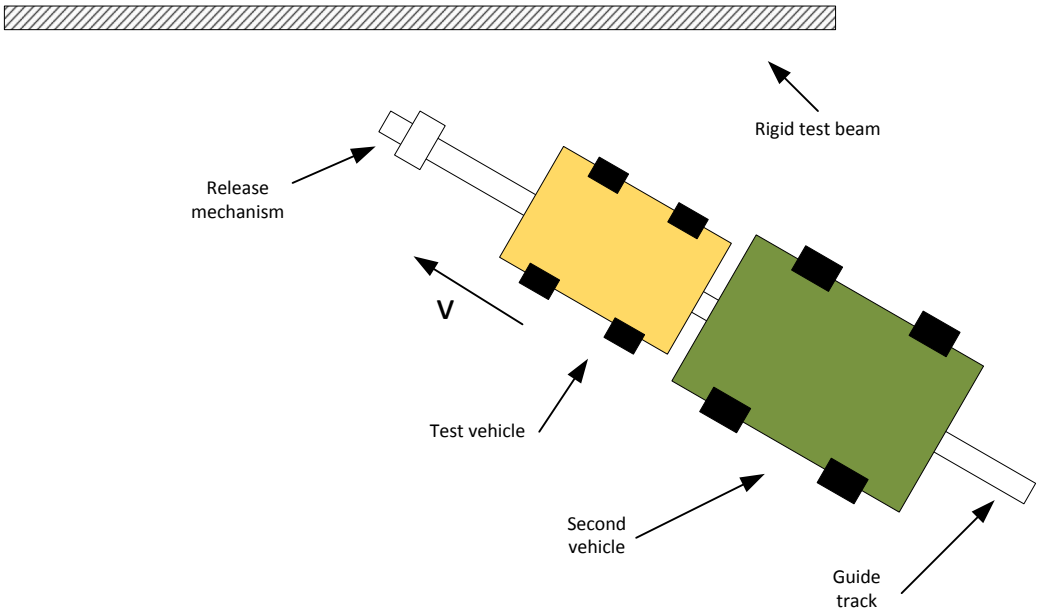

FIGURE 6.24: *Scheme of the Vehicle to road safety barrier oblique collision [9].*

A 3D accelerometer was used to record the accelerations for the test vehicles in three axes of directions (x-longitudinal, y-lateral, and z-vertical) at the center of gravity of the vehicle during the collision. A gyro meter is also used to measure the yaw-rate of the vehicle. The dimensions of the car and more important information about the test setup is described in [9].

The spring stiffness and the damping coefficients are calculated in similar procedure to the previous discussions for the 2D and 3D models. The acceleration data from the accelerometer in the longitudinal and lateral directions as well as the yaw rate are used in obtaining the values.

The complete two-dimensional model which is used to reproduce the described crash test was shown in the Figure 5.4. The center of gravity(COG) of the system model is assumed to be located at exactly the same position as the car's COG and the global coordinate system of the model is exactly the same as the global reference frame of the vehicle crash which is shown in Figure 6.25.

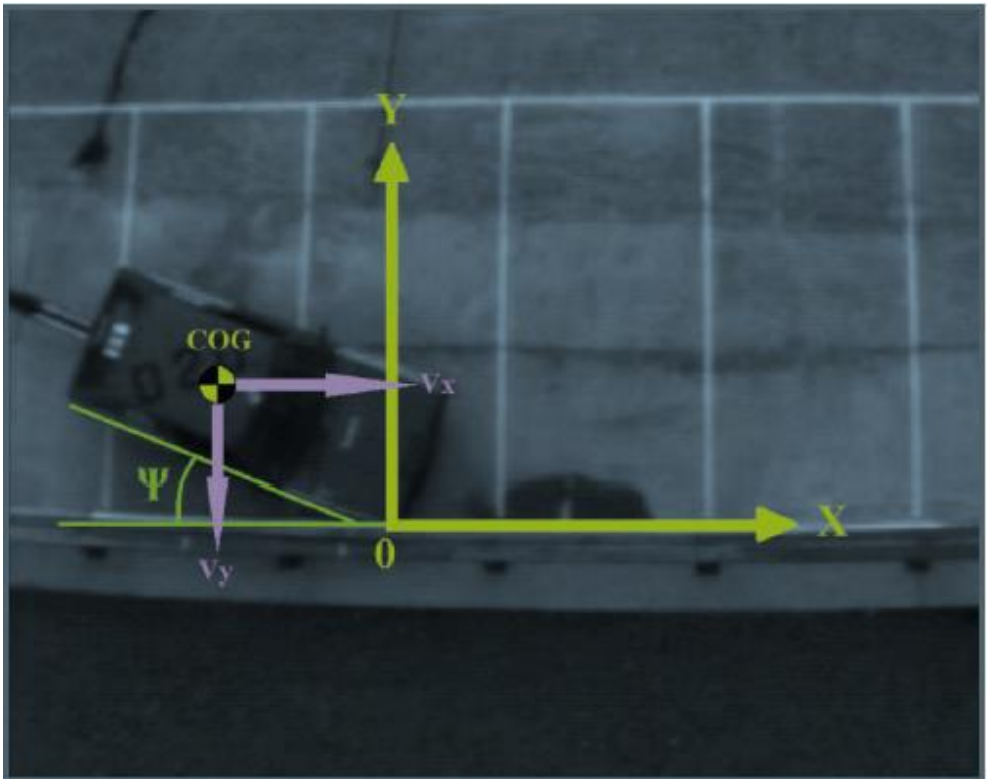

FIGURE 6.25: *The global coordinate frame for the vehicle and its COG[9].*

.

A simple trigonometric relationship is used to calculate the components of initial vehicle impact speed in the X-axis direction and Y-axis direction. The component values of the initial velocity are calculated to be:

$v_x = v_0 cos\psi = 98\ km/h,$

$v_y = v_0 sin\psi = 36\ km/h.$

6.4.2 Simulation Result for the Validation data set

The model simulation is performed using the Matlab simulink model already established and it is shown in Figure 6.4. The known parameters of the model are: mass $m = 893[kg]$ - the same as the vehicle's mass, X-direction initial impact velocity component $V_x = 98\ [km/h]$, and Y-direction initial impact velocity component $V_y = 36\ [km/h]$. The unknown structural parameters: K_x, C_x, K_y, and C_y are all determined by using the techniques of identifying the parameter which was previously described in the parameter estimation section. The parameters values are determined to be:

X-direction spring stiffness: $K_x = 1,108.7\ [N/m]$;

X-direction damping coefficient: $C_x = 2,737\ [Ns/m]$;

Y-direction spring stiffness: $K_y = 15,547\ [N/m]$;
Y-direction damping coefficient: $C_y = 5,869.1\ [Ns/m]$.

The measured yaw-rate is used in the model and it is integrated to find the value of yaw-angle which is also used in combination with other input parameters. The model acceleration response vs the global reference data from vehicle crash acceleration are shown in the Figure 6.26 for the longitudinal direction and in the Figure 6.27 for the lateral direction.

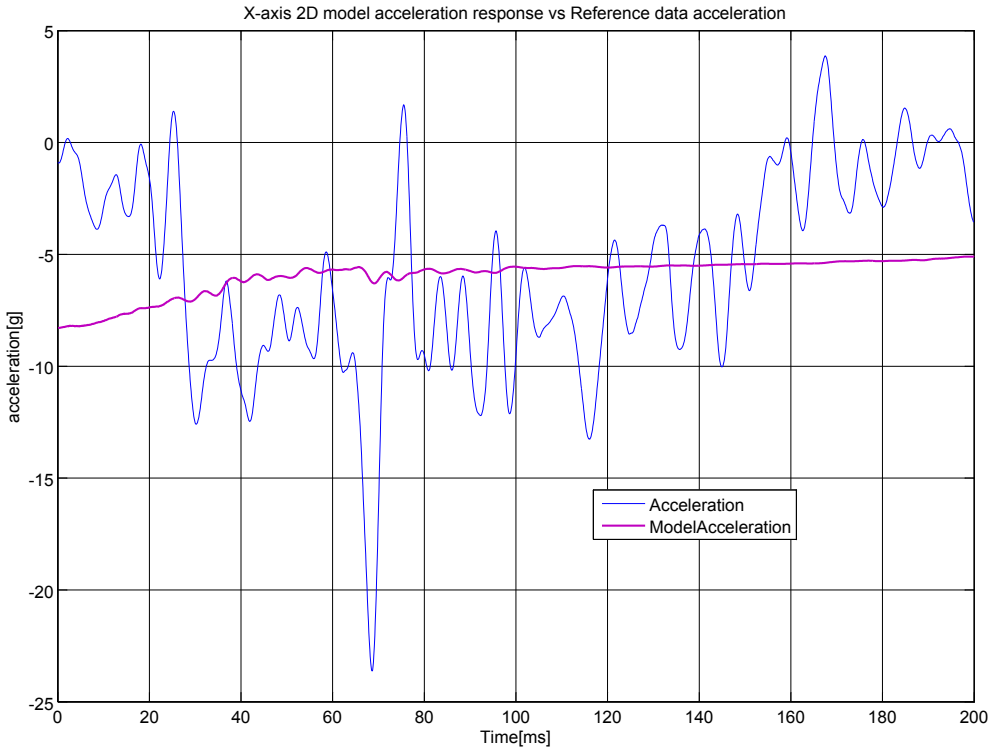

FIGURE 6.26: *2D Model acceleration response vs Oblique collision global frame reference acceleration in X-axis.*

The velocity response of the model and the global frame reference velocity of the oblique collision of the vehicle are also shown as in the Figure 6.28 for the longitudinal direction, and the other velocity pair are shown for lateral direction as in the Figure 6.29.

Finally, the displacement response of the model and the displacement of global frame reference of the oblique collision are shown in the Figure 6.30 for X-axis direction and as in the Figure 6.31 for Y-axis direction.

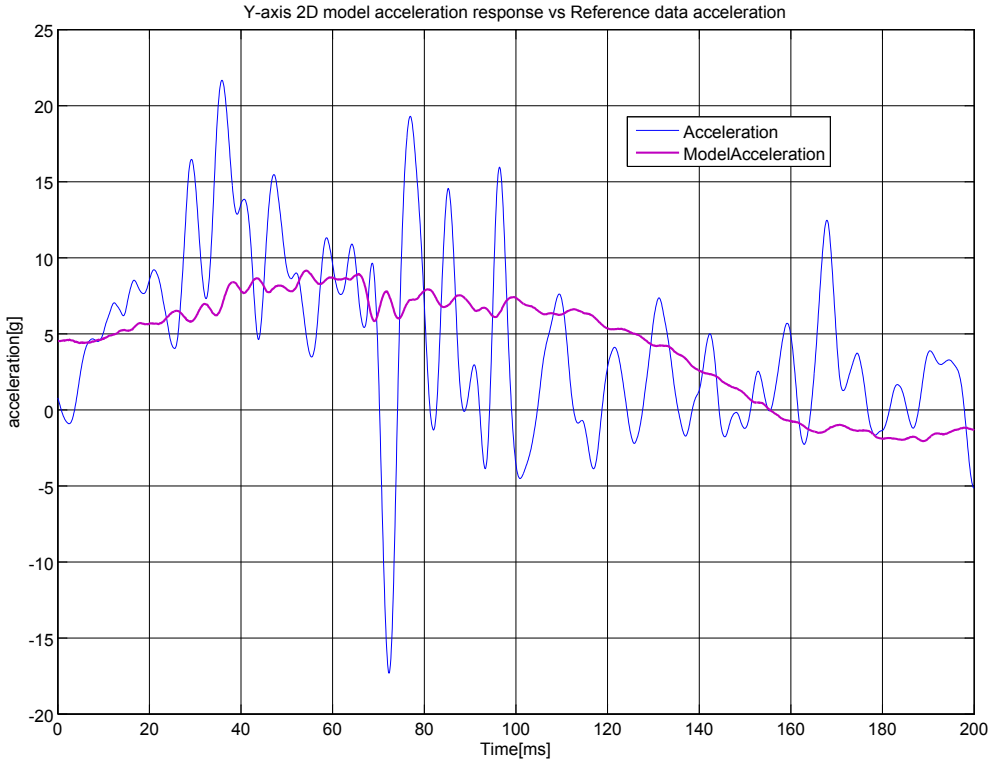

FIGURE 6.27: *2D Model acceleration response vs Oblique collision global frame reference acceleration in Y-axis.*

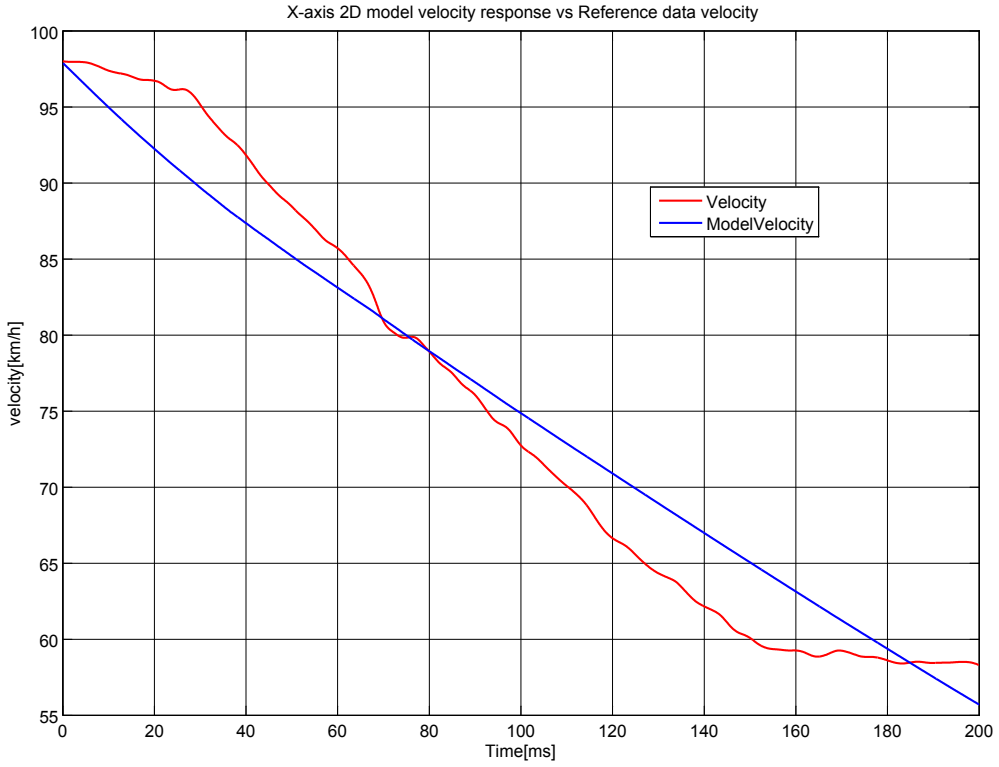

FIGURE 6.28: *2D Model velocity response vs Oblique collision global frame reference velocity in X-axis direction.*

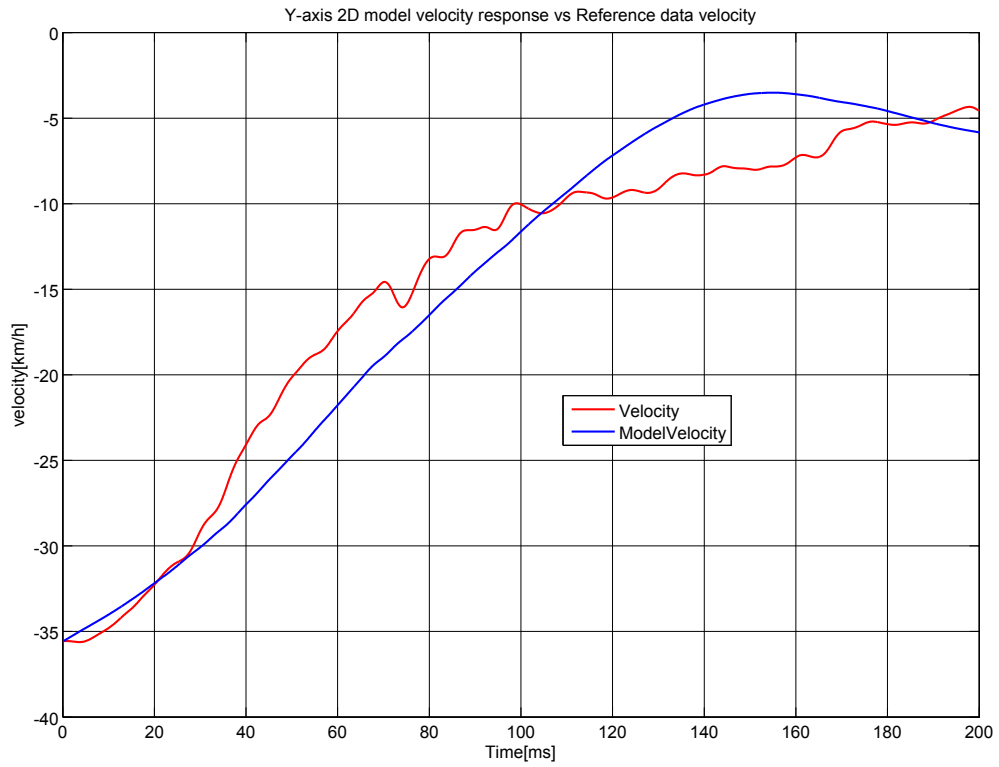

FIGURE 6.29: *2D model velocity response vs Oblique collision global frame reference velocity in Y-axis direction.*

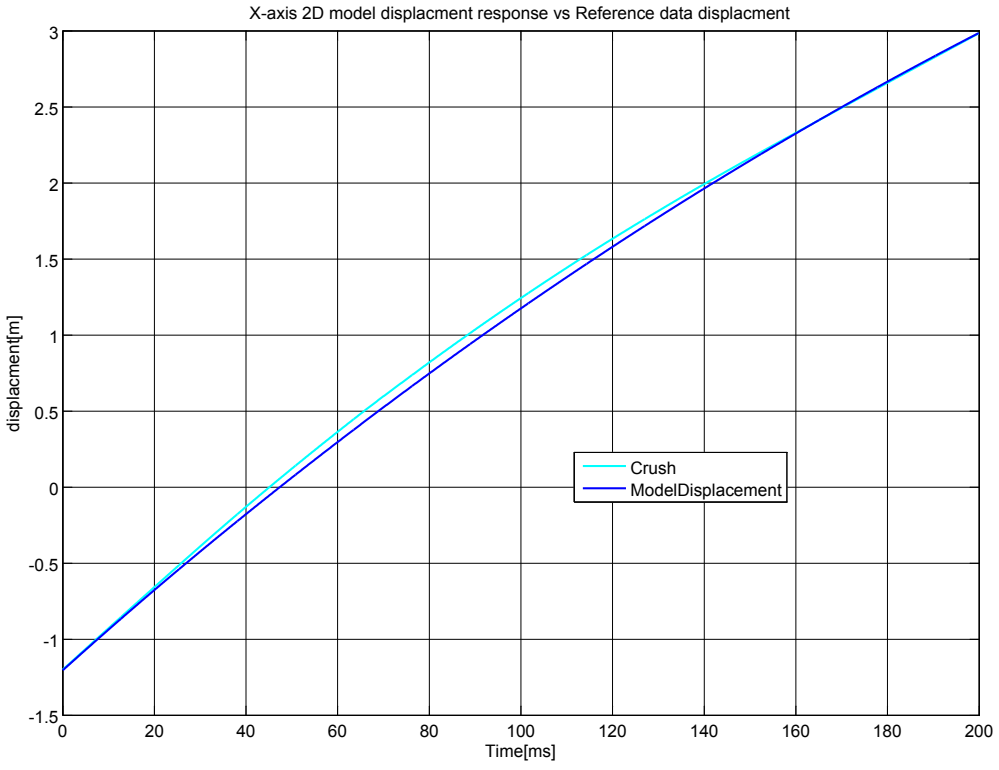

FIGURE 6.30: *2D Model displacement response vs global frame reference displacement of oblique collision in X-axis direction.*

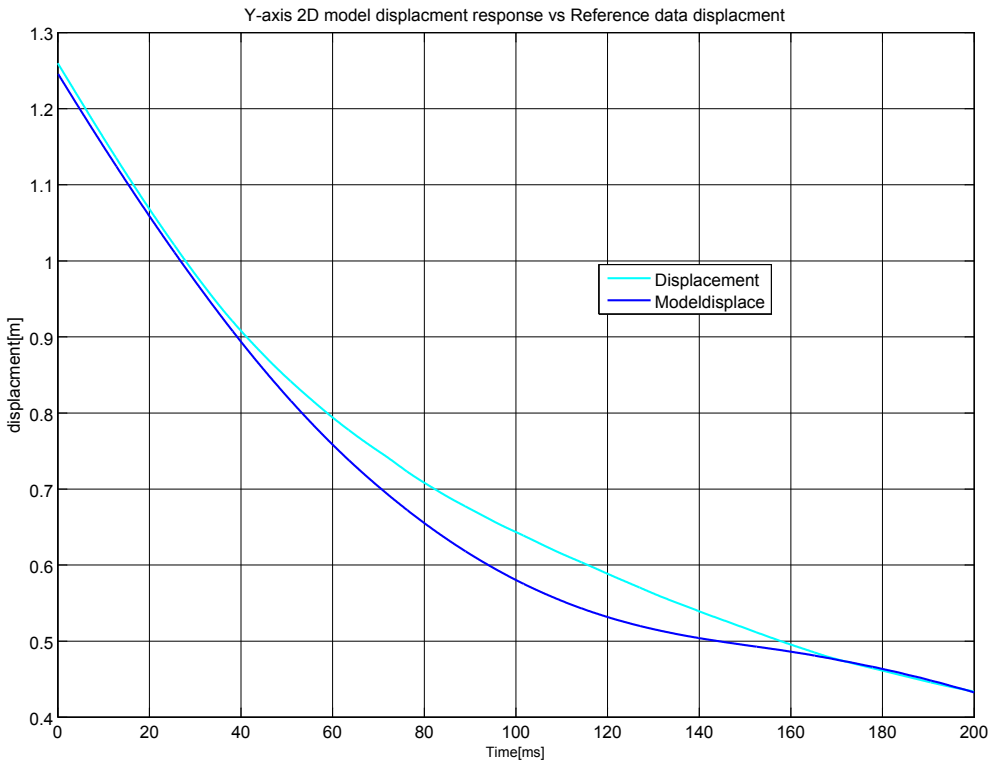

FIGURE 6.31: *2D Model displacement response vs global frame reference displacement of oblique collision inY-axis direction.*

Chapter 7

Discussion and Evaluation of Results

In the signal analysis part of the project an observation is made that raw data gathered from the accelerometer and the gyro sensors have some unwanted high frequency signal values. The graph of the wideband signal has been shown to have some discrepancy when used directly for signal analysis. A curve fitting technique can be utilized to make smooth curve out of the distorted data to obtain a better velocity and displacement output after the integration of the fitted curve. It can be seen that unfiltered signal can be used to analyze the velocity and displacement with good approximations comparing it to the filtered signal. Moreover, digital filtering is a better solution to get rid of the unnecessary features in the signal or to make the signal in its useful frequency range. The digital filters are selected in such away to meet the requirement of frequency response corridors specified in ISO standard. The differences between the channel classes are also investigated and CFC-180 is used for the filtering of the signal for the kinematic plots of the vehicle crash.

The signal is also analyzed in its frequency domain by plotting the FFT graph for the crash pulses in the X, Y and Z coordinate axis. The FFT has helped in the analysis for the filtered data by showing the cut-off frequency effect of the channel classes applied. From the FFT graphs it was also easy to observe that a higher amplitude values occur at lower frequencies for both Y and Z-axis than the X-axis direction for vehicle crash acceleration. It is also noted that there is fast changing amplitude values at subsequent frequencies. Due to this fact, the curve of the velocity and displacement in the time domain of the Y-axis and Z-axis are shown to be unstable when compared to the X-axis direction signal. These phenomena further created the discrepancy between the response output of the derived models and the reference data.

After explicit signal analysis has been made, two mathematical models (2D and 3D models) have been successfully derived for reproduction of the vehicle to barrier collision. Then the parameter estimation for the models has been made. Next the derived models are implemented in the MATLAB simulink to find their responses using the parameters. The verification yields good result for the kinematic values. The general attribute of both 2D and 3D models match the real crush, velocity and acceleration time histories of a car. The highest deformation of a car and the time at which it occurs are the two main parameters characterizing the collision of a vehicle to a barrier

or another car. The maximum dynamic crushe for the comparison between the vehicle to barrier frontal collision and mass-spring-damper model responses for both 2D and 3D mode are shown in the Table 7.1. It can be seen from the table that the maximum dynamic crush and the time it occurs are better represented by the 3D model response than the 2D model. Maximum dynamic crush and maximum time of crush are important to assess the crashworthiness of the vehicle. They can be used to indicate the maximum intrusion to the compartment of a passenger and influence the airbag activation time [42].

Quantity	*Maximum Dynamic Crush [cm]*	*Maximum Dynamic Crush Time [ms]*
2D-Model	44.50	62.95
Reference data (2D)	50.16	74.58
3D-Model	49.54	67.50
Reference data (3D)	50.57	74.76

TABLE 7.1: *Maximum dynamic crush and time of dynamic crush comparison.*

The displacement values in the Y-axis and Z-axis are very small values that are shown in millimeters on the graphs. Higher discrepancies have been observed between the real reference data and the model response in the Y-axis for the 2D model. Similarly higher discrepancies have been observed between the real reference data and the model response in the Y-axis and Z-axis for the 3D model.

The Root-Mean-Square errors are calculated for the acceleration, velocity and displacement for model responses and the reference data that are shown below.

Root-Mean-Square Errors between 2D Model Response and Real Data from Full-Scale Frontal Vehicle Crash

A mean squared error is one of many ways to quantify the difference between the values implied by the model and the true values of reference data. The formula for RMSE is as shown in Equation 7.1.

$$RMSE = \sqrt{\frac{\sum_{i=1}^{n}(x_i - \hat{x}i)^2}{n}} \tag{7.1}$$

where:

- n=number of samples,
- x_i-reference value,
- $\hat{x}_i$-estimated value,

The calculated root-mean-square errors between the 2D model response and the real data from the full-scale frontal vehicle to the barrier collision is shown in Table 7.2 for the 2D model.

Quantity	*Acceleration [g]*	*Velocity [m/s]*	*Displacement [m]*
X-direction	1.88	2.88	0.81
Y-Direction	1.94	9.88	1.69

TABLE 7.2: *Root-mean-square errors(RMSE) between 3D model response and real data from Frontal Collision.*

Root-Mean-Square Errors between 3D Model Response and Real Data from Full-Scale Frontal Vehicle Crash

The calculated root-mean-square errors between the 3D model response and the real data from the full-scale frontal vehicle crash is shown in Table 7.3.

Quantity	*Acceleration [g]*	*Velocity [m/s]*	*Displacement [m]*
X-direction	2.89	5.84	0.41
Y-direction	6.33	1.22	0.11
Z-direction	24.44	27.39	1.45

TABLE 7.3: *Root-mean-square errors(RMSE) between 3D model response and real data from Frontal collision.*

For both the 2D and 3D cases the RMSE values between the reference and estimated data acceleration are relatively high. This is because the reference acceleration signals are complex and not smooth. Particularly the value of the RSME for the acceleration and velocity for the Z-axis are very high in the 3D model response compared to the rest of the values. This is because of the rough estimations of the missing data. The overall behavior of the vehicle is reproduced with a good accuracy for the Kelvin model since the relative values of the velocity and displacement graphs show low RSME values for X-axis direction and the experiment is frontal vehicle crash.

RMSE between 2D Model Response and Real Data from vehicle to road safety barrier oblique collision

The root-mean-square errors between the validation data and the 2D model response are calculated to give ruslts shown in Table 7.4.

The graphs from the simulation results in combination with the values of the root-mean-square-errors shown in Table 7.4 and Table 7.2 clearly show that the 2D model established can represent

Quantity	*Acceleration [g]*	*Velocity [m/s]*	*Displacement [m]*
X-direction	13.90	5.07	1.38
Y-direction	3.73	0.87	0.67

TABLE 7.4: *Root-mean-square errors(RMSE) 2D model response and real data from vehicle to road safety barrier oblique collision.*

either full-scale frontal vehicle to barrier collision or vehicle to road safety barrier oblique collision. The overall behavior of the vehicle to barrier collision is well represented in both cases, but the high RMSE values indicate non-linear parameter estimation method is needed to minimize the differences.

Chapter 8

Conclusions and Future work

.

The intial problem was to make a signal anaysis, mathematical modeling and simulation of a vehicle crash. A thorough anslysis was carried out for a collected vehicle crash data. As a result of this work one viscoelastic model for 2D and a second viscoelastic model for 3D were created to simulate a vehicle to safety barrier collision. There were some assumptions made during modeling to simplify the analysis and to make the model to represent the kinematics of the reference experimental vehicle with a high degree of accuracy. The vehicle is assumed to be a rigid body and the deformation of the barrier is assumed to be negligible. Making these assumptions the mass-spring-damper models for both the 2D and 3D cases have been shown to reproduce the kinematics of the reference experimental vehicle crash with a high degree of accuracy.

The overall attributes of the vehicle crash and the models have been presented to be equivalent and one can use them interchangeably. The recorded acceleration pulses measured in the coordinate frame associated with the car have been decomposed into separate directions related with the global coordinate system and the details of motion was described for the vehicle throughout the collision in the global frame. This is essential, since only then it is possible to establish a complete model of the collision using the approach elaborated in this project. However, there are missing reference data for the 3D model which are very necessary to verify the accuracy of the 3D model established. In this case estimations of the missing reference data values are made by looking at the yaw-rate and yaw-angle to verify the 3D model which give a satisfactory output in comparison of the model with the obtained data.

On the other hand, there is a significant limitation of the proposed methodology. The derived mathematical models are lumped parameter models which represent the crash event. The parameters are estimated by fitting procedure which makes them valid only for a particular crash event. That means parameter values will change with different initial impact velocity. To overcome this issue the suggestion is to create a viscoelastic model with nonlinear parameters which are functions of the initial impact velocity. This kind of system would be capable helping in the reproduction of a wide range of collisions which depend on their changeable initial impact velocities [9].

The parameter estimation used in this project is a simple forward linear equation solving technique. The estimation method is used by making an assumption of the system equations as linear systems. The result obtained from the estimation has proved show some discrepancies. Therefore a better and advance curve fitting procedure is recommended for future identification of parameters for the proposed models. For example, LevenbergMarquardt algorithm curve fitting procedure or other method of solving non-linear system can be used to estimate the parameters.

Finally, the missing data for the 3D model should be collected for future work for the complete 3D dynamic and kinematic modeling and analysis, and it is also advisable to analyze other important aspects of crash test besides the comparing of the kinematics of the model with the colliding vehicle.

Appendix A

Gantt chart

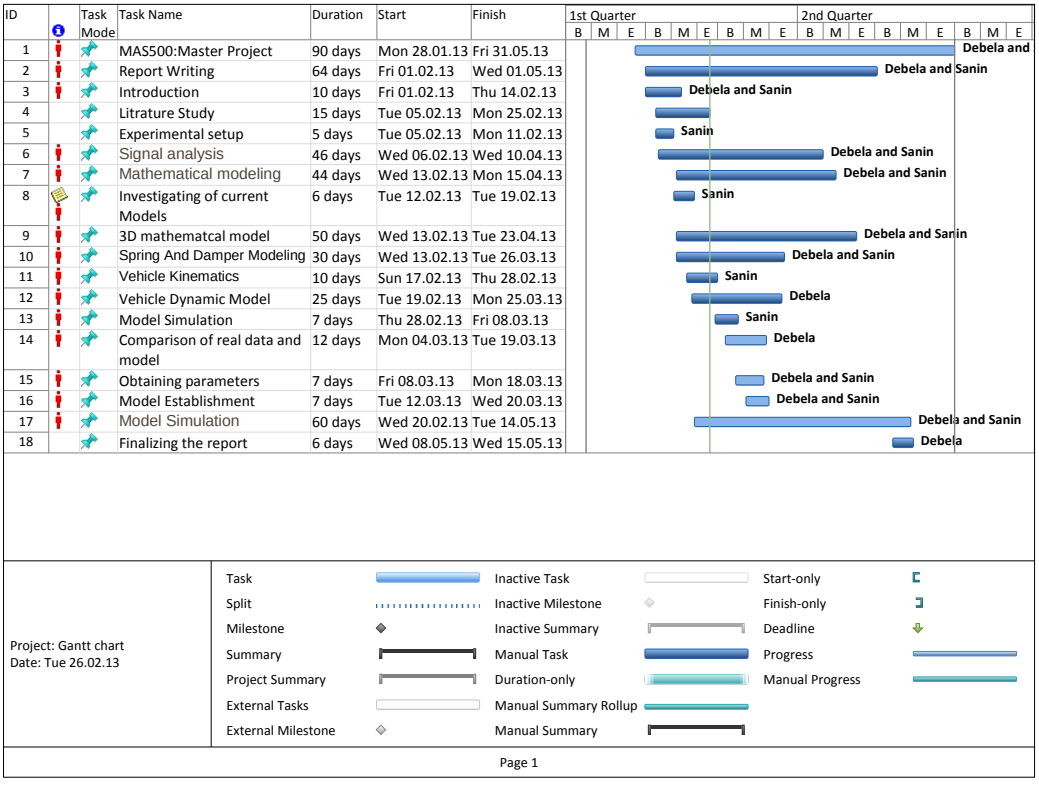

ID	Task Mode	Task Name	Duration	Start	Finish
1		MAS500:Master Project	90 days	Mon 28.01.13	Fri 31.05.13
2		Report Writing	64 days	Fri 01.02.13	Wed 01.05.13
3		Introduction	10 days	Fri 01.02.13	Thu 14.02.13
4		Litrature Study	15 days	Tue 05.02.13	Mon 25.02.13
5		Experimental setup	5 days	Tue 05.02.13	Mon 11.02.13
6		Signal analysis	46 days	Wed 06.02.13	Wed 10.04.13
7		Mathematical modeling	44 days	Wed 13.02.13	Mon 15.04.13
8		Investigating of current Models	6 days	Tue 12.02.13	Tue 19.02.13
9		3D mathematcal model	50 days	Wed 13.02.13	Tue 23.04.13
10		Spring And Damper Modeling	30 days	Wed 13.02.13	Tue 26.03.13
11		Vehicle Kinematics	10 days	Sun 17.02.13	Thu 28.02.13
12		Vehicle Dynamic Model	25 days	Tue 19.02.13	Mon 25.03.13
13		Model Simulation	7 days	Thu 28.02.13	Fri 08.03.13
14		Comparison of real data and model	12 days	Mon 04.03.13	Tue 19.03.13
15		Obtaining parameters	7 days	Fri 08.03.13	Mon 18.03.13
16		Model Establishment	7 days	Tue 12.03.13	Wed 20.03.13
17		Model Simulation	60 days	Wed 20.02.13	Tue 14.05.13
18		Finalizing the report	6 days	Wed 08.05.13	Wed 15.05.13

Appendix B

ISO 6487

INTERNATIONAL STANDARD

ISO 6487

Fourth edition
2002-10-01

Road vehicles — Measurement techniques in impact tests — Instrumentation

Véhicules routiers — Techniques de mesurage lors des essais de choc — Instrumentation

Reference number
ISO 6487:2002(E)

ISO copyright office
Case postale 56 • CH-1211 Geneva 20
Tel. + 41 22 749 01 11
Fax + 41 22 749 09 47
E-mail copyright@iso.ch
Web www.iso.ch

Printed in Switzerland

Contents

Page

Foreword

ISO (the International Organization for Standardization) is a worldwide federation of national standards bodies (ISO member bodies). The work of preparing International Standards is normally carried out through ISO technical committees. Each member body interested in a subject for which a technical committee has been established has the right to be represented on that committee. International organizations, governmental and non-governmental, in liaison with ISO, also take part in the work. ISO collaborates closely with the International Electrotechnical Commission (IEC) on all matters of electrotechnical standardization.

International Standards are drafted in accordance with the rules given in the ISO/IEC Directives, Part 3.

The main task of technical committees is to prepare International Standards. Draft International Standards adopted by the technical committees are circulated to the member bodies for voting. Publication as an International Standard requires approval by at least 75 % of the member bodies casting a vote.

Attention is drawn to the possibility that some of the elements of this International Standard may be the subject of patent rights. ISO shall not be held responsible for identifying any or all such patent rights.

ISO 6487 was prepared by Technical Committee ISO/TC 22, *Road vehicles*, Subcommittee SC 12, *Passive safety crash protection systems*.

This fourth edition cancels and replaces the third edition (ISO 6487:2000), which has been technically revised.

Annex A forms a normative part of this International Standard. Annex B is for information only.

Introduction

This edition of ISO 6487 is the result of a willingness to harmonize the previous edition, ISO 6487:2000, and the American Society of Automotive Engineers' standard, SAE J211:1995.

It presents a series of performance requirements concerning the whole measurement sequence of impact shocks.

These requirements may not be altered by the user and all are obligatory for any agency conducting tests to this International Standard. However, the method of demonstrating compliance with them is flexible and can be adapted to suit the needs of the particular equipment used by a testing agency.

This approach affects the interpretation of requirements. For example, there is a requirement to calibrate within the working range of the channel, i.e. between F_L and $F_H/2{,}5$. This cannot be interpreted literally, as low-frequency calibration of accelerometers requires large displacement inputs beyond the capacity of virtually any laboratory.

It is not intended that each requirement be taken as necessitating proof by a single test. Rather, it is intended that any agency proposing to conduct tests to this International Standard certify that if a particular test could be and were to be carried out then their equipment would meet the requirements. This certification would be based on reasonable deductions from existing data, such as the results of partial tests. The agency would normally be expected to make the basis of their certification available to users of their test results.

The basis of certification of some subjects can be very direct, in that a single test can demonstrate compliance. For others, a less direct form of certification will be necessary. To continue with the above example, the agency could have obtained similar calibrations with direct current at a medium frequency and, from knowledge of the transducer, might infer that calibrations at intermediate frequencies would have been the same.

Similar considerations apply to the practical need to divide the whole channel into subsystems, for calibration and checking purposes. The requirements are valid only for the whole channel, as this is the sole route by which subsystem performance affects the output quality. If it is difficult to measure the whole channel performance, which is often the case, the test agency may treat the channel as two or more convenient subsystems. The whole channel will be certified on the basis of subsystem results, together with a rationale for combining them.

To summarize, this International Standard enables users of impact test results to call up a set of relevant instrumentation requirements by merely specifying ISO 6487. Their test agency then has the primary responsibility for certifying that the ISO 6487 requirements are met by their instrumentation system. The evidence on which they have based this certification will be available to the user on request. In this way, fixed requirements, guaranteeing the suitability of the instrumentation for impact testing, can be combined with flexible methods of demonstrating compliance with those requirements.

Road vehicles — Measurement techniques in impact tests — Instrumentation

1 Scope

This International Standard gives requirements and recommendations for measurement techniques involving the instrumentation used in impact tests carried out on road vehicles. Its requirements are aimed at facilitating comparisons between results obtained by different testing laboratories, while its recommendations will assist such laboratories in meeting those requirements. It is applicable to instrumentation including that used in the impact testing of vehicle subassemblies. It does not include optical methods, which are the subject of ISO 8721.

2 Normative references

The following normative documents contain provisions which, through reference in this text, constitute provisions of this International Standard. For dated references, subsequent amendments to, or revisions of, any of these publications do not apply. However, parties to agreements based on this International Standard are encouraged to investigate the possibility of applying the most recent editions of the normative documents indicated below. For undated references, the latest edition of the normative document referred to applies. Members of ISO and IEC maintain registers of currently valid International Standards.

ISO 2041:1990, *Vibration and shock — Vocabulary*

ISO 3784, *Road vehicles — Measurement of impact velocity in collision tests*

ISO 4130, *Road vehicles — Three-dimensional reference system and fiducial marks — Definitions*

SAE J211/1, *Instrumentation for impact test — Part 1: Electronic instrumentation*

3 Terms and definitions

For the purposes of this International Standard, the terms and definitions given in ISO 2041 and the following apply.

3.1
data channel
all the instrumentation from, and including, a single transducer (or multiple transducers, the outputs of which are combined in some specified way) to, and including, any analysis procedures that may alter the frequency content or the amplitude content of data

3.2
transducer
first device in a data channel used to convert a physical quantity to be measured into a second quantity (such as an electrical voltage), which can be processed by the remainder of the channel

3.3
channel amplitude class
CAC
designation for a data channel that meets certain amplitude characteristics as specified by this International Standard

NOTE The CAC number is numerically equal to the upper limit of the measurement range.

3.4
channel frequency class
CFC
frequency class designated by a number indicating that the channel frequency response lies within limits specified by Figure 1 for CFCs 1 000 and 600, or is filtered using the algorithm given in annex A

NOTE This number and the value of the frequency F_H (see Figure 1), in hertz, are numerically equal.

3.5
calibration value
mean value measured and read during calibration of a data channel

3.6
sensitivity
ratio of the output signal (in equivalent physical units) to the input signal (physical excitation) when an excitation is applied to the transducer

EXAMPLE 10,24 mV/*g*/V for a strain gauge accelerometer.

3.7
sensitivity coefficient
slope of the straight line representing the best fit to the calibration values, determined by the method of least squares within the channel amplitude class

3.8
calibration factor of a data channel
mean value of the sensitivity coefficients evaluated over frequencies evenly spaced on a logarithmic scale between F_L and $F_H/2,5$

3.9
linearity error
ratio of the maximum difference between the calibration value and the corresponding value read on the straight line at the upper limit of the channel amplitude class

NOTE It is expressed as a percentage.

See 4.6.

3.10
transverse sensitivity of a rectilinear transducer
sensitivity to excitation in a nominal direction perpendicular to its sensitive axis

NOTE 1 The transverse sensitivity of a rectilinear transducer is usually a function of the nominal direction of the axis chosen.

NOTE 2 The cross sensitivity of force and bending moment transducers is complicated by the complexity of loading cases. At time of publication, this situation had yet to be resolved.

3.11
transverse sensitivity ratio of a rectilinear transducer
ratio of the transverse sensitivity of a rectilinear transducer to its sensitivity along its sensitive axis

NOTE The cross sensitivity of force and bending moment transducers is complicated by the complexity of loading cases. At time of publication, this situation had yet to be resolved.

3.12
phase delay time of a data channel
time equal to the phase delay, expressed in radians, of a sinusoidal signal, divided by the angular frequency of that signal, and expressed in radians per second

3.13
environment
aggregate, at a given moment, of all external conditions and influences to which the data channel is subject

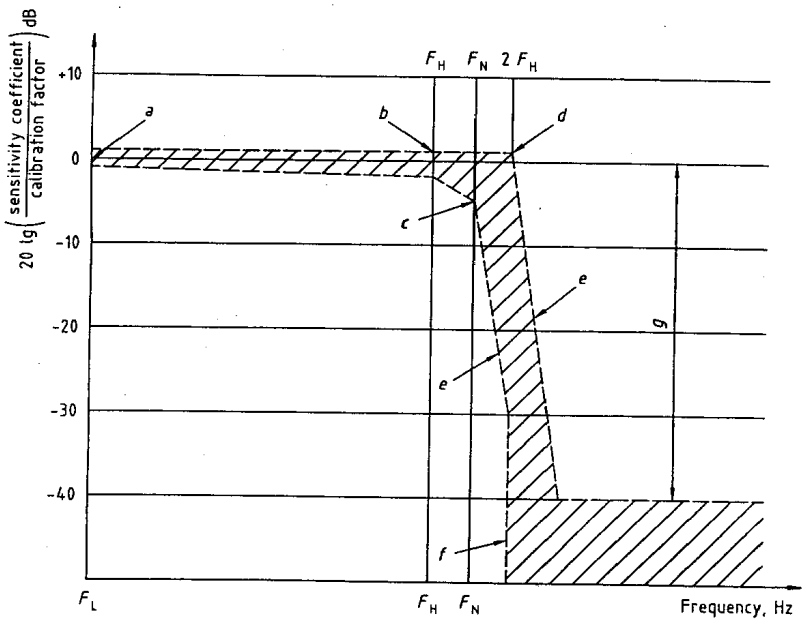

Logarithmic scale	
a	± 0,5 dB
b	+ 0,5; – 1 dB
c	+ 0,5; – 4 dB
d	+ 0,5 dB
e	– 24 dB/octave
f	– ∞
g	– 40 dB

CFC	F_L Hz	F_H Hz	F_N Hz
1 000	⩽ 0,1	1 000	1 650
600	⩽ 0,1	600	1 000

Figure 1 — Frequency response limits — CFC 1000 and CFC 600

4 Performance requirements

4.1 Linearity error

The absolute value of the linearity error of a data channel at any frequency in the CFC (channel frequency class) shall be less than or equal to 2,5 % of the value of the CAC over the whole measurement range.

4.2 Amplitude against frequency

The frequency response of a data channel shall lie within the limiting curves given in Figure 1 for CFCs 1 000 and 600. For CFCs 180 and 60, the frequency response of the channel is determined by the filter algorithm given in annex A. The zero decibels line is defined by the calibration factor. For CFCs 180 and 60, the frequency response of the data channel shall remain within 0,5 dB of the zero decibel line at frequencies ranging from 0,1 Hz to the CFC, before the digital filter is applied.

See 4.6.2.3.2.

4.3 Phase delay time of a data channel

The phase delay time of a data channel between its input and output shall be determined; it shall not vary by more than $1/10 F_H$ s between 0,03 F_H and F_H.

4.4 Time

4.4.1 Timebase

A timebase shall be recorded that shall give at least 0,01 s with an accuracy of 1 %.

4.4.2 Relative time delay

The relative time delay between the signals of two or more data channels, regardless of their frequency class, shall not exceed 1 ms, excluding phase delay caused by phase shift. Two or more data channels whose signals are combined shall have the same frequency class and shall have a relative time delay not greater than $1/10 F_H$ s.

This requirement is applicable to analog signals, synchronization pulses and digital signals.

4.5 Transducer transverse sensitivity ratio of a rectilinear transducer

The transducer transverse sensitivity ratio of a rectilinear transducer shall be less than 5 % in any direction.

4.6 Calibration

4.6.1 General

A data channel shall be calibrated at least once a year against reference equipment traceable to known standards. The methods used to carry out a comparison with reference equipment shall not cause an error greater than 1 % of the CAC. The use of reference equipment is limited to the range of frequencies for which it has been calibrated.

Data channel subsystems may be evaluated individually and the results factored into the accuracy of the total data channel. This can be made, for example, by an electrical signal of known amplitude simulating the output signal of the transducer, allowing a check to be made on the gain of the data channel, excluding the transducer.

4.6.2 Accuracy of reference equipment for calibration

4.6.2.1 General

The accuracy of the reference equipment shall be certified or endorsed by an approved metrology service.

4.6.2.2 Static calibration

4.6.2.2.1 Acceleration

The error shall be less than 1,5% of the channel amplitude class.

4.6.2.2.2 Force and displacement

The error shall be less than 1 % of the channel amplitude class.

4.6.2.3 Dynamic calibration

4.6.2.3.1 Acceleration

The error in the reference accelerations expressed as a percentage of the channel amplitude class shall be less than 1,5 % at below 400 Hz, less than 2 % between 400 Hz and 900 Hz, and less than 2,5 % between 900 Hz and the maximum frequency at which the reference acceleration is used (see 4.6.4).

4.6.2.3.2 Forces and displacements

A method for the evaluation of the dynamic response during the calibration of data channels for forces and displacements has not been included in this International Standard, since no satisfactory method is known at present. The problem is to be reconsidered at a later date.

4.6.2.4 Time

The relative error in the reference time shall be less than 10^{-5}.

4.6.3 Sensitivity coefficient and linearity error

The sensitivity coefficient and the linearity error shall be determined by measuring the output signal of the data channel against a known input signal, for various values of this signal.

The calibration of the data channel shall cover the whole range of the amplitude class.

For bi-directional channels, both the positive and negative values shall be used.

If the calibration equipment cannot produce the required input, due to the excessively high values of the quantity to be measured, calibrations shall be carried out within the limits of these calibration standards, and these limits shall be recorded in the report.

A total data channel shall be calibrated at a frequency or at spectrum of frequencies, with its significant value being between F_L and $F_H/2,5$.

4.6.4 Calibration of frequency response

The response curves of phase and amplitude against frequency shall be determined by measuring the output signals of the data channel in terms of phase and amplitude against a known input signal, for various values of this signal varying between F_L and ten times the CFC or 3 000 Hz, whichever is the lower.

4.7 Environmental effects

The existence or nonexistence of an influence of environmental effects shall be checked regularly (i.e. electric or magnetic flux, cable velocity, etc.). This can be done, for example, by recording the output of spare channels equipped with dummy transducers.

If significant output signals are obtained, corrective action shall be taken — for example, the re-allocation or replacement of cables.

4.8 Choice and designation of data channel

The CAC and CFC define the data channel, and their values are chosen for a given application by the party requiring the application.

A data channel in accordance with this International Standard shall be designated as follows.

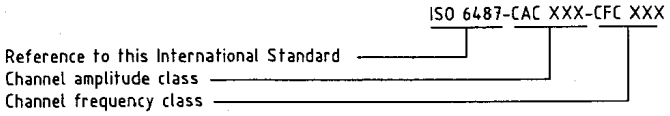

The type of filter used, phaseless or phase shifting, shall be declared for each channel.

For CFCs 180 and 60, the Butterworth four-pole phaseless filter, as specified in annex A, shall be used.

If the calibration of the amplitude or frequency response does not cover the complete CAC or CFC, owing to limited properties of the calibration equipment, then the CAC or CFC shall be marked with an asterisk.

EXAMPLE A measurement carried out in accordance with this International Standard, where the channel amplitude class is 200 m/s^2, the channel frequency class 1 000, and the calibration of the amplitude response did not cover the complete CAC, is designated as follows:

ISO 6487 – CAC* 200 m/s^2 – CFC 1 000

The test report shall indicate the calibration limits.

4.9 Choice of reference coordinate system

The following coordinate systems shall be used.

— For the dummy measurements: SAE J211/1.

— For the vehicle measurements: ISO 4130 or SAE J211/1.

The coordinate reference system used shall be clearly defined for each measurement.

4.10 Impact velocity measurement

Impact velocity measurement shall be in accordance with ISO 3784.

Annex A
(normative)

Butterworth four-pole phaseless digital filter (including initial-condition treatment) algorithm

The following algorithm is unsuitable for filter frequencies above CFC 180, since, at high frequencies, the frequency response of this digital filter varies as a function of the sampling rate used.

```
/*  ------------------------------------------------------------------------------------------  */
/*                                  Butterworth phaseless filter                               */
/*  ------------------------------------------------------------------------------------------  */

//  Author : NHTSA
//  for CFC 60 :      F-3db = 100
//  for CFC 180 :     F-3db = 300

/*  ------------------------------------------------------------------------------------------  */
/*                                  Variables used                                             */
/*  ------------------------------------------------------------------------------------------  */
```

F-3db = cutoff frequency at -3dB
F-6db = cutoff frequency at -6dB = 1,25 * F-3db

SampleRate = sampling interval in seconds
Pi = 3,141592654
a1, a2, b0, b1, b2 filter coefficients
Samples = initial table of samples
NumberOfSamples = length of **Samples** table ***(! note ! : the index of a table is between zero and length of table -1)***
FilterTab = table of filtering samples
IndexLastPoint + 1 = length of **FilterTab** table
NumberOfAddPoints = number of points to be added to **NumberOfSamples**

```
/*  ------------------------------------------------------------------------------------------  */
/*                                  Initial condition                                          */
/*  ------------------------------------------------------------------------------------------  */
```

//The table **Samples** is completed with anti-symmetry around t = 0. Gives table **FilterTab**

/*compute the number of points to be added to the table **Samples** */
NumberOfAddpoints = 0,01 / **SampleRate**
NumberOfAddPoints = min (max(**NumberOfAddPoints**,100), **NumberOfSamples**-1)
IndexLastPoint = **NumberOfSamples** + 2 * **NumberOfAddPoints** - 1

```
/* Generation of table to be filtered FilterTab */
for i = NumberOfAddPoints to NumberOfAddPoints + NumberOfSamples -1 by step 1
            FilterTab[i] = Samples[i - NumberOfAddPoints]
endfor

for i = 0 to NumberOfAddPoints - 1 by step 1
        FilterTab[NumberOfAddPoints - i - 1] = 2 * Samples[0] - Samples[i+1];
        FilterTab[NumberOfSamples + NumberOfAddPoints + i] =
              2 * Samples[NumberOfSamples - 1] - Samples[NumberOfSamples - i - 2]
endfor

/*  ----------------------------------------------------------------------------------------  */
/*                              compute filter coefficients                                  */
/*  ----------------------------------------------------------------------------------------  */

Wd = 2. * Pi * F-6db
Wa = sin( Wd * SampleRate / 2,0) / cos( Wd * SampleRate / 2,0)
b0 = Wa² / (1 + √2 * Wa + Wa²)
b1 = 2. * b0
b2 = b0
a1 = -2 * (Wa² - 1 ) / ( 1 + √2 * Wa + Wa² )
a2 = ( -1 + √2 * Wa - Wa² ) / ( 1 + √2 * Wa + Wa²)

/*  ----------------------------------------------------------------------------------------  */
/*                                   Filter forward                                           */
/*  ----------------------------------------------------------------------------------------  */

y1 = 0
for i = 0 to i = 9 by step 1
          y1 = y 1 + FilterTab[i]
endfor

y1 = y1 / 10,0
x2 = 0.
x1 = FilterTab[0]
x0 = FilterTab[1]
FilterTab[0] = y1
FilterTab[1] = y1
for i = 2 to i = IndexLastPoint by step 1
          x2 = x1
          x1 = x0
          x0 = FilterTab[i]
          FilterTab[i] = b0 * x0 + b1 * x1 + b2 * x2 +a1 * FilterTab[i-1] +a2 * FilterTab[i-2]
endfor

/*  ----------------------------------------------------------------------------------------  */
/*                                   Filter backward                                          */
/*  ----------------------------------------------------------------------------------------  */

y1 = 0
for i = IndexLastPoint to IndexLastPoint - 9 by step -1
          y1 = y1 + FilterTab[i]
endfor
```



```
y1 = y1/10,0
x2 = 0.
x1 = FilterTab[IndexLastPoint]
x0 = FilterTab[IndexLastPoint - 1]
FilterTab[IndexLastPoint] = y1
FilterTab[IndexLastPoint - 1] = y1
for i = IndexLastPoint - 2 to i = 0 by step -1
        x2 = x1
        x1 = x0
        x0 = FilterTab[i]
        FilterTab[i] = b0 * x0 +b1 * x1 +b2 * x2 + a1 * FilterTab[i+1] + a2 * FilterTab[i+2]
endfor

/*  ------------------------------------------------------------------------------------------------------------  */
/*                                              Filtering of samples                                              */
/*  ------------------------------------------------------------------------------------------------------------  */

for i = NumberOfAddPoints to i = NumberOfAddPoints + NumberOfSamples -1 by step 1
    Samples[i - NumberOfAddPoints] = FilterTab[i]
endfor
```

Annex B
(informative)

Recommendations for enabling requirements to be met

B.1 Mounting of transducers

Transducers should be rigidly mounted so that their recordings are affected as little as possible by vibration. Any transducer mounting component assembly having a lowest resonance frequency equal to at least five times the frequency F_H of the given data channel should be considered valid.

Acceleration transducers, excluding transducers in dummies, should be mounted such that the initial angle of the actual measurement axis to the corresponding axis of the reference axis system is not greater than 5°, unless analytical or experimental assessment of the effect of the mounting on the collected data is made. When multi-axial accelerations at a point are to be measured, each acceleration transducer axis should pass within 10 mm, and the centre of seismic mass of each accelerometer within 30 mm, of that point.

Transducers should be mounted on the dummies using a support specially provided for that purpose.

B.2 Data processing

B.2.1 Filtering

Filtering corresponding to the frequencies of the data channel class may be carried out either during recording or processing of data.

However, before recording, analog filtering at a level greater than or equal to CFC 1 000 should take place in order to use at least 50 % of the dynamic range of the recorder and reduce the risk of high frequencies saturating the recorder or of aliasing error in the digitizing process.

If no pre-impact event data is recorded, then the initial conditions algorithm defined in annex A or an alternative procedure should be used.

If filtering is to be performed, it should precede all non-linear operations, such as calculation of resultant vectors or injury indices.

B.2.2 Digitizing

B.2.2.1 Sampling frequencies

The sampling frequency should be at least 10 F_H.

The analog anti-aliasing filters should have an attenuation of at least 30dB at half the sampling rate.

In the case of analog recording, when the recording and reading speeds are different, the sampling frequency can be divided by the speed ratio.

B.2.2.2 Amplitude resolution

The length of digital words should permit a resolution of at least 0,2 % of CAC.

B.3 Presentation of results

The results should be presented on A4 size paper, in accordance with ISO 216.

The measurements may be recorded at various locations on the vehicle. These locations shall be stated in the test report.

Results presented as diagrams should have axes scaled with one measurement unit corresponding to a suitable multiple of the chosen unit (for example 1 mm, 2 mm, 5 mm, 10 mm, 20 mm).

SI units shall be used. For vehicle velocity, kilometres per hour may be used, and for accelerations due to an impact, g may be used (where $g = 9{,}81\ m/s^2$).

Bibliography

[1] ISO 216, *Writing paper and certain classes of printed matter — Trimmed sizes — A and B series*

[2] ISO 8721, *Road vehicles — Measurement techniques in impact tests — Optical instrumentation*

[3] SAE J182, *Motor vehicle fiducial marks and three-dimensional reference system*

[4] SAE J670, *Vehicle dynamics terminology*

Appendix C

Channel Class Selection-SAE J211

Typical Test Measurement	Channel Class
Vehicle structural acceleration for use in:	
Total vehicle comparison	**60**
Collision simulation (for example, impact sled) input	60
Component analysis	600
Integration for velocity or displacement	180
Barrier face force	**60**
Belt restraint system load	**60**
Occupant	
Head acceleration	**1000**
Chest acceleration	**180**
deflection	180
Pelvis	
acceleration	**1000**
forces	1000
moments	1000
Femur/knee/tibia/ankle	
forces	**600**
moments	600
displacements	180
Sled acceleration	**60**
Steering column load	**600**
Headform acceleration	**1000**

TABLE C.1: *Channel Class Selection-SAE J211 [5].*

Bibliography

[1] Euro NCAP. Euro ncap @ONLINE. http://www.euroncap.com, February 2013.

[2] W.T. HOLLOWELL, H.C. GABLER, S.L. STUCKI, and S. SUMMERS. Updated review of potential test procedures for fmvss no. 208. 1999.

[3] IIHS. Insurance institute for highway safety@ONLINE. http://www.iihs.org, February 2013.

[4] KG Robbersmyr. Project report 43/2004, calibration test of a standard ford fiesta 1.1 l, model year 1987, according to ns–en 12767, 2004.

[5] M. Huang. *Vehicle Crash Mechanics*. Taylor & Francis, 2010. ISBN 9780849301049. URL http://books.google.no/books?id=-vec1_mU-uMC.

[6] B. Balachandran and E.B. Magrab. *Vibrations*. Cengage Learning, 2008. ISBN 9780534552060. URL http://books.google.no/books?id=ySCUry0VabQC.

[7] R.N. Jazar. *Vehicle Dynamics: Theory and Application*. Springer, 2008. ISBN 9780387742434. URL http://books.google.no/books?id=Pvsv78xj7UIC.

[8] Jörg Lampe and Heinrich Voss. Large-scale tikhonov regularization of total least squares. *Journal of Computational and Applied Mathematics*, 2012.

[9] Witold Pawlus, Hamid Reza Karimi, and Kjell G. Robbersmyr. Reconstruction and simulation of the vehicle to road safety barrier oblique collision based on the levenberg-marquardt algorithm. *International Journal of Crashworthiness*, 17(6):676–692, 2012. doi: 10.1080/13588265.2012.714300. URL http://www.tandfonline.com/doi/abs/10.1080/13588265.2012.714300.

[10] NRMA. Australasian new car assessment program (ancap)@ONLINE. http://www.mynrma.com.au, February 2013.

[11] JNCAP. Japan new car assessment program (jncap)@ONLINE. http://www.nasva.go.jp, February 2013.

[12] E. Toccalino. Passenger vehicle safety rating (euro , us-ncap and iihs): Performance overview and energy management solutions. *SAE Technical Paper 2003-01-0230*, 2003. doi: 10.4271/2003-01-0230.

[13] Witold Pawlus, Hamid Reza, and Kjell Gunnar Robbersmyr. Application of viscoelastic hybrid models to vehicle crash simulation. *International Journal of Crashworthiness*, 16(2):195–205, 2011. doi: 10.1080/13588265.2011.553362. URL http://www.tandfonline.com/doi/abs/10.1080/13588265.2011.553362.

[14] W. Pawlus, H.R. Karimi, and K.G. Robbersmyr. Reconstruction of crash pulse of a vehicle involved in central localized collision based on morlet wavelets. In *Control Conference (CCC), 2012 31st Chinese*, pages 1811 –1816, july 2012.

[15] F. Amato, V. Moscato, A. Picariello, and C. Sansone. Reconstruction of car crash scenes using a 3d building and query algebra. In *Signal Image Technology and Internet Based Systems (SITIS), 2012 Eighth International Conference on*, pages 891 –897, nov. 2012. doi: 10.1109/SITIS.2012.132.

[16] M. Murad, K.C. Cheok, and M. Das. Intelligent adaptive occupant restraint system. In *Southeastcon, 2009. SOUTHEASTCON '09. IEEE*, march 2009.

[17] Wikipedia. Traffic collision — wikipedia, the free encyclopedia. http://en.wikipedia.org/w/index.php?title=Traffic_collision&oldid=535638660, 2013. [Online; accessed 4-February-2013].

[18] CN Kloeden, AJ McLean, MRJ Baldock, and AJT Cockington. Severe and fatal car crashes due to roadside hazards.

[19] MM Peden, R. Scurfield, D. Sleet, D. Mohan, A.A. Hyder, E. Jarawan, C.D. Mathers, et al. World report on road traffic injury prevention, 2004.

[20] C.D. Mathers, C. Stein, C. Rao, M. Inoue, N. Tomijima, C. Bernard, A.D. Lopez, and C.J.L. Murray. Global burden of disease 2000: Version 2 methods and results. 2002.

[21] H.P. Snider. Vehicle instrumentation for crash testing. *Industrial Electronics and Control Instrumentation, IEEE Transactions on*, IECI-11(1):44 –49, feb. 1964. ISSN 0018-9421. doi: 10.1109/TIECI.1964.229528.

[22] Karim Nice. How crash testing works. http://auto.howstuffworks.com/car-driving-safety/accidents-hazardous-conditions/crash-test.htm, 02 March 2001. [Online; accessed 4-February-2013].

[23] G.W. Miyasaki. *Automobile Crash Test Facility and Preliminary Analysis of Low Speed Crush Characteristics*. Thesis: M.A.Sc. University of British Columbia, 1987. URL http://books.google.no/books?id=hKrpSgAACAAJ.

[24] Robert (Thesis) Rice. Crash analysis: an investigation of current speed estimation techniques. Master's thesis, Dublin Institute of Technology, Ireland, 2004. URL http://arrow.dit.ie/scienmas/39.

[25] M. Pecht, A. Ramakrishnan, J. Fazio, and C.E. Nash. The role of the u.s national highway traffic safety administration in automotive electronics reliability and safety assessment. *Components and Packaging Technologies, IEEE Transactions on*, 28(3):571 – 580, sept. 2005. ISSN 1521-3331. doi: 10.1109/TCAPT.2005.851597.

[26] Witold Pawlus, Hamid Reza Karimi, and Kjell G Robbersmyr. A fuzzy logic approach to modeling a vehicle crash test. *Central European Journal of Engineering*, pages 1–13, 2012.

[27] Matej Borovinšek, Matej Vesenjak, Miran Ulbin, and Zoran Ren. Simulation of crash tests for high containment levels of road safety barriers. *Engineering Failure Analysis*, 14(8):1711–1718, 2007.

[28] A Deb and KC Srinivas. Development of a new lumped-parameter model for vehicle side-impact safety simulation. *Proceedings of the Institution of Mechanical Engineers, Part D: Journal of Automobile Engineering*, 222(10):1793–1811, 2008.

[29] Zeng Liang, Peng Shao-xiong, Zou Qiang, and Zhu Xu-cheng. Applying ls-dyna to construct virtual experiment system. In *Education Technology and Computer (ICETC), 2010 2nd International Conference on*, volume 2, pages V2–37 –V2–39, june 2010. doi: 10.1109/ICETC.2010.5529439.

[30] Livermore Software Technology Corporation. Livermore software technology corporation:-ls-dyna @ONLINE. http://www.lstc.com, February 2013.

[31] IMPETUS Afea AS. Impetus afea solver @ONLINE. http://www.impetus-afea.com, February 2013.

[32] Witold Pawlus, Hamid Reza Karimi, and Kjell Gunnar Robbersmyr. Development of lumped-parameter mathematical models for a vehicle localized impact. *Journal of mechanical science and technology*, 25(7):1737–1747, 2011.

[33] Hamid Reza Karimi, Witold Pawlus, and Kjell G. Robbersmyr. Signal reconstruction, modeling and simulation of a vehicle full-scale crash test based on morlet wavelets. *Neurocomputing*, 93(0):88 – 99, 2012. ISSN 0925-2312. doi: 10.1016/j.neucom.2012.04.010. URL http://www.sciencedirect.com/science/article/pii/S0925231212003451.

[34] ISO. Vehicles measurement techniques in impact tests instrumentation, 2000.

[35] Wikipedia. System of linear equations — wikipedia, the free encyclopedia, 2013. URL http://en.wikipedia.org/w/index.php?title=System_of_linear_equations&oldid=551640828. [Online; accessed 27-April-2013].

[36] Encyclopedia of Mathematics. Linear algebraic equation., 2013. URL http://www.encyclopediaofmath.org/index.php?title=Linear_algebraic_equation&oldid=21576. [Online; accessed 27-April-2013].

[37] Ivo Petráš and Dagmar Bednárová. Total least squares approach to modeling: a matlab toolbox. *Acta Montanistica Slovaca*, 15(2):158, 2010.

[38] Valerio Lucarini. Total least squares.

[39] Gene H Golub. Some modified matrix eigenvalue problems. *Siam Review*, 15(2):318–334, 1973.

[40] Gene H Golub and Charles F Van Loan. An analysis of the total least squares problem. *SIAM Journal on Numerical Analysis*, 17(6):883–893, 1980.

[41] Ivan Markovsky and Sabine Van Huffel. Overview of total least-squares methods. *Signal processing*, 87(10):2283–2302, 2007.

[42] Witold Pawlus, Kjell Gunnar Robbersmyr, Hamid Reza Karimi, and Arnfinn Fanghol. The performance investigation of viscoelastic hybrid models in vehicle crash event representation. In *World Congress*, volume 18, pages 2138–2143, 2011.